博士論文

論文題目　A Study on the Degradation Mechanism and Lifetime Enhancement of Microwave Discharge Neutralizers
(マイクロ波放電式中和器の劣化機構と長寿命化に関する研究)

氏名　大道　渉

A Study on the Degradation Mechanism and Lifetime Enhancement of Microwave Discharge Neutralizers

Wataru OHMICHI

March, 2014

Abstract

An ion thruster is a form of electric propulsion used for spacecraft propulsion that creates thrust by accelerating ions. Electric propulsion thrusters are external combustion engines using electric power and generate a thrust force by means of a physical reaction of exhaust propellant. Electric propulsion thrusters typically use much less propellant than chemical propulsion thrusters because they operate at a higher exhaust velocities. These characteristic enable spacecraft to achieve low-cost, long-distance missions due to weight savings. The unmanned Japanese asteroid sample-return mission of Hayabusa is a deep-space mission. The Hayabusa asteroid explorer spacecraft is the first spacecraft to use an electron cyclotron resonance (ECR) microwave discharge ion thruster as the primary propulsion system. The total accumulated operation time of Hayabusa's four "μ10" ion thrusters reached approximately 40,000 hours. This achievement depends to a large extent on the ECR discharge method. In this plasma generation method, electrodes in the discharge chamber are not subject to erosion, which is the typical failure mechanism in conventional ion thrusters. However, μ10 experienced an autonomous stop during the final phase of the Hayabusa project due to degradation of the neutralizer. The neutralizer is a critical element that limits the lifetime of the thruster. Therefore, it is necessary to enhance the endurance of the neutralizer in order to extend the lifetime of the spacecraft.

The objectives of the present study are to clarify the mechanism of performance degradation of the neutralizer and to determine methods by which to extend the lifetime of the neutralizer for the next-generation μ10 thrusters. In order to achieve these objectives, we

- assume and verify the degradation mechanism of the neutralizer,
- propose a novel neutralizer that uses countermeasures to reduce performance degradation, and
- demonstrate the performance of the novel neutralizer through long time experiment.

We first investigate the neutralizer, which was subjected to a 20,000-hour endurance test, and for which degradation had already occurred. The investigation revealed that the principal cause of the performance degradation of the neutralizer was the contamination of the dielectric surface due to sputtering from flakes on the magnetic circuit. This degradation can be avoided by suppressing the sputtering by means of a lower contact voltage and by inhibiting flakes formation.

In order to achieve a lower contact voltage, we determined which assembly should be improved by net ion current distribution measurement. This measurement revealed which assembly is collecting ions, which is the counterpart of electron emission. Based on these findings, we refurbished the magnet, and orifice plate, and suppressed the contact voltage by 5 V, which extend 25% the lifetime of μ10 flight model neutralizer. In order to investigate the long-term performance, we conducted 10,000-hour class endurance tests.

In order to inhibit flake formation, we designed a full molybdenum-covered neutralizer. Moreover, we conducted a 1,500-hour endurance test in order to verify the long-term performance of the full molybdenum-covered neutralizer.

Contents

List of Figures

List of Tables

1 Introduction

The ion thruster is an electric propulsion system used in spacecraft propulsion that creates thrust by accelerating ions. Electric propulsion thrusters are external combustion engines using electric power and generate a thrust force by means of a physical reaction of exhaust propellant. Electric propulsion thrusters typically use much less propellant than chemical propulsion thrusters because electric propulsion thrusters operate at higher exhaust velocities. These characteristic enable to low-cost, long-distance missions due to weight savings [6] [7].

The unmanned Japanese asteroid sample return mission aboard Hayabusa is a deep-space mission. The Hayabusa asteroid exploration spacecraft is the first spacecraft that uses an electron cyclotron resonance (ECR) microwave discharge ion thruster [8] as the primary propulsion system. The total accumulated operation time of Hayabusa's four "μ10" ion thrusters reached approximately 40,000 hours [9]. This achievement depends to a large extent on the ECR discharge method. In this plasma generation method, electrodes in the discharge chamber can be released by erosion of the chamber, which is a typical failure of conventional ion thrusters [10]. However, the μ10 experienced an autonomous stop during the final phase of the Hayabusa project as a result of degradation of the neutralizer. The neutralizer has been found to be a critical element that limits the lifetime of the thruster. Therefore, it is necessary to extend the lifetime of the neutralizer in order to extend the lifetime of the spacecraft [11] [12]. In this chapter, fundamentals of ion thurster and neutralizer are firstly introduced, and the objective of present study is also introduced in detail.

1.1 Ion thruster

[13] [14] In this section, the principal of ion thrusters is explained. Ion thrusters create very small levels of thrust compared to conventional chemical rockets but achieve very high specific impulses, or propellant mass efficiencies. An ion thruster basically consists of three components: a plasma generator, accelerator grids, and a neutralizer, which acts as an electron source. Fig.1.1 shows a schematic of an ion thruster. Plasma is generated by the plasma generator, and ions are accelerated by the grid system and are neutralized by the neutralizer, which acts as an electron source.

Plasma generator

The power consumption of plasma generation does not contribute to the thrust force. Thus, in terms of thruster efficiency, the power consumption should be low. Ion thrusters are classified according to the plasma generating process, i.e., the primary electron generation process. This is because the ion production process is the same in all ion thrusters and uses ionizing collisions by electrons. For effective ionization, a low ionization energy and a high collision cross section are important. Xenon, which is the conventional propellant used in ion thrusters, satisfies these requirements. In addition, xenon has a large molecular size, which has two advantages, The first is a relatively low thermal velocity, which provides a higher efficiency of ion confinement in the discharge chamber, and the second is that the thrust force can be more easily increased by increasing the specific impulse, as compared to an atom having a smaller molecular size. Fig.1.2 shows the excitation and ionization cross-section of xenon [1] [2]. A primary electron energy of approximately 30 eV is optimal for ionizing xenon with high efficiency. Accelerating multiple ionized xenon atoms requires more energy, but its velocity which produce thrust force increases with the square root of multiplied charge. Thus, singly ionized xenon atoms are the most effective means of producing a thrust force. In addition, the energy of excitation does not contribute to the thrust force. As such, the energy consumption of excitation must be lower than the energy consumption of ionization.

Ion accelerator

The ion velocity is accelerated by the electrostatic field formed by the difference in the grid voltage. The velocity thrust force of the ion thruster F is given as follows:

$$F = J_b\sqrt{\frac{2m_iV_b}{q}} \tag{1.1.1}$$

where J_b is the ion beam current flux in A/m^2, m_i is the mass of the ion, q is the quantum of electricity, and V_b is the voltage between the grids. This ion beam current flux is defined by the grid design and the plasma parameters. The ion current flux from the plasma is given as follows:

$$j_i = qe^{-\frac{1}{2}}n_0\sqrt{\frac{kT_e}{m_i}} \tag{1.1.2}$$

where j_i is the ion current flux in A/m^2, n_0 is number density of plasma, k is the Boltzmann coefficient, and T_e is the electron temperature. However, the maximum ion current flux j_{max} that can obtained from the electric field formed by two plane electrodes is given as follows:

$$j_{max} = \frac{4}{9}\varepsilon_0\sqrt{\frac{2q}{m_i}}\frac{V^{\frac{3}{2}}}{L^2} \tag{1.1.3}$$

where ε_0 is the vacuum permittivity, and L is the electrode gap distance. The grids are designed to consistently maintain $j_i = j_{max}$. The flux is J_b.

However, the grids are sputtered by ions that are generated by charge exchange collision due to accelerated ions. This is one factor that limits the thruster lifetime.

Neutralization

Ions from the plasma generator are accelerated at the grids and form the thrust beam. The neutralizer provides electrons at the same rate as the ions in order to avoid a charge imbalance with the spacecraft. The neutralizer does not contribute to the thrust force, the low operational gas consumption and power consumption are required. The neutralizer is placed near the ion beam, but not in the ion beam, so as to avoid degradation by ion beam sputtering. The electrons are provided to the ion beam plasma by the plasma inside the neutralizer. The electrons from the neutralizer are provided by the voltage difference

between the neutralizer and the ion beam. This is referred to as the contact voltage. However, if the neutralizer is emitting only electrons, the emission current is limited by the space-charge-limited current. In order to achieve the mitigation of the limited current, plasma connection of the ion beam plasma and the plasma inside the neutralizer is required. This connection is achieved by additional plasma generated by collisions between neutral particles and emitted electrons, which are sketched in Fig.1.3. This is referred to as a plasma bridge. The plasma bridge realizes a low contact voltage.

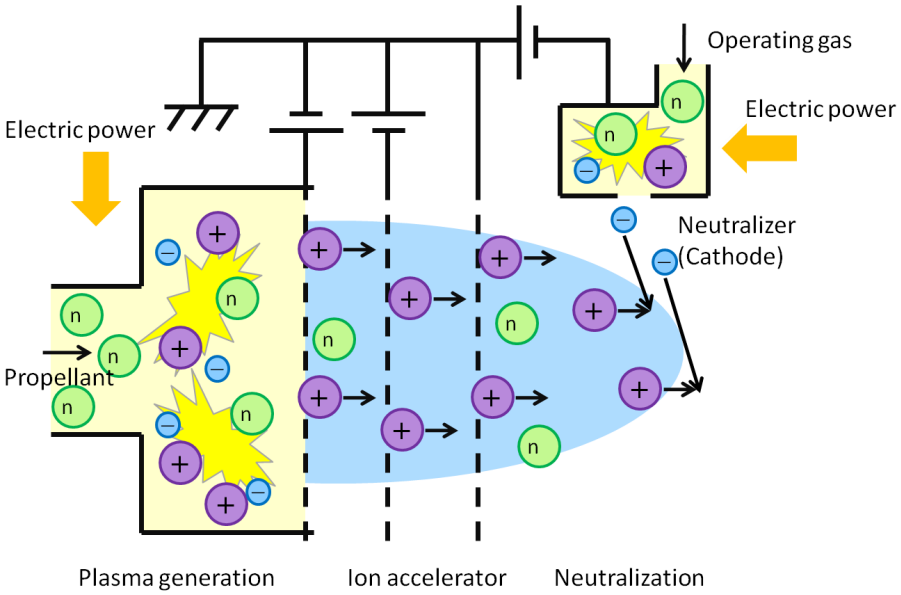

Figure1.1: Schematic diagram of the ion thruster.

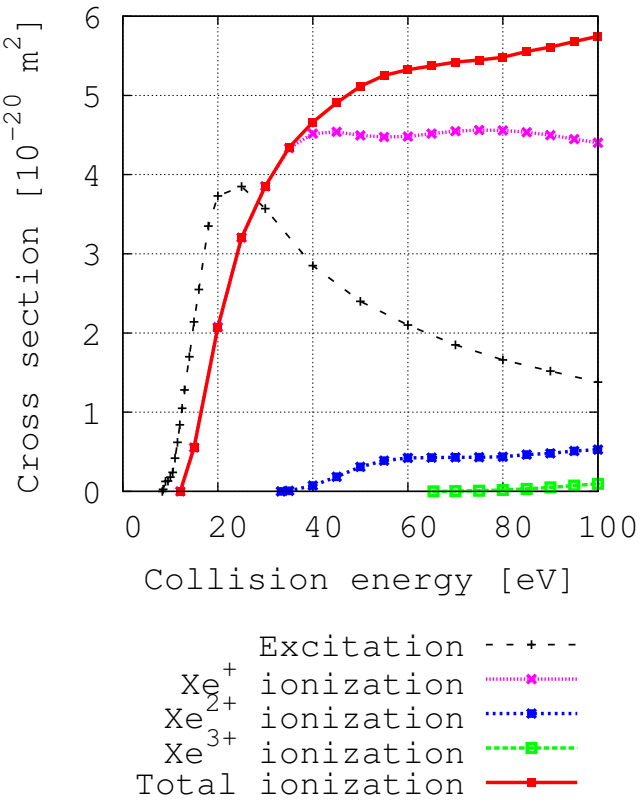

Figure1.2: Cross section of Xe. [1] [2]

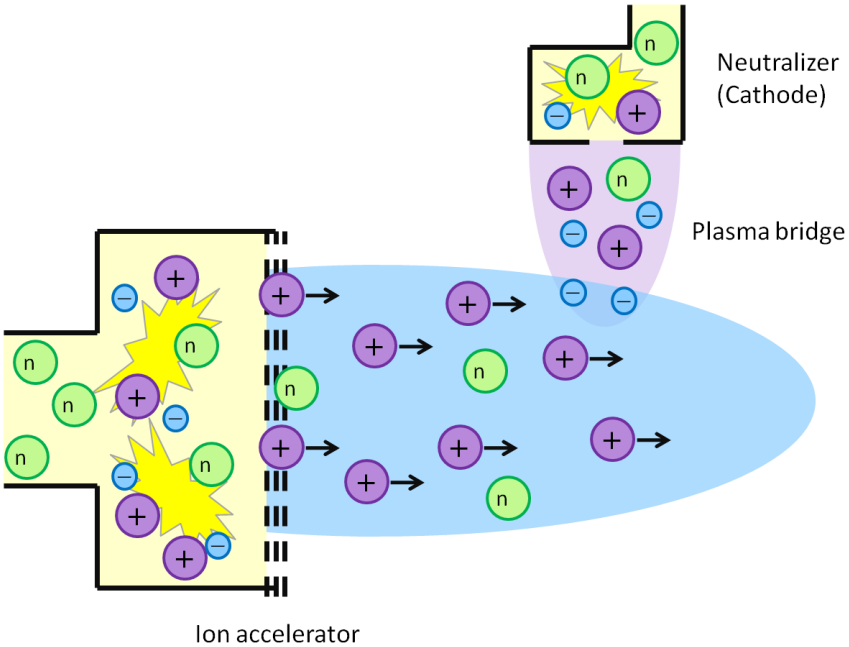

Figure1.3: Schematic diagram of the plasma connection.

1.2 Ion thruster types

As mentioned in 1.1, ion thrusters are classified according to the primary electron generation method. These methods include direct current (DC), radio frequency (RF), and microwave discharge (Microwave). DC ion thrusters, which use hollow cathodes as an ion source and a neutralizer, are the most common type of ion thruster. The most serious problem associated with DC ion thrusters is that the lifetime of the thruster is limited by the lifetime of the hollow cathodes and the lifetime of the grids. In order to eliminate the limit caused by the lifetime of the cathode, RF or Microwave heating are adopted for plasma generation.

1.2.1 DC ion thruster

DC ion thrusters are classified according to the geometry of the magnetic field. Fig.1.4 shows the cusp and Kaufmann type thrusters, which are typical DC ion thrusters. Permanent magnets are placed on the wall in the cusp type ion thruster. The discharge cathode, which is a hollow cathode, is placed in the discharge chamber, and thermionic electrons are generated as the primary electrons. In order to increase the probability of ionization collisions, a magnetic mirror is formed in order to decrease the probability of extinguishing thermionic electrons by collisions with the wall. The magnetic mirror is also used for plasma confinement. The NEXT ion thruster, which has the longest lifetime, is this type of ion thruster. Table 1.1 lists the specification of the NEXT ion thruster [15]. The Kaufman type ion thruster has a divergent magnetic field from upstream to downstream. The primary electrons twist around the magnetic lines and are electrostatically reflected by the grid. The reflected electron is again reflected by the potential of the discharge cathode. This system enables a higher ionization probability.

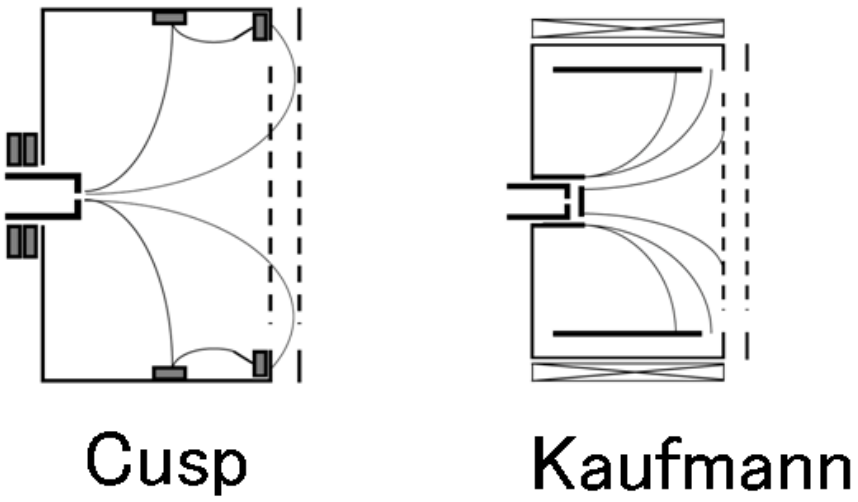

Figure1.4: Schematic diagram of the DC ion thruster.

1.2.2 RF ion thruster

RF thruster consists of a dielectric wall discharge chamber and an induction coil, which is wrapped around the chamber. Applying an alternate current to the coil, the magnetic field is formed in the axial direction. This magnetic field leads to

an inductive electric field. This electric field provides energy to the electrons, which ionize the propellant. This thruster requires a hollow cathode in order to ignite the plasma in the discharge chamber. The plasma is maintained by the thermionic electrons that are generated by ionization. The RIT-10 is a space-qualified RF ion thruster. Table 1.2 shows the specifications of the RIT-10 thruster [16] [17] [18] [19].

1.2.3 Microwave ion thruster

The typical microwave ion thruster is an electron cyclotron resonance (ECR) discharge ion thruster. This thruster generates primary electrons by ECR. An electron in a static, uniform magnetic field will move in a circle due to the Lorentz force. The angular frequency ω_{ce} of this circular motion for a given magnetic field strength B is given by (1.2.1)

$$\omega_{ce} = \frac{qB}{m_i}. \tag{1.2.1}$$

where q is the elementary charge and m_i is the mass of the electron. When ω_{ce} matches the microwave frequency, electrons are continuously accelerated by the microwave electrical oscillations because electrons always feel the accelerating electric field to the velocity direction results in electron acceleration. The electrons that ignite the plasma are the electron that exist in the discharge chamber. The plasma is maintained by the thermionic electrons that are generated by ionization. The μ10 space-qualified thrusters installed on Hayabusa were developed at the Institute of Space and Astronautical Science (ISAS).

1.3 $\mu-$ series microwave ion thrusters

[20] [21] [22] Microwaves provide an alternative method by which to produce plasma without the need for a hollow cathode. Fig.1.5 shows a schematic diagram of a μ10 microwave ion thruster. The ISAS has developed microwave thrusters of various sizes, ranging from the 1-cm class "μ1" to the 20-cm class "μ20". Four μ10 thrusters, labeled A through D were installed in the asteroid explorer spacecraft Hayabusa as a primary propulsion system, as shown in Fig.1.6. Table 1.3 lists the nominal specifications of the μ10 thruster. On the way to the Itokawa asteroid, Hayabusa successfully conducted a swing-by using its ion thrusters. In total, the thrusters operated for 40,000 hours and consumed 45 kg of xenon by the end of the mission [10].

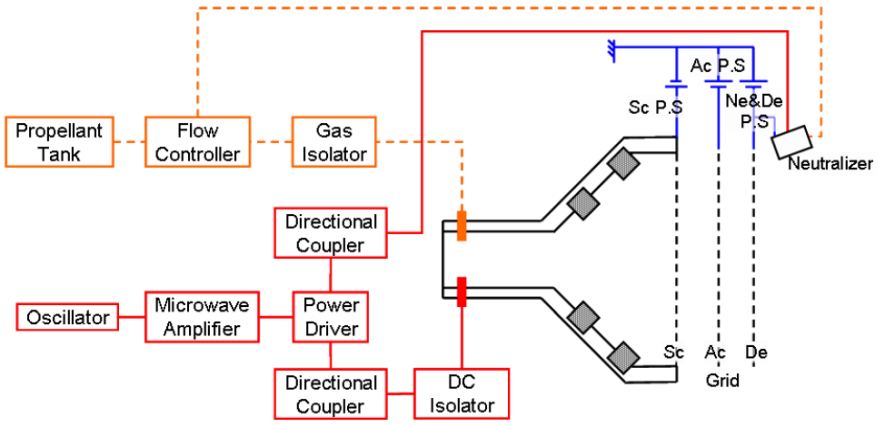

Figure1.5: Schematic diagram of the μ10 microwave ion thruster system.

Table1.1: Specifications of the NEXT ion thruster.

Parameter	
Beam diameter, cm	36
Electric power, W	6,830
Specific impulse, sec	4,160
Thrust, mN	236
Propulsion efficiency, %	70.7
Mass utilization efficiency, %	89
Screen voltage, V	1,800
Beam current, mA	3,540

Table1.2: Specifications of the RIT-10 ion thruster.

Parameter	
Beam diameter, cm	10
Electric power, W	459
Specific impulse, s	3,400
Thrust, mN	15
Propulsion efficiency, %	52
Mass utilization efficiency, %	69.3
Screen voltage, V	1,500
Beam current, mA	234

Table1.3: Specifications of the μ10 microwave ion thruster.

Parameter	
Beam diameter, cm	10
Electric power, W	350
Microwave frequency, GHz	4.25
Specific impulse, sec	3,200
Thrust, mN	8.0
Propulsion efficiency, %	36
Mass utilization efficiency, %	85
Microwave efficiency, %	55
Screen voltage, V	1,500
Beam current, mA	135

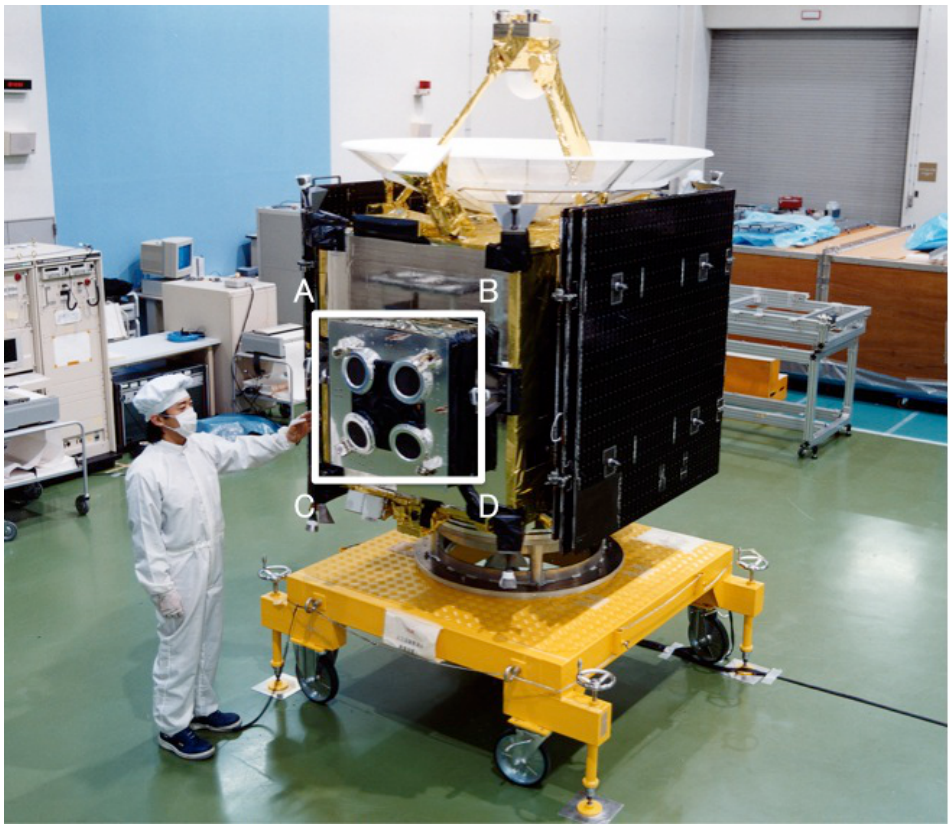

Figure1.6: Four μ10 microwave ion thrusters installed in Hayabusa.

1.4 Neutralizer

Two types of neutralizer are described in this section. One is the typical neutralizer, i.e., a hollow cathode, and the other is the ECR neutralizer, which is primarily discussed herein.

1.4.1 Hollow cathode

A hollow cathode is typically used as the discharge cathode of the DC and RF ion thrusters and is also typically used as an electron source. Fig.1.7 shows a schematic diagram of the hollow cathode. The hollow cathode has an electrode for emitting thermionic electrons inside the discharge chamber, which has an orifice on the downstream side. The electrode, referred to as the insert, which is heated by a heater, emits a thermionic electron current flux J_t A/m^2 determined by the Richardson-Dushman equation:

$$J_t = AT^2 e^{\frac{-q\phi_w}{kT}} \tag{1.4.1}$$

where A is the thermionic emission coefficient, T is the insert temperature in K, and ϕ_w is the work function V of the insert. For the low work function, the common design of the insert, which consists of a porous tungsten matrix impregnated with a mixture of barium oxide [23]. LaB_6 is common used as a material for the insert. This material can achieve an ion current flux of 10 A/cm^2 at 1,800 K. A keeper electrode exists in the downstream side. The thermionic electrons from the insert accelerated by the electric field between the keeper electrode and the discharge chamber ionize the operational gas. Only a heater is needed for ignition. Once the plasma is ignited, the insert maintains the temperature through self-heating, which is achieved by Joule heating by means of the plasma discharge passing through the orifice due to the high internal pressure, and the ion and electron bombardment against the insert surface. Cathodes operate in two characteristic modes, i.e., spot mode and plume mode. The spot mode is characterized by relatively low oscillations in the electron current. As the pgas flow rate is reduced for a given discharge current, the cathode begins to transition to the plume mode, in which the contact voltage and oscillation increase. The spot mode is used in the ion thruster in order to achieve a long lifetime [23].

The hollow cathode can emit a large amount of electrons with low energy and low consumption of the operating gas. Hollow cathodes can have lifetimes exceeding 40,000 hours, but have problems of erosion of the insert, handling in the oxygen atmosphere, and compatibility of operational gases due to the insert material.

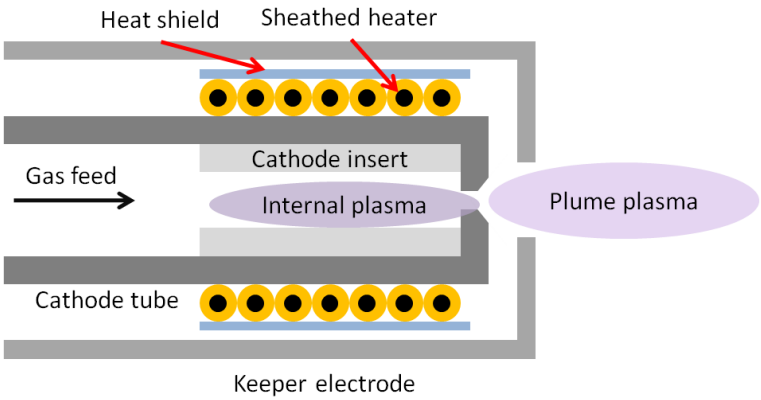

Figure1.7: Schematic diagram of the hollow cathode.

1.4.2 ECR neutralizer

The ECR neutralizer generates plasma by ECR heating, as mentioned in Section 1.2.3. In this method, plasma is generated without a cathode, and electrons are emitted by the applied negative voltage of the neutralizer. Ions are generated at the same rate that the electrons bombard the inside of the neutralizer. Therefore, erosion of the inside of the neutralizer is of concern. However, the ECR neutralizer can permanently supply electrons in the existence of the operational gas because the electrons are supplied by the generated plasma, not the thermionic electrons emitted from the low-work-function material. Thus, ECR neutralizers are space-qualified alternatives to hollow cathodes [10]. Fig.1.8 shows a μ10 prototype model neutralizer, which consists of magnets, magnetic circuits, a discharge chamber, an antenna, and an orifice. Table 1.4 lists the surface area which contact to the plasma. Microwaves are transmitted from the antenna to the discharge chamber at a frequency of 4.25 *GHz*. A magnetic circuit generates an azimuthal mirror-like magnetic field, within which a region with a field strength of 0.15 T gives rise to ECR. Xenon operating gas is injected into the discharge chamber, where electrons are continuously accelerated by the microwave electrical oscillations and are trapped by the mirror magnetic field due to the ECR. As a result of the electron-neutral collisions, an ECR plasma is formed. During ECR heating, high-energy electrons exhibit three types of motion: Larmor motion around the magnetic field lines, reciprocating motion between the magnetic mirrors, and azimuthal motion due to the curvature and gradient B drifts. The ECR neutralizer generates a plasma, from which electrons are emitted into the ion beam by the negative applied voltage. Thus, if the neutralizer cannot emit the amount of electrons required for a certain applied voltage, the negative applied voltage will be increased. This is why degradation of the neutralizer occurs as the contact voltage between the neutralizer and the plasma increases. Ions, which are generated at the same rate at which the electrons are ejected, bombard the interior of the neutralizer so as to complete the electrical circuit. These ions are reused as an operational gas after bombardment and recombination. However, thermionic electrons are not dominant in the ECR neutralizer. Ion bombardment in the interior arises from sputtering.

Table 1.5 lists the nominal specifications of the μ10 neutralizer. The operational range is 85 to 135 *mA* for the electron emission current. Degradation of the neutralizer produces an increase in the contact voltage between the neutralizer and the plasma. The neutralizers onboard Hayabusa stopped working due to the excess contact voltage above the capacity of the power sources after 10,000 hours of space operation [24]. The neutralizer is also installed on the Dubai-sat 2 for cathode of Hall Effect Thruster as a primary propulsion [25]. DubaiSat-2 is an electro-optical Earth observation satellite built by the Emirates Institution for Advanced Science and Technology under an agreement with Satrec Initiative, a satellite manufacturing company in South Korea. It was launched in 21th November 2013, and the mission duration is 5 years. The neutralizer was provided by ISAS/JAXA. This neutralizer emits 500 *mA* with in 1.2 *sccm* operational gas flow rate.

Table1.4: Surface area of the neutralizer.

Name	Surface area mm^2
Antenna	70
Upstream magnetic circuit	400
Side wall	600
Downstream magnetic circuit	300
Orifice plate	300

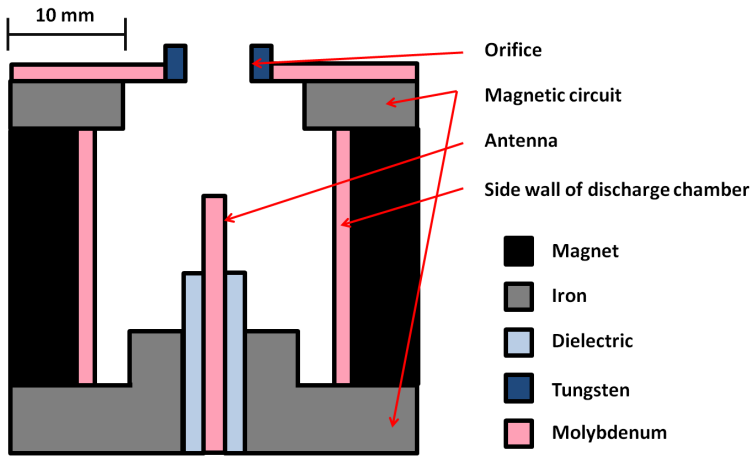

Figure1.8: Schematic diagram of the μ10 prototype model neutralizer.

1.5 Comparison of the hollow cathode and the ECR neutralizer

Table 1.6, Fig.1.9, and Fig.1.10, Fig.1.11, and Fig.1.12 shows the parameters of the neutralizers of the ion thruster [3] [26] [27]. The neutralization cost and gas utilization efficiency are given as follows:

$$C_{cHC} = \frac{I_k V_k + I_e V_c}{I_e} \tag{1.5.1}$$

or

$$C_{cECR} = \frac{P + I_e V_c}{I_e} \tag{1.5.2}$$

$$\eta_g = \frac{I_e}{\dot{m}} \tag{1.5.3}$$

where C_{cHC} is the neutralization cost W/A of the hollow cathode, I_k is the keeper current A, V_k is the keeper voltage V, I_e is the electron emission current A, V_c is the contact voltage V, C_{cECR} is the neutralization cost W/A of the ECR neutralizer, P is the input microwave power W, eta_g is the gas utilization efficiency, and $\dot{m}$ is the neutralizer flow rate Aeq. Although, the electron current of the ECR neutralizer is significantly lower than that of the hollow cathode, the neutralization costs are equivalent. The gas utilization efficiency of the ECR neutralizer is lower than that of the hollow cathode because, in the ECR neutralizer, thermionic electrons do not contribute to the electron emission, i.e., it can be operated without thermionic electron emission material so that it is released from the problems due to it as mentioned in 1.4.2. Thus, the gas utilization efficiency is sacrificed for robustness.

Table1.5: Specifications of the μ10 neutralizer.

Parameter	μ10 neutralizer
Microwave frequency, GHz	4.25
Xenon flow rate, sccm, μg/s	0.5, 0.49
Electron emission current, mA	135 at 8 mN
Contact voltage between neutralizer and beam plasma, V	22

Table1.6: Parameters of the ion thruster neutralizer.

Ion thruster	NSTAR	NEXT	μ10	μ20
Electron current, A	1.76	3.84	0.135	0.5
Contact voltage, V	13.4	10.25	22	40
Neutralization cost, W/A	25	70	81	72
Gas utilization efficiency	8.2	12.2	3.8	5.8
(Thrust force of ion source, mN)	92	237	8	30

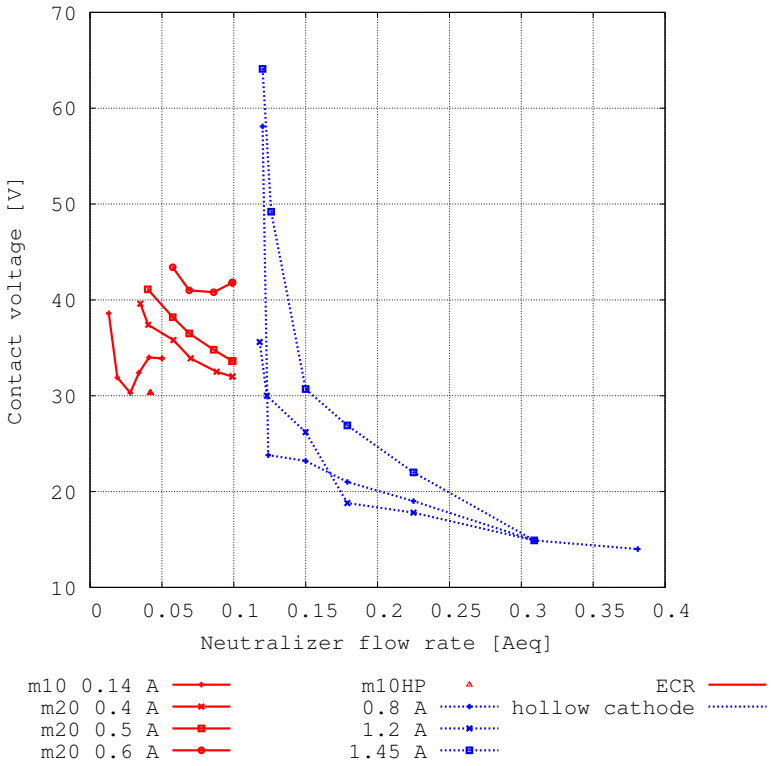

Figure1.9: Contact voltage v.s. flow rate of ECR neutralizers and hollow cathodes. [3]

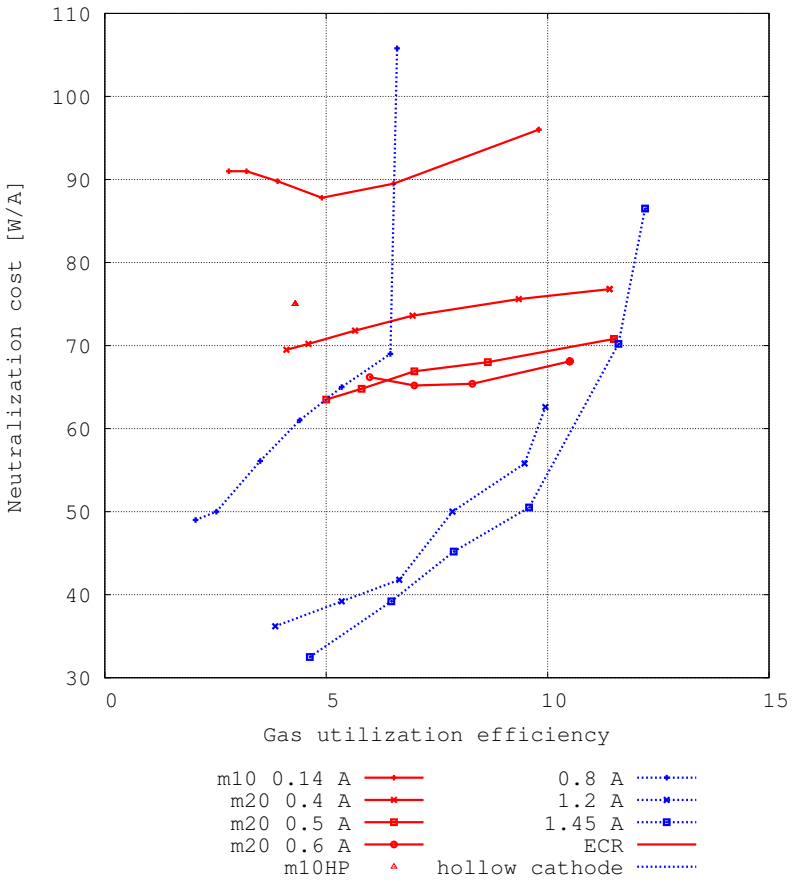

Figure1.10: Neutralization cost v.s. gas utilization efficiency of ECR neutralizers and hollow cathodes. [3]

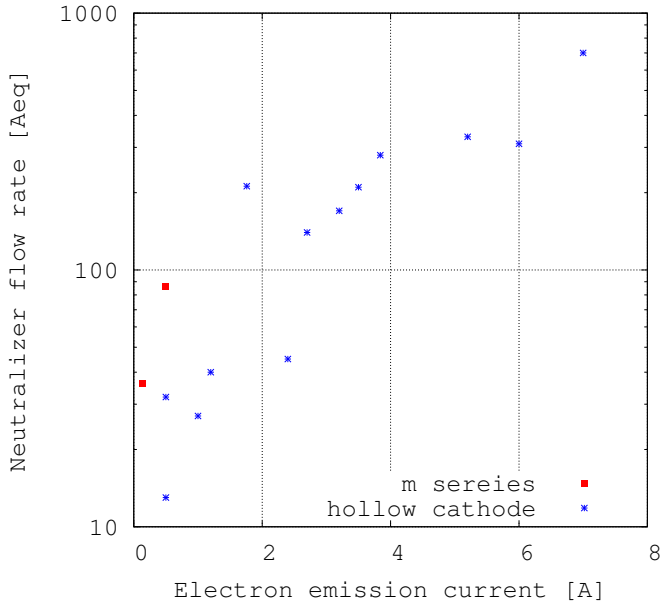

Figure1.11: Flow rate v.s. emission current of ECR neutralizers and hollow cathodes. [3]

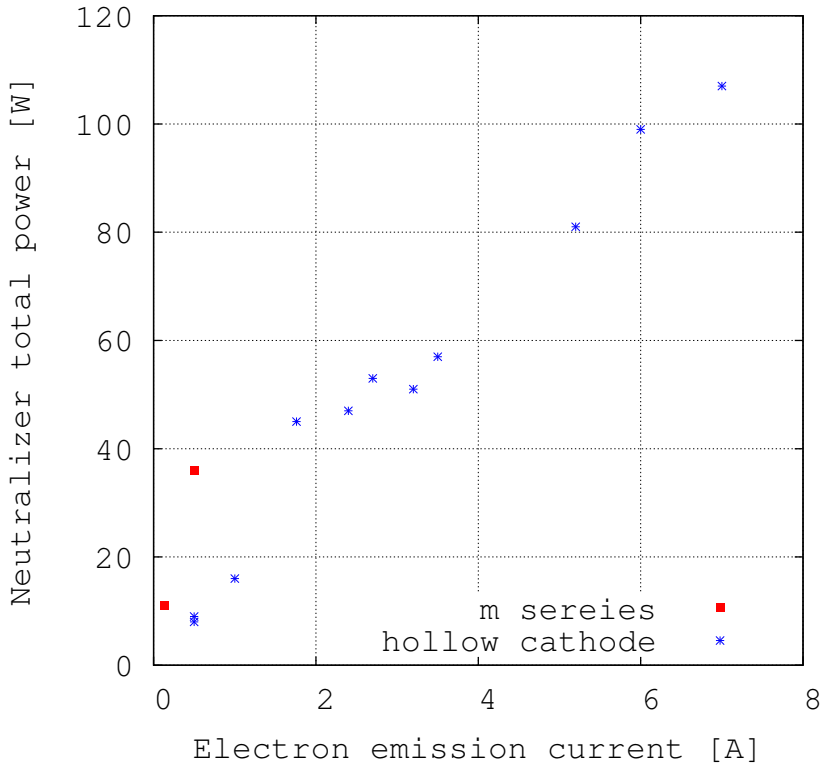

Figure1.12: Neutralizer power v.s. emission current of ECR neutralizers and hollow cathodes. [3]

Neutralization cost

In this section, the maximum theoretical performance of the neutralization cost of ECR neutralizer is explained as the following:

$$C_n = \frac{P_\mu}{I_n} \tag{1.5.4}$$

where C_n is neutralization cost W/A, P_μ is microwave input power W, and I_n is electron emission current A. Define the plasma ion production cost as

$$C_p = \frac{I_F V_\mu}{I_p} \tag{1.5.5}$$

where C_p is plasma ion production cost W/A, I_F is primary electron current A, V_μ is accelerated voltage of the primary electron V, and I_p is produced ion current A. It is known that 60 % of microwave power contributes to accelerate the primary electron [28]. Assuming of the produced ion current produce the electron emission current, $I_p = I_n$. C_p is also written as the following:

$$C_p = \frac{\varepsilon_p^*}{1 - exp(-\sigma nL)} \tag{1.5.6}$$

where ε_p^* is baseline plasma ion energy cost eV which is the theoretical minimum energy to produce an ion, σ is the summary of the cross section of ionization and excitation m^2, n is the plasma density $1/m^3$, and L as the mean free path m to be accelerated to 30 eV in ECR area while doing a round trip between magnetic mirror. ε_p^* is 40 eV [29], σ is $7 \cdot 10^{-20}$ m^2, and n is 10^{20} $1/m^3$, L is much more than 0.5 m. This results in C_n is approximately 66 W/A.

1.6 Previous research on ECR neutralizers and position of this study

The ECR neutralizer is new application of the technology of plasma cathode which was used for plasma ignition. In our laboratory, the ECR neutralizer was developed alongside the ECR ion source [30] [31] [32]. This is the current $\mu 10$ system. The goal of the present research was to realize a microwave discharge ion thruster. The motivation for the present research is, as mentioned in Section 1.4.2, this ion thruster is cathodeless and so does not have the problems of handling difficulty in an oxygen atmosphere, propellant compatibility due to the insert material, and poor response speed of ignition due to heating. The first microwave discharge ion thruster developed in our laboratory was the YOSHINO-I, a resonant cavity microwave discharge type ion thruster. Microwaves are injected from a standing wave in the cavity, and electrons are accelerated in a short time. The ion production cost of this ion thruster exceeds 3,000 eV/ion and the propellant utilization efficiency is less than 40%. Because of these performances, the other plasma generating method was concerned, using the heritage of microwave heating technology. This was the ECR heating. As shown in Fig.1.13 and Fig.1.14, two types of ECR heating, i.e., the waveguide type and the axisymmetric type, which are classified according to the shape of the discharge chamber, were developed. By adopting ECR heating in the newly developed thruster, YOSHINO-III had an ion production cost of less than 1,000 eV/ion and a propellant utilization efficiency of more than 40%. From the positive prospect of ECR discharge ion thruster, the ECR neutralizer was developed along with the ECR ion source because of the advantage of the simple structure of the ion thruster system provided by the compatibility of the ECR ion source and the power source. The waveguide type plasma generator was developed into the $\mu 10$ ion thruster ion source, and the axisymmetric type was developed into the $\mu 10$ ion thruster neutralizer.

The ECR neutralizer was developed with the objective of emitting sufficient electrons to the ion source. In order to efficiently emit electrons, a sufficient charge complement is needed. In the conventional hollow cathode, this is handled by thermo-electrons. In the ECR neutralizer, Onodera et al. revealed that 95% of the charge is complemented by the neutralization of singly charged ions through collisions with the wall. The secondary electrons, which were generated by singly charged ion collisions, complement the several percent of the charge, which can be improved to 10% by using a low-work-function material for the wall [33]. Onodera et al. also clarified the ECR neutralizer plasma parameters. Table 1.7 lists the parameters for each area shown in Fig.1.15. In this experiment, the space potential, electron temperature, and number density of plasma were measured by single probe, number density of metastable Xe I was measured by 823 nm laser absorption spectrometry, and the ratio of number density between singly ionized and doubly ionized xenon was measured by quadrupole mass spectrometer outside the neutralizer.

These studies indicate that the ECR neutralizer has sufficient ability to emit electrons. In order to enhance the lifetime of the ion thruster system, the ECR ion source configuration, e.g., the grid configuration [34], has been investigated. However, the lifetime is limited by the lifetime of the ECR neutralizer, as mentioned in Section 1.3. This is the first study that focuses on improving the lifetime of the ECR neutralizer.

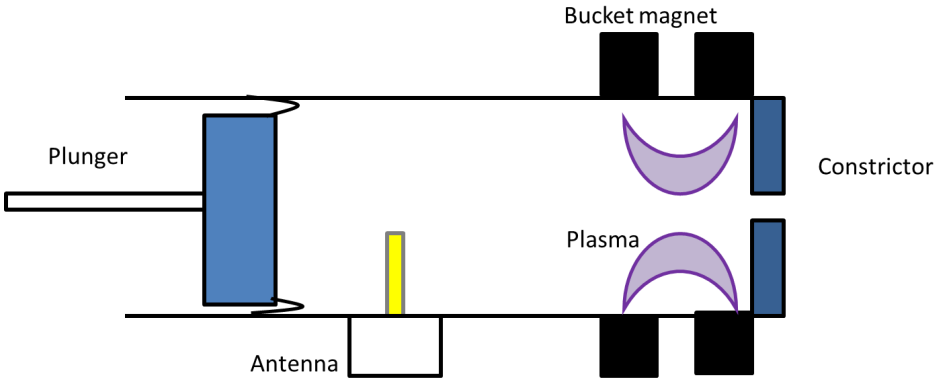

Figure1.13: Schematic diagram of the waveguide type ECR heating plasma generator.

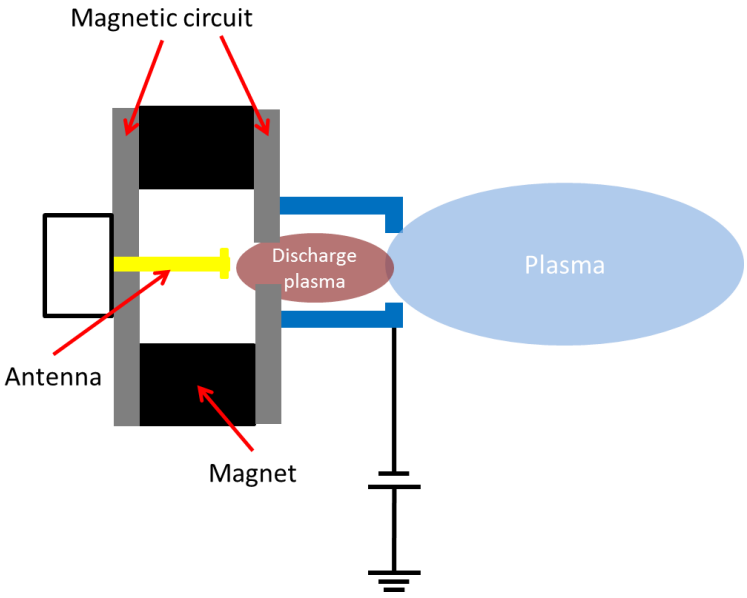

Figure1.14: Schematic diagram of the axisymmetric type ECR heating plasma generator.

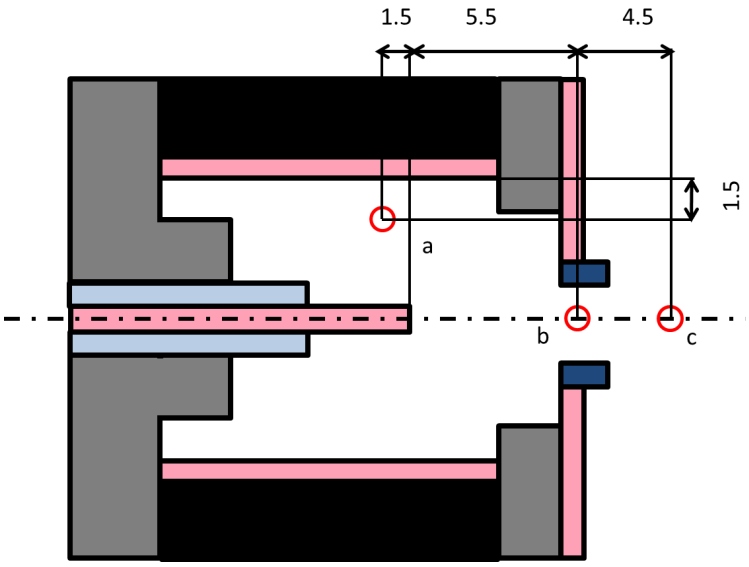

Figure1.15: Schematic diagram of the neutralizer and measured position of the plasma parameter.

Table1.7: Plasma parameters of the neutralizer.

Positon	Space potential V	Electron temperature eV	Gas/ion temperature K	Xe^{+} number density $\times 10^{17} m^{-3}$	Xe^{2+} number density $\times 10^{15} m^{-3}$	Xe^{m} number density $\times 10^{17} m^{-3}$
Inside discharge chamber (a)	19.5	2.35	350	6.25	-	1.30
Inside orifice (b)	21.3	3.21	350	8.66	-	1.31
Outside neutralizer (c)	20.1	3.57	350	1.38	0.293	0.927

1.7 Outline of the present study

1.7.1 Objective of the present study

The objectives of the present study are to clarify the mechanism of performance degradation of the neutralizer and to find out the methods to extend the lifetime of neutralizer for the next generation μ10 thrusters. In order to realize these objectives we

- assume and verify the degradation mechanism of the neutralizer, and
- propose a novel neutralizer and demonstrate its performance by means of a long-term experiment.

1.7.2 Progression of the present study

The present study was conducted as follows.

1. A neutralizer that had been subjected to a 20,000-hour endurance test, for which degradation had already occurred, was investigated.
2. The degradation mechanism was assumed.
3. The degradation mechanism was verified experimentally.
4. Novel neutralizers that use lifetime-extending countermeasures were investigated and proposed.
5. The proposed neutralizers were evaluated through a long-term experiment.

1.7.3 Contents of the present study

The contents of the present study are as follows.

Chapter 1. Introduction

The objectives and contents of the present study are introduced. The ion thruster and the ECR neutralizer criteria are also introduced.

Chapter 2. Hypothetical degradation mechanism

The degradation of neutralizers is explained, and the degradation mechanism is assumed.

Chapter 3. Experimental facilities and errors

Introduces the experimental facilities and errors.

Chapter 4. Verification of the degradation mechanism

The degradation mechanism is verified through experiments, and two countermeasures for endurance enhancement are proposed.

Chapter 5. Experimental investigation

The countermeasures for endurance enhancement are proposed and discussed.

Chapter 6. Lifetime enhancement

The lifetime enhancement of the neutralizer is described.

Chapter 7. Conclusion

The present study is summarized.

2 Hypothetical degradation mechanism

In this chapter, the performance transition and degradation mechanism of the μ10 neutralizers will be explained.

2.1 Performance degradation of the Hayabusa onboard neutralizers

Fig.2.1, Fig.2.2, and Fig.2.3 show the performance transition of the three Hayabusa onboard neutralizers [35]. The neutralizer is expected to sustain 18,000-hour on ground test, but onboard neutralizers didin't sustain the performance for that hours [36]. For neutralizer B, the emission current rapidly decreased three times, at 6,000 hours, 7,000 hours, and 9,000 hours of operation. The first and second times, the contact voltage also decreased with the decrease in the emission current. These indicate decreases occurred when the ion thruster was throttled due to mission requirements. However, the third time, the contact voltage increased despite the decrease in the emission current. After 9,000 hours, the contact voltage could not be suppressed by emitting fewer electrons. Finally, at 10,000 hours, neutralizer B ceased to function because the contact voltage exceeded the capacity of the power sources. Neutralizer D also ceased to function after 15,000 hours of operation and experienced six decreases in the emission current at 5,000, 6,000, 7,700, 8,500, 10,500, and 14,500 hours of operation, the first five decreases were due to mission requirements. Neutralizer C continued to function throughout the Hayabusa mission, although its performance did decrease. After 11,000 hours of operation, the neutralizer could no longer emit electrons at a constant contact voltage. The performance of the neutralizer had been got worse in several hundreds hour despite performing at a constant level for thousands of hours.

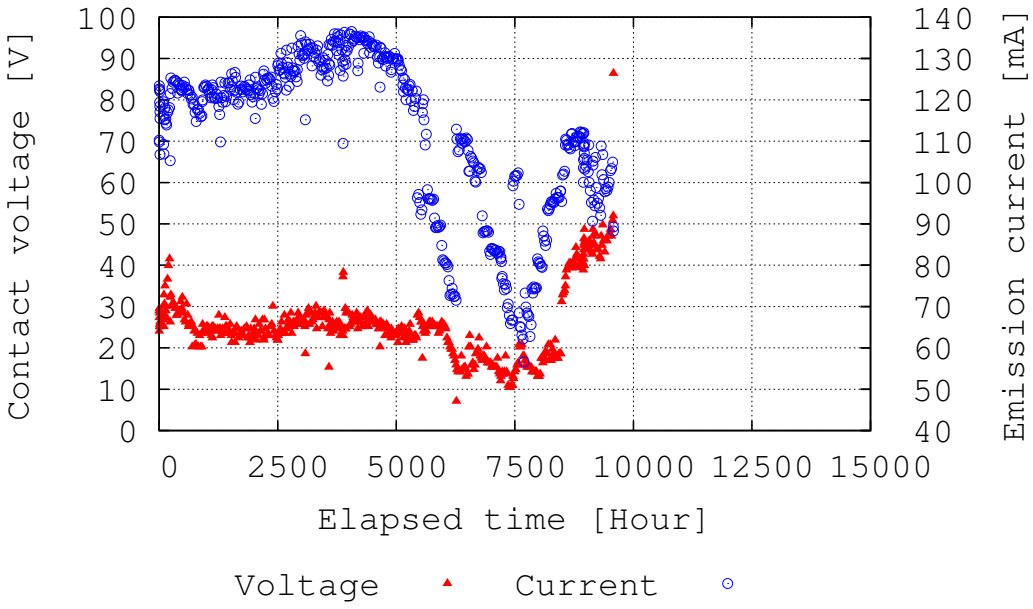

Figure2.1: Performance transition of Hayabusa onboard neutralizer B.

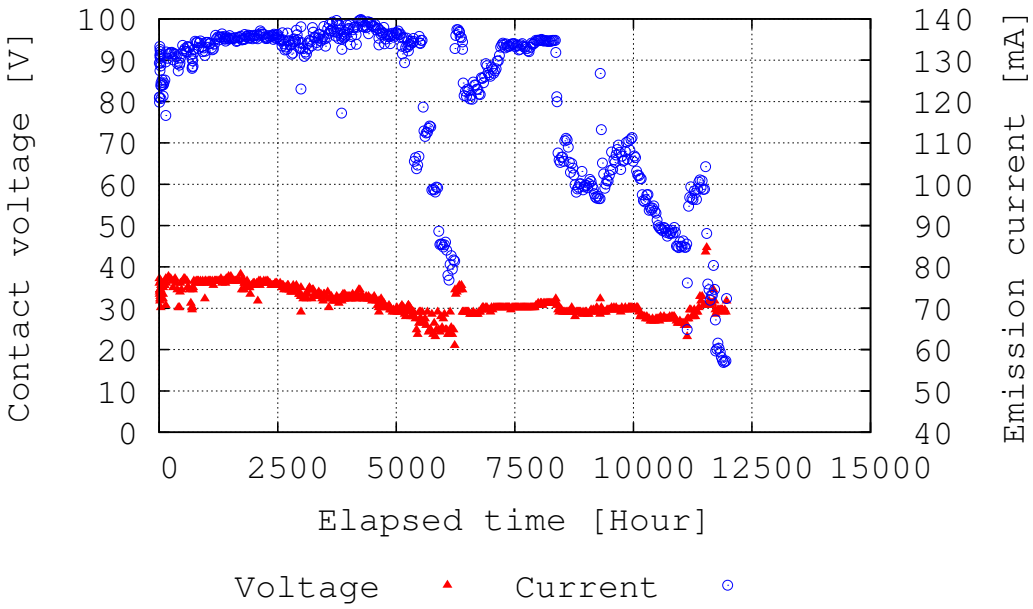

Figure2.2: Performance transition of Hayabusa onboard neutralizer C.

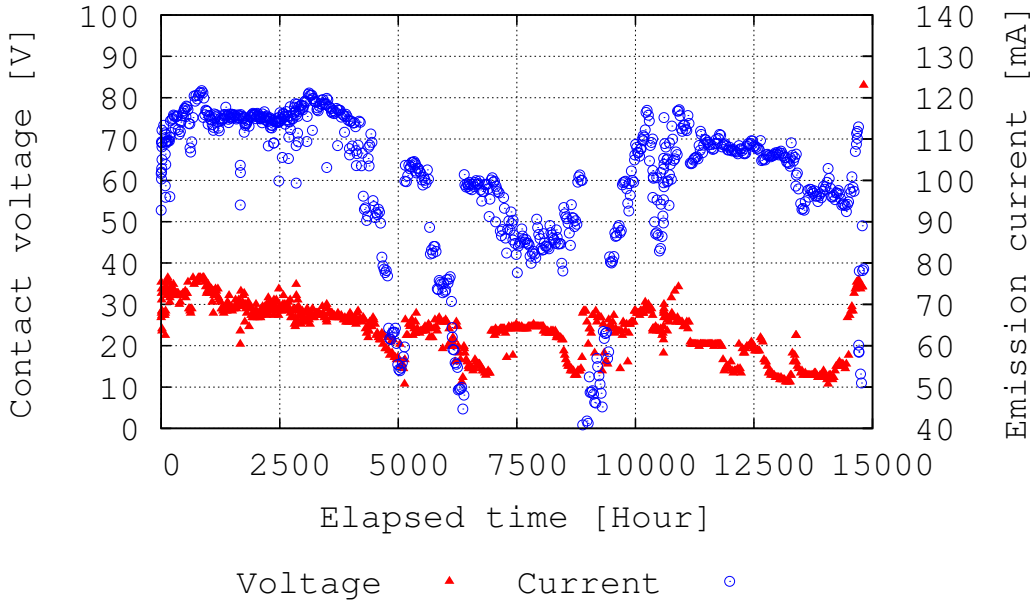

Figure2.3: Performance transition of Hayabusa onboard neutralizer D.

2.1.1 Performance degradation of the endurance test neutralizer

The prototype model neutralizer was subjected to a 20,000-hour endurance test. The experimental facility is described in Section 3.3. During the final 2,000 hours of the 20,000-hour test, the performance of the μ10 prototype model neutralizer decreased abruptly and became exponentially worse for each 20-V increase in the contact voltage, as shown in Fig.2.4. Simultaneously, the reflected microwave power increased tenfold. In this endurance test, the test was suspended 81 times. This indicates there were 81 thermal cycles.

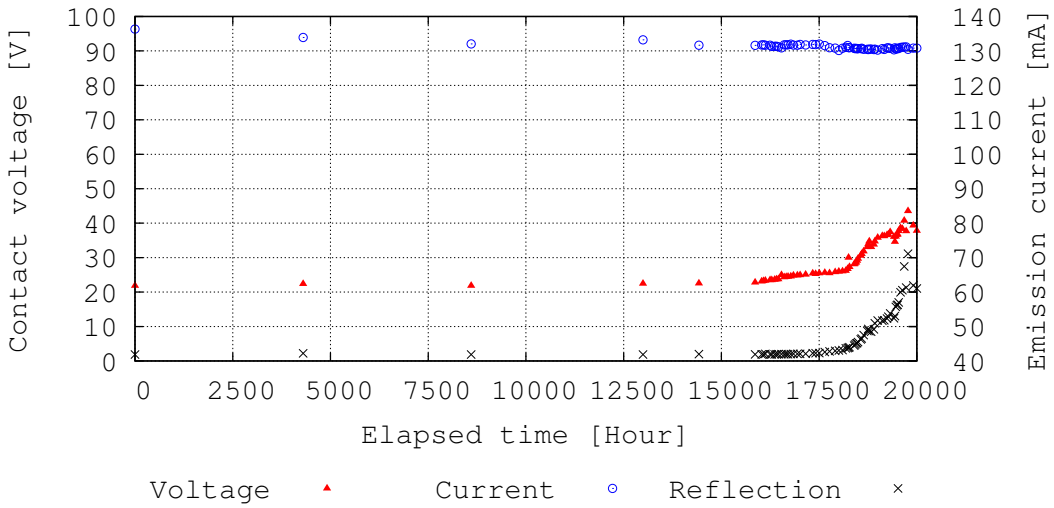

Figure2.4: Performance transition during the endurance test of the Hayabusa prototype model neutralizer. The microwave reflection power is in arbitrary units. It is less than 1 W in maximum.

2.2 Inspection of the prototype model neutralizer

Fig.1.8 shows the prototype model neutralizer. The antenna, the side wall of the discharge chamber, and the orifice plate are made of molybdenum. The magnetic circuit is created of iron. The antenna is protected by ceramic. The orifice is made of thoriated tungsten in order to increase the emission current by a low work function. The composition of the neutralizer parts, which were exposed to plasma, were as follows:

- Iron, nickel coat: $Fe, C(0.03\%), Si(0.04\%), Mn(0.06\%), P(0.03\%), S(0.003\%), Ni$
- Ceramic: $SiO_2(46\%), MgO(17\%), Al_2O_5(16\%), K_2O(10\%)$
- Molybdenum alloy 363: $Mo, Ti(0.5\%), Zr(0.1\%)$
- Thoriated tungsten: W, Th
- Silver alloy blazing: $Ag, Cu, Zn, (Cd, Sn, Ni, Mn)$

Internal inspection of the $\mu 10$ prototype model neutralizer after the 20,000-hour endurance test revealed the following. Numerous metal flakes were attached to the tips of the magnetic circuits, and the dielectric part of the microwave antenna was contaminated with metal. However, the antenna, the orifice, and the internal surfaces were not seriously worn. The metal flakes were magnetically attached, which indicate that the flakes were ferromagnetic. Most of the flakes were approximately 1 *mm* square, and none exceeded 4 *mm* square. The thickness of the flakes was ten and several micrometers. The summary volume of all flakes is several mm^3. Compositional analysis by a scanning electron microscopy and X-ray energy dispersion DX-4 system, the specifications of which are shown in Table 2.1, revealed that the contamination on the surface of the dielectric was 30% tungsten, 30% iron, and 10% molybdenum. The metal flakes were found to be composed of 35% iron, 30% molybdenum, and 15% nickel.

Table2.1: Specifications of the scanning electron microscopy and X-ray energy dispersion facility.

Company	Philips
Model	DX-4
Sensitivity	Na(11)-U(92)

2.3 Assumed degradation mechanism

Fig.2.5 and Fig.2.6 list the candidates for the degradation mechanism of the μ10 neutralizer. The green symbols indicate physical causes of degradation. The red symbols indicate observational evidence. The blue symbols indicate implied phenomena. The ovals indicate fundamental causes. Fig.2.5 shows the degradation mechanism in sequential form, and Fig.2.6 shows the degradation mechanism as a fault tree. Low-probability events have been omitted. The assumed performance degradation mechanism were as follows.

The performance degradation was triggered by doubly ionized xenon ions bombarding the magnetic circuit. First, surface materials are sputtered by doubly ionized xenon ions and accumulate on other surfaces, subsequently forming thin films of iron, molybdenum, and tungsten. Second, thermal cycling results in peeling off of thin films due to the different thermal expansivities of the films and the base plates. Third, thin films containing iron, i.e., ferromagnetic flakes, are magnetically attracted to the tips of the magnetic circuit. The metal flakes observed on the tips of the magnetic circuit may obstruct high-energy electrons and extinguish the generated plasma. The metal flakes also contaminate the surface of the dielectric, which had been cleaned by the generated plasma. This contamination reduces microwave transmission and decreases plasma production.

A decrease in plasma production is also associated with a decrease in magnetic performance. This is caused by a distortion of the magnetic field caused by the attached flakes and a reduction in the magnetic field caused by a transformation of the magnetic circuit due to sputtering [37].

Basic cause of the degradation

The basic cause of the decrease in plasma production is thought to be sputtering by doubly ionized xenon ions. The primary reason for this thinking is that the degradation requires a 10,000-hour time span because there are only 0.2% which is shown by Table 1.7. The secondary reason for this is that doubly ionized xenon ions can acquire sufficient energy to cause sputtering, even at the low contact voltage of the neutralizer [33] [38]. Fig.2.7 shows the sputtering yield using Yamamura model [38] against 1 C current from the plasma which is concerning number ratio of singly and doubly ionized xenon.

Peeling mechanism

Peeling occurs when film strain energy exceeds the attachment energy [39] [40]. The strain energy U_s is given by

$$U_s = \frac{E_f}{1-\nu_f}(\Delta\alpha\Delta T)^2 d \tag{2.3.1}$$

where E_f and ν_f are the Young's modulus and Poisson's ratio, respectively, of the film, $\Delta\alpha$ is the difference in the coefficient of linear expansion between the film and the base material, ΔT is the difference between the maximum and the minimum temperature, and d is the film thickness. The attachment energy of the metal is approximately 2 J/m^2 [39]. In the present case, E_f is 200 GPa, ν_f is 0.3, $\Delta\alpha$, $12.1-4.8\times10^{-6}1/K$, and ΔT is 100 K, U_s is 2 when d is 13 μm. In other words, peeling occures when the film thickness is approximately 13 μm, which corresponds to the flake thickness being ten and several micrometers, as mentioned in Section 2.2. The difference between maximum and minimum temperature is larger in the Hayabusa mission which is held in space than the endurance test which is held on ground. The problem that the lifetime of the neutralizers onboard Hayabusa were shorter than the prototype model neutralizer is also explained in this peeling mechanism.

Surface cleaning by the generated plasma

Under the usual condition, ions from the plasma bombard the entire surface of the neutralizer. This ion bombardment harms the surface but it also helps clean the surface, preventing the accumulation of contaminants. If the rate of contamination accumulation exceeds the rate of cleaning, the contamination becomes more serious.

The ion bombardment also helps to inhibit the flake forming. The flakes only formed at the low ion bombardment area results in the accumulating and vanishing repetition, i.e, the thin film which can become the flakes formed at high ion bombardment area vanished and they accumulated on the surfaces, while the thin film formed at low ion bombardment not vanished. The flakes which were attracted to the tips of the magnetic circuit are the latter films.

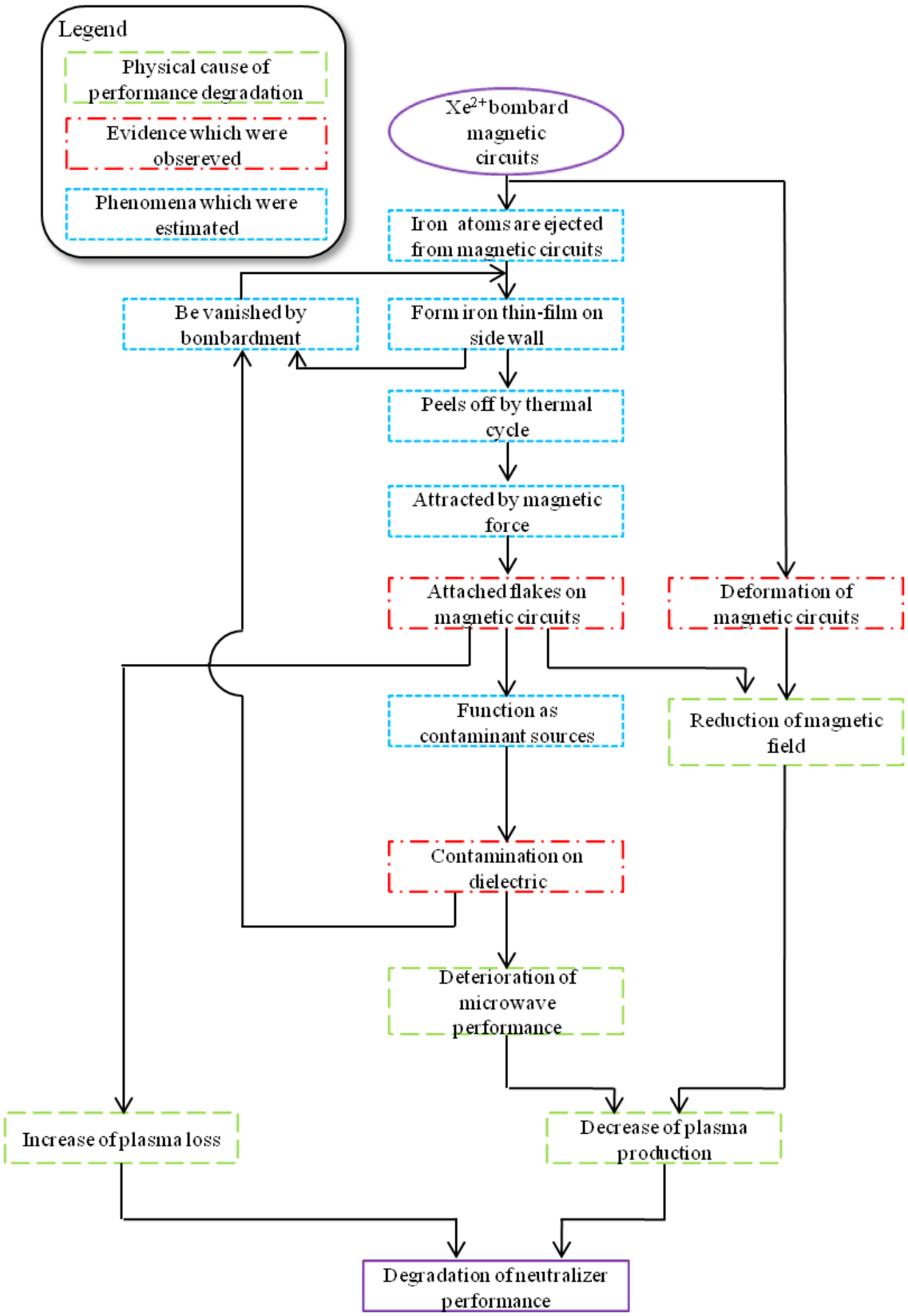

Figure2.5: Assumed degradation mechanism. Sequential form.

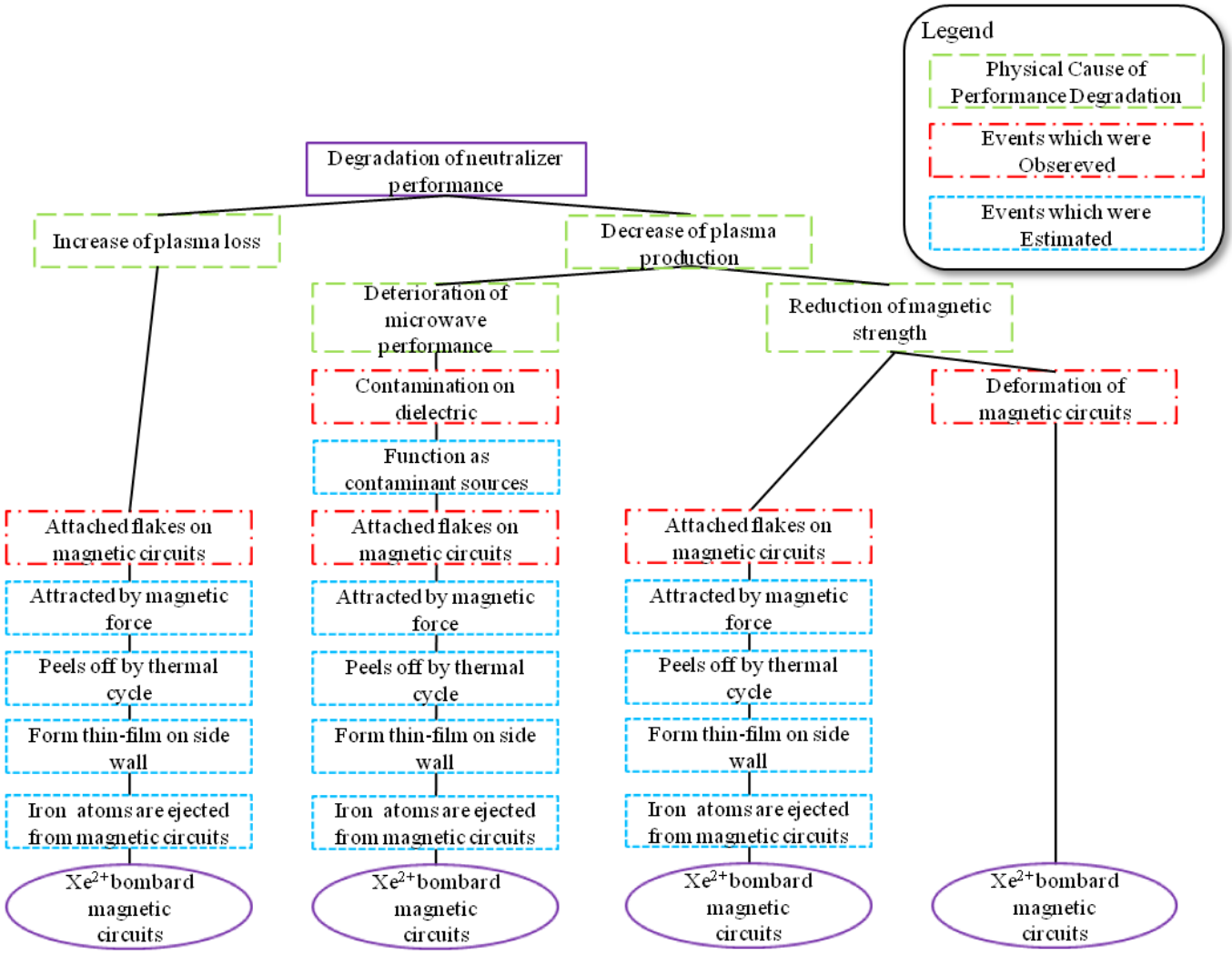

Figure2.6: Assumed degradation mechanism. Fault tree analysis form.

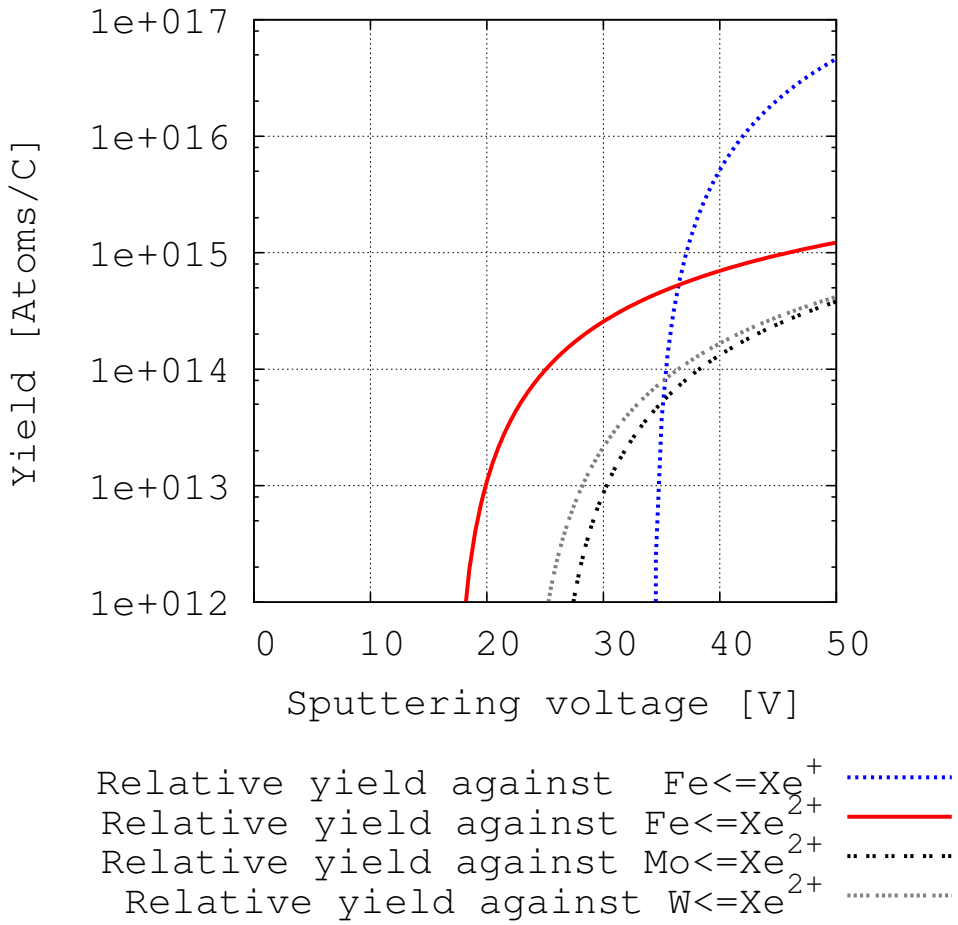

Figure2.7: Sputtering yield from inner plasma of neutralizer.

3 Experimental facilities and errors

In order to verify the degradation mechanism and evaluate countermeasures applied to the neutralizers, operation of neutralizers are conducted. For instance, prototype model neutralizer, newly constructed neutralizers, et. al. In this section, the neutralizer operating facilities are explained.

3.1 Experimental used neutralizers

In this section, the neutralizers which were used in this study are introduced. The specification and the criteria are already mentioned in Section 1.4.2. All the neutralizers have the same structure, but some assemblies are changed, i.e., stronger magnet, different material, molybdenum-covered.

Prototype model neutralizer

This neutralizer is mainly used in 20,000-hour endurance test. The details are mentioned in Section 1.4.2.

Experimental neutralizer

Fig.3.1 shows the experimental neutralizers used in the present study. The neutralizer was designed to be inexpensive and easy to use. The orifice plate and the antenna material are changed for usefulness.

Net ion current distribution measurement neutralizer

This neutralizer has the same structure as the experimental neutralizer, but all assemblies are isolated from each other. This neutralizer is mainly used in chapter 6 experiments. The details are mentioned in Section 5.1.1.

Lower-contact-voltage neutralizer

This neutralizer has the same structure as the prototype model neutralizer, but using x1.15 stronger magnet. This neutralizer is mainly used in Section 6.2.2.

Molybdenum-covered neutralizers

These neutralizers have two different models. These neutralizers are mainly used in Section 6.3. The details are mentioned in Section 6.3.

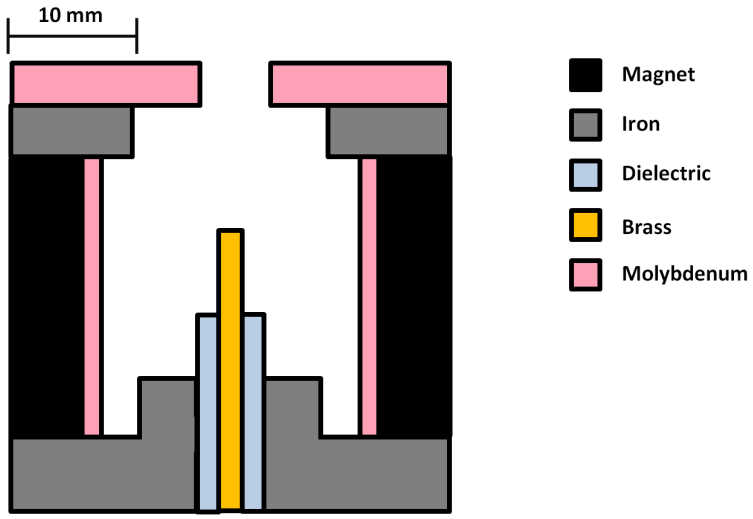

Figure3.1: Schematic diagram of the μ10 experimental neutralizer

3.2 Neutralizer operating system

Fig.3.2 and Fig.3.3 show a schematic diagram and a photograph, respectively, of the operating system of the neutralizer in diode mode. The neutralizer is evacuated by a turbo molecular pump to 3 *mPa*. Table 3.1 lists the specifications of the chamber. The length of the matching circuit is adjusted in order to minimize the reflected power at a nominal electron emission current of 135 *mA*. The input microwave power is measured at the entrance of the matching circuit. The loss between the neutralizer and the matching circuit is approximately -0.2 *dB*. In the present experiments, the electron emission current is between 60 and 150 *mA*. The contact voltage is the potential difference between the anode and the neutralizer in diode mode, for which electrons emitted by the neutralizer are collected by the anode is located 1.1 cm from the exit of the neutralizer orifice. The following experiments were conducted under nominal conditions, with an input microwave power of 8 *W* and a xenon flow rate of 0.5 *sccm*, unless stated otherwise.

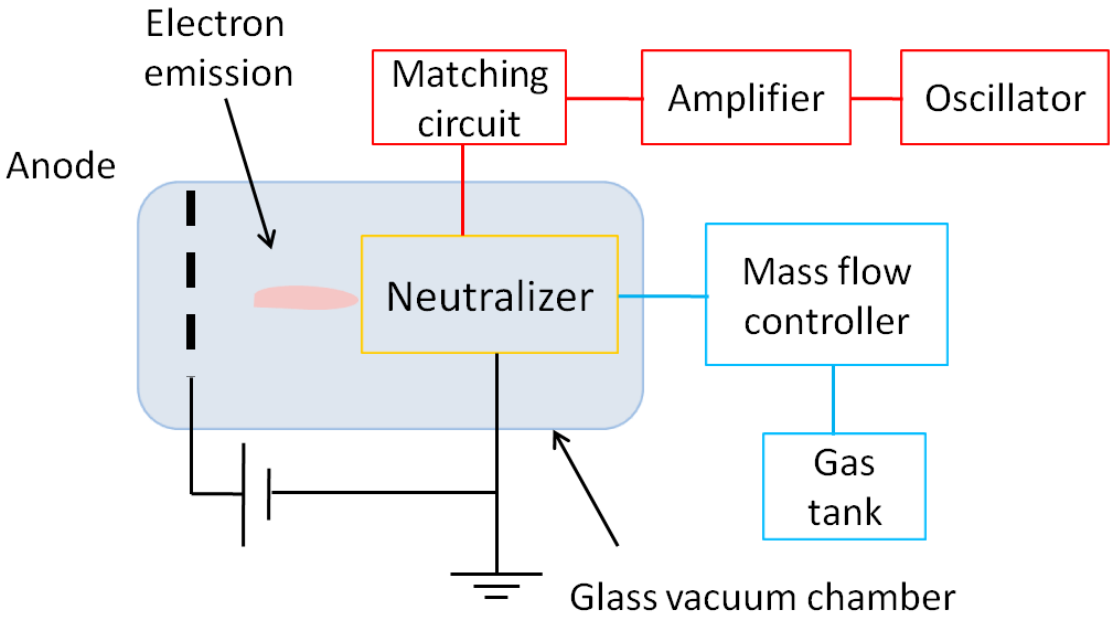

Figure3.2: Schematic diagram of the neutralizer performance measurement system.

Table3.1: Specifications of the vacuum chamber of the neutralizer performance measurement system.

Specification	Number
Glass cross chamber $\phi 15cm \times 30cm \times 4$	1
Turbomolecular pump (750 l/s)	1
Rotary pump (208 l/min)	1

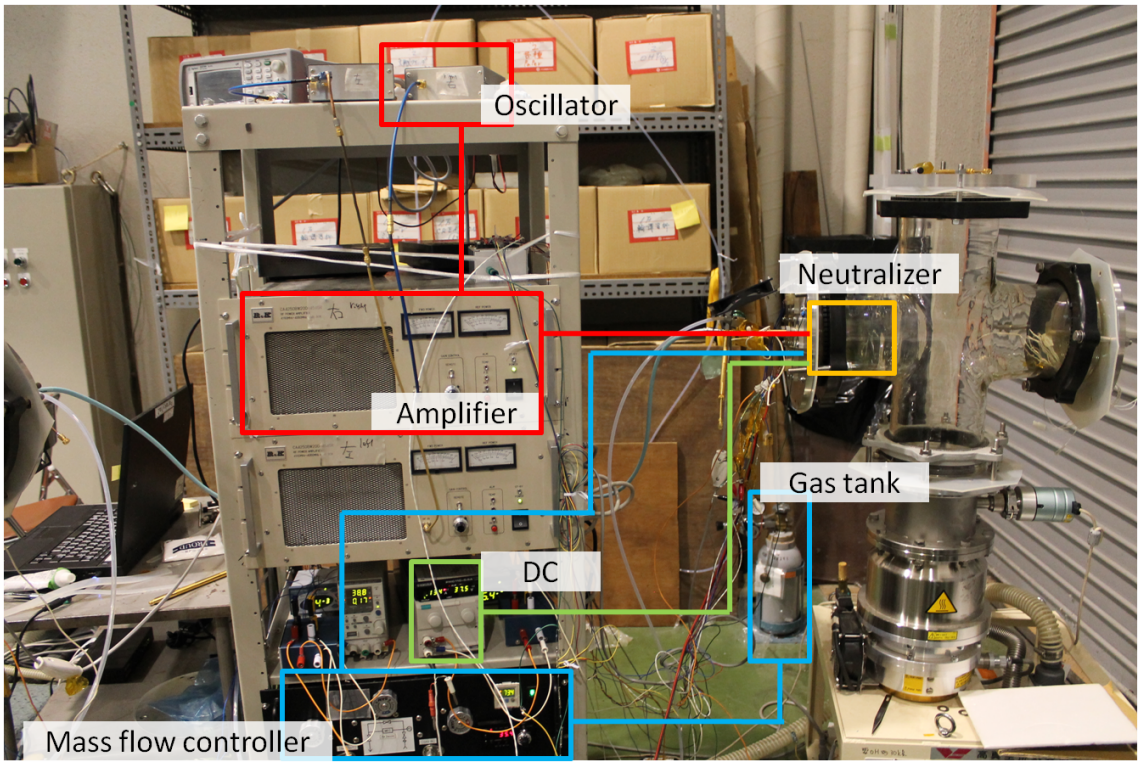

Figure3.3: Photograph of the neutralizer performance measurement system.

3.3 Neutralizer operation system that includes an ion source

Fig.1.5, Fig.3.4, and Fig.3.5 show the operating system of the neutralizer that includes an ion source in its coupling mode. The vacuum chamber has a diameter of 2 *m* and a length of 5 *m* [41] [42] [43]. Table 3.2 lists the specifications of the chamber. Four cryogenic pumps having diameters of 800 *mm* evacuated the vacuum chamber to a gas pressure of less than 0.2 *mPa* during thruster operation at a rate of 28,000 l/s. The two sub-chambers, sub-A and sub-B, are partitioned by gate valves from the main chamber. The internal surface was covered with a titanium shroud and a beam damper was refrigerated to -40 °C. The endurance test mentioned in Subsection 2.1.1 was also performed in this facility from 1999 to 2003.

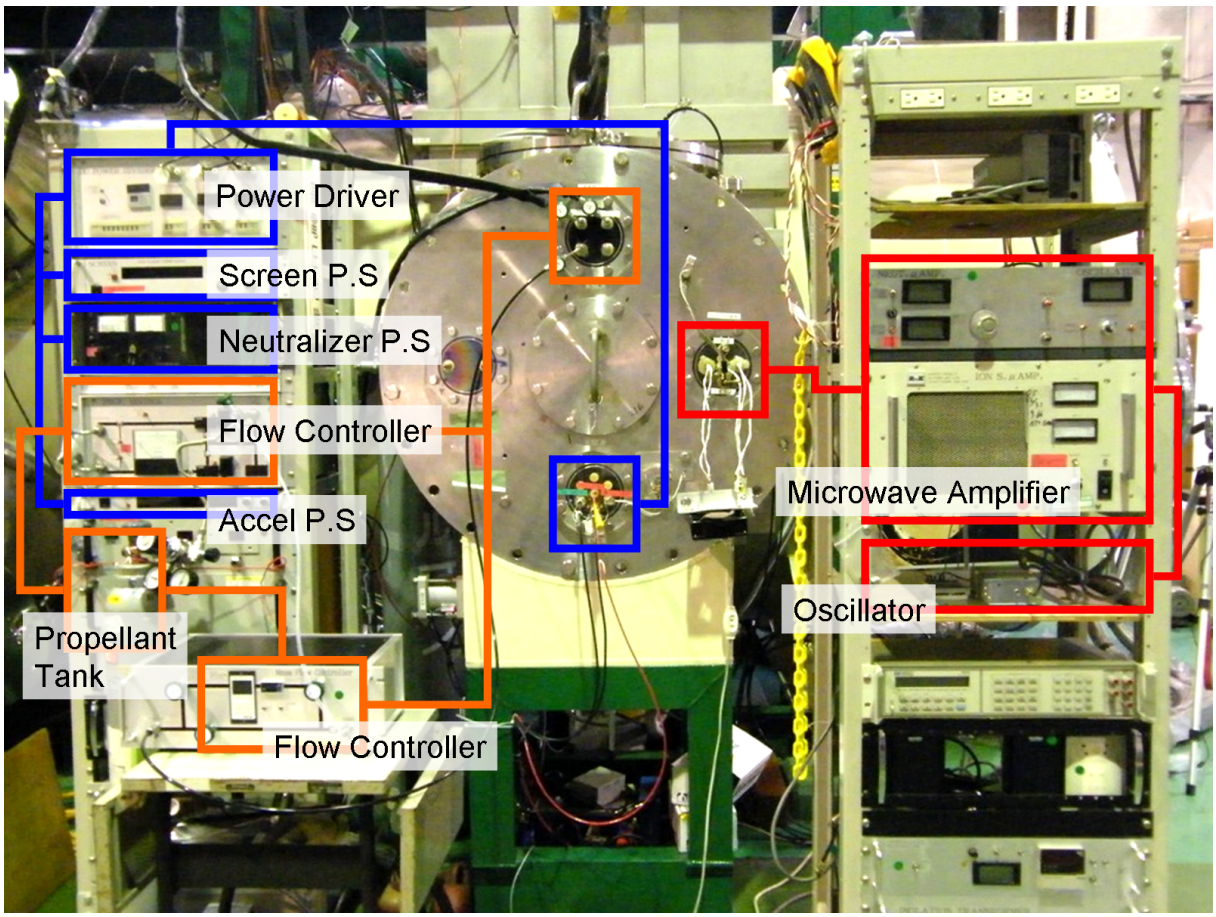

Figure3.4: Photograph of the neutralizer performance measurement system including the ion source.

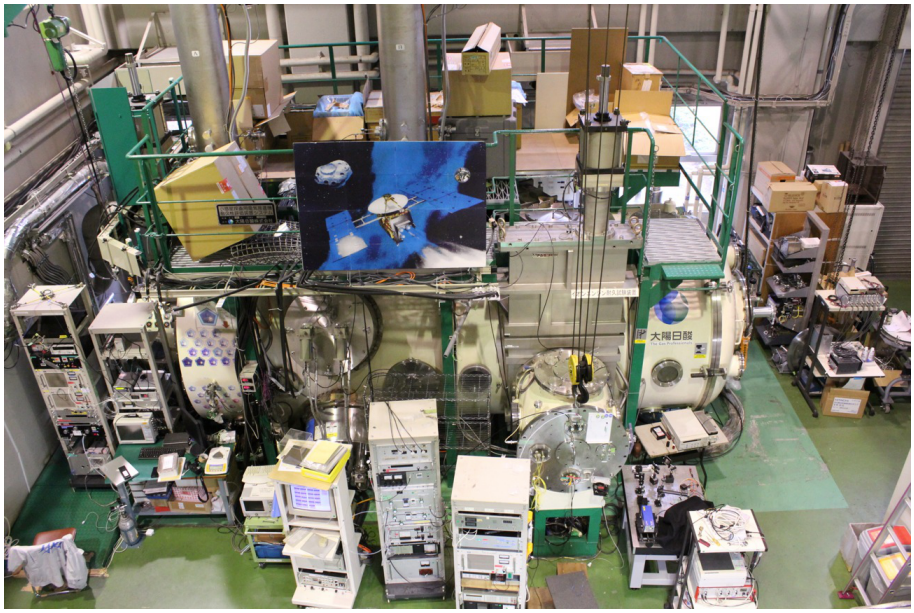

Figure3.5: Vacuum chamber (diameter: 2 m, length 5 m).

Table3.2: Specifications of the vacuum chamber used in the endurance test.

	Specification	Number
Main chamber	SUS316 cylindrical chamber ($\phi 2m, \times 5m$)	1
	Cryopump (28,000 l/s)	4
	Turbomolecular pump	1
	Cryopump	1
	Rotary pump	1
	Mechanical booster pump	1
	Titanium shroud panel / Ion beam target	1
	1.4×10^{-5} Pa in ambient	
	3.4×10^{-4} Pa at Xe 8 sccm	
	-35 °C in 5 hours	
Sub chamber	SUS316 cylindrical chamber ($\phi 0.8m \times 0.6m, 0.8m$)	2
	Turbomolecular pump (200 l/s)	2
	Gate valve 0.8 m	2
	Titanium shroud panel	1
	-50 °C in 5 hours	
Large airlock	SUS316 (0.5 m 2 m)	2
	Turbomolecular pump (200 l/s)	2
	X-Z traversing arrangement	2
	Gate valve 0.4 m	2
Small airlock	SUS316 cylindrical chamber $\phi 0.2m$	2
	Gate valve 0.2 m	2

3.4 Difference between neutralizers with and without an ion source

In order to discuss the neutralizer performance in the diode mode, it is necessary to determine the difference in performance between operating a neutralizer with an ion source (coupling mode) and a neutralizer without an ion source (diode mode). The experimental result is plotted in Fig.3.6 which shows that the difference in contact voltages between the coupling and diode modes is less than 4 V and the contact voltage for the diode mode is always higher, which is negligible compared to the performance degradation, which exceeds 20 V, observed in the endurance test. This is because, in the coupling mode the plasma sheath potential drop does not occur on the anode plate. This is discussed in Section 6.1.2. Moreover, the voltage differences between the diode mode and coupling mode are approximately parallel just the certain voltage is biased.

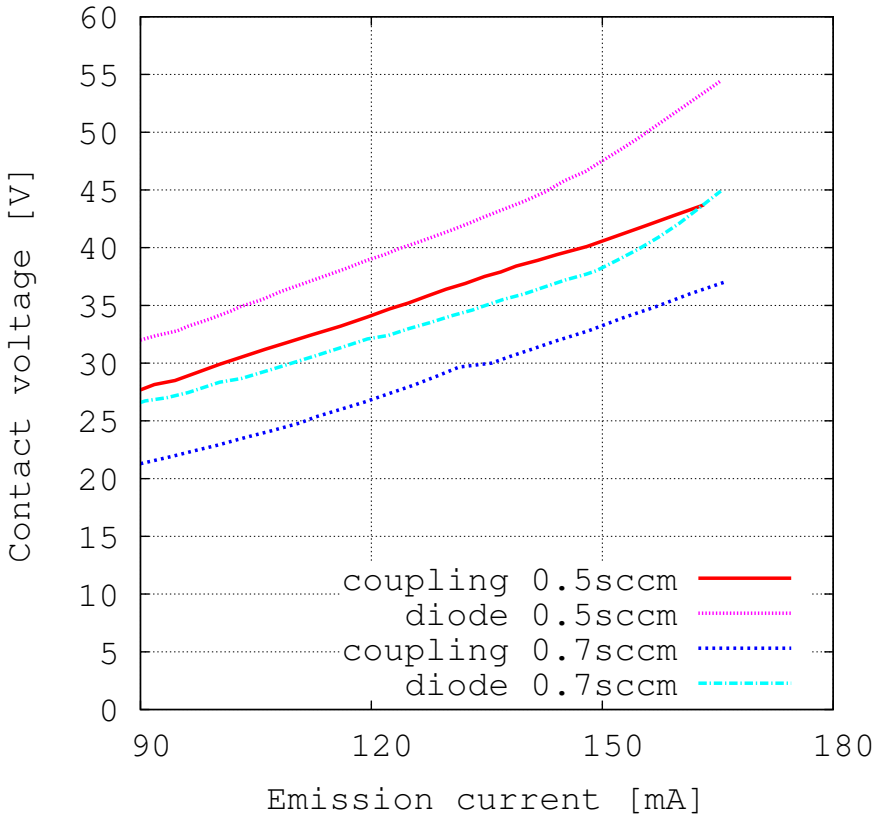

Figure3.6: Difference in performance between the coupling mode and the diode mode.

3.5 Difference in performance between before and after rebuild the neutralizer.

In the following experiments, we rebuild the neutralizer numerous times, for instance, by swapping out the orifice plate, and measure the resulting difference in performance. In order to discuss changes in performance, we need to determine how the performance changes when the assemblies are swapped for different assemblies of the same design. Fig.3.7 shows the change in performance before and after rebuilding. As shown in Fig.3.7, the changes were less than 0.5 V, so changes of more than 1 V are significant.

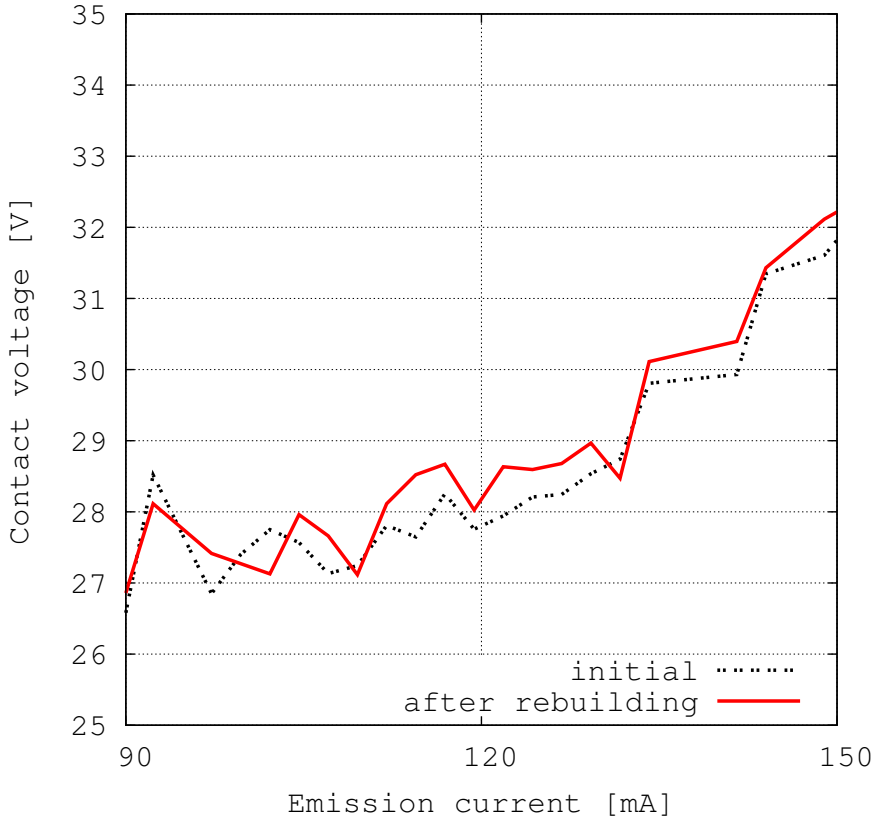

Figure3.7: Changes in performance before and after rebuilding

3.6 Difference in performance between different assemblies of the same design.

Fig.3.1 shows the experimental neutralizers used in the present study. These neutralizers were designed to be inexpensive and easy to use. The orifice plate and the antenna material are changed for usefulness. Since the orifice plates and antennas were all constructed by hand, the performance of each neutralizer is different, even thought the designs are the same. Fig.3.8 shows the changes in performance when an assembly was swapped out with another of the same design. As shown in Fig.3.8, when we change upstream magnetic circuit and antenna, performance changes significantly. The upstream magnetic circuit and antenna could not distributed because of the structural reason. For the accurate experiments, we conducted the experiments using the neutralizer with the highest performance, which was chosen from among the neutralizers that we constructed.

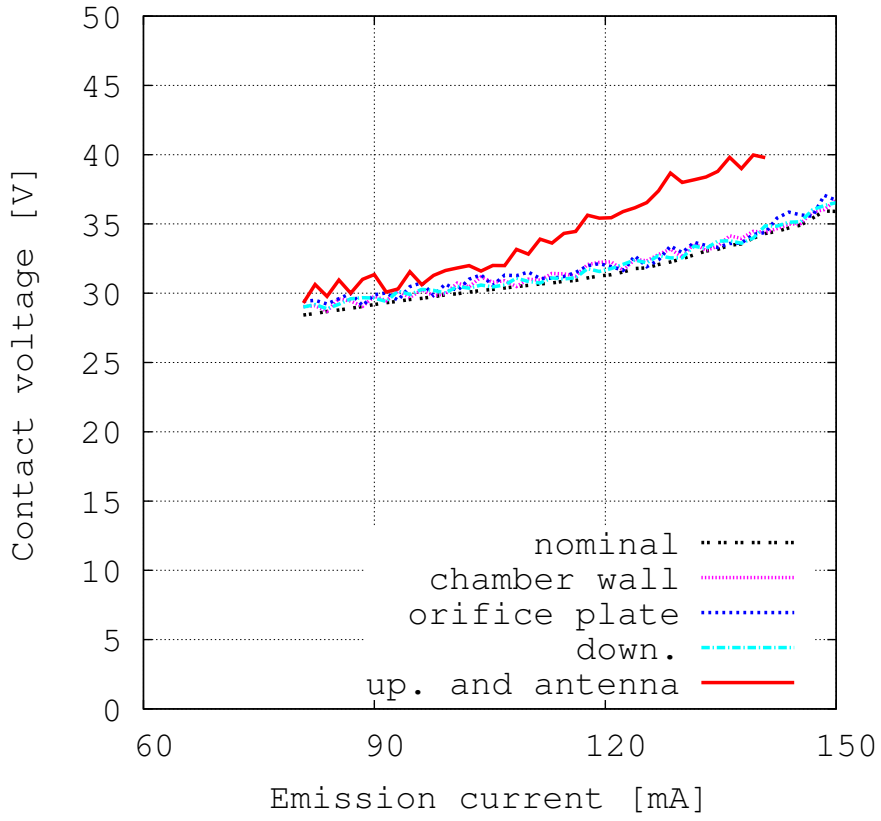

Figure3.8: Changes in performance between different assemblies of the same design.

4 Verification of degradation mechanism

In this section, the degradation mechanism of the neutralizer is explained. We verified the assumed degradation mechanism, which is explained in Section 2.3 based on a number of experiments.

4.1 Magnetic performance

The magnetic performance can change as a result of the deformation of the magnet circuit or the attachment of metal flakes. Sputtering leads to the deformation of the magnetic circuit. In the prototype model neutralizer, the tip of the magnetic circuit, which the magnetic field is the strongest, was worn. The attached flakes may also affect the configuration of the magnetic field because the flakes gather the magnetic line due to the higher magnetic permeability of its than vacuum. An on-the-spot-inspection indicated that the magnetic field in the μ10 prototype model neutralizer was unchanged after the endurance test. This inspection was conducted using a magnetic probe MG-601, the specifications of which are listed in Table 4.1. Any deformation of the magnetic circuits by sputtering had a negligible effect on the performance of the neutralizers. In addition, the flakes on the magnetic circuit were too thin to create a significant magnetic flux due to their saturation. For this reason, the flakes did not affect the performance of the neutralizers. In conclusion, ”Reduction of magnetic field” in Fig.2.5 and Fig.2.6 cannot be the physical cause of the performance degradation.

Table4.1: Specifications of the magnetic probe.

Conmapny	Magna
Model	MG-601
Indication range	0-3000 mT
Resolution	0.01-1 mT

4.2 Plasma loss caused by flakes

Next, we investigated the effect of plasma loss due to the flakes on the neutralizer performance. Performance recovery occurs after the flakes are removed from the $\mu 10$ prototype model neutralizer. Fig.4.1 shows the performance before and after cleaning. The contact voltage drops by approximately 4 V due to the cleaning. The neutralizer was tested using imitation flakes made of non-ferromagnetic stainless steel that are approximately 50 times larger than the actual flakes. The flakes have a thickness of 25 μm, a width of 11 mm, and a length of 6 mm. The relative permeability of the flakes is 2,000. The use of such large flakes sets an upper limit on the negative effects on the neutralizer. Fig.4.2 shows three possible orientations of the imitation flakes: parallel, transverse, and perpendicular to the magnetic field. In order to realize the setups of the B_t and B_{pp}, since the flakes are not self sustainable, we produced these flakes as a unit with a thin film oriented along the side wall. In order to verify the mean effects of the B_t and B_{pp} flakes, we also made a thin film oriented along the side wall and determined the performance difference between the setups of the B_t and $wall$, or B_{pp} and $wall$, or B_{pp} and $wall$. Fig.4.3 shows an example of the results for each setup. In order to simplify the graph, we defined the differences in the contact voltage compared to operation without flakes as

- $B_{pr} := B_{pr} - none\,flake$
- $B_t := B_t - wall\,film$
- $B_{pp} := B_{pp} - wall\,film$

The results are shown in Fig.4.4 and Fig.4.5. Fig.4.4 and Fig.4.5 show the differences in the contact voltage as compared to operation without the flakes. Positive values indicate an increase in the contact voltage due to the presence of the imitation flakes.

Discussion

Considering an emission current of 135 mA, the parallel configuration has a minor effect on the neutralizer. On the other hand, the transverse and perpendicular configurations increase the contact voltage by 7 V in the 0.5-$sccm$ condition. Ion collisions with the flakes result in plasma loss and in efficient charge transfer to the neutralizer. The plasma loss has an adverse effect, whereas the charge transfer has a favorable effect on the electron-emitting neutralizer. High-energy electrons, traveling back and forth in the magnetic tube and drifting azimuthally in the discharge chamber, collide with the flakes in the transverse and perpendicular configurations, resulting in plasma loss. Although the voltage recovery by removal of the flakes indicated in Fig.4.1 and the voltage increase by the imitation flakes in Fig.4.4 are consistent with each other, they involve voltages lower than the performance degradation of 20 V or greater. In addition, this effect decreases at higher propellant flow rates. In summary, the item ”Increase of plasma loss” generated by the flakes in Fig.2.5 and Fig.2.6 is not a major factor in the performance degradation.

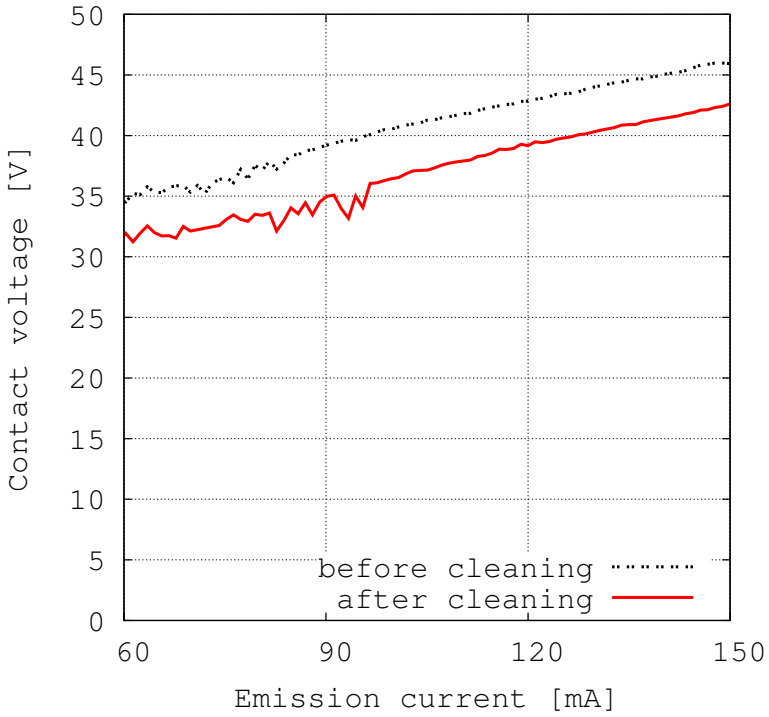

Figure4.1: Change in performance before and after cleaning off the flakes in the prototype model neutralizer.

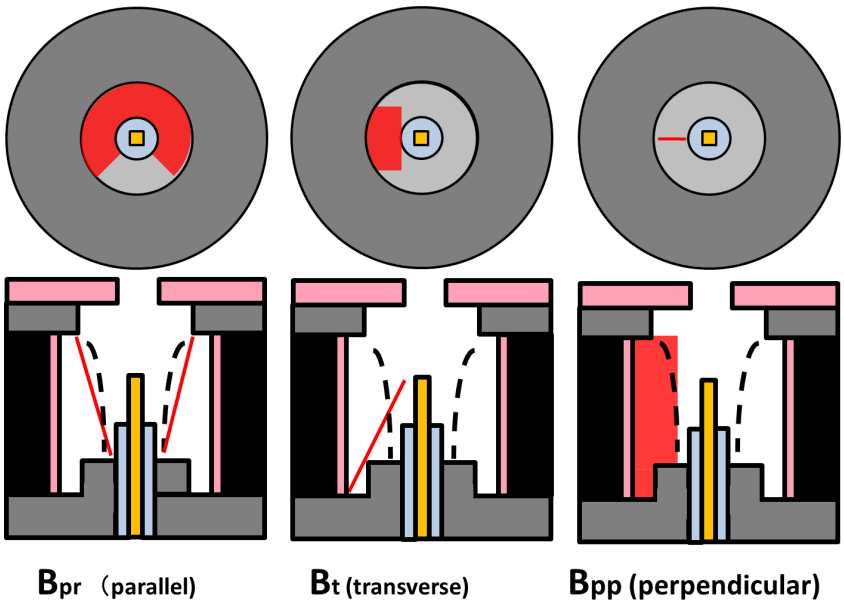

Figure4.2: Three arrangements of imitation flakes. The red lines indicate the flakes, and are parallel to the magnetic field (B_{pr}), transverse to the magnetic field (B_t), or perpendicular to the magnetic field (B_{pp}). The dashed lines indicate magnetic field lines.

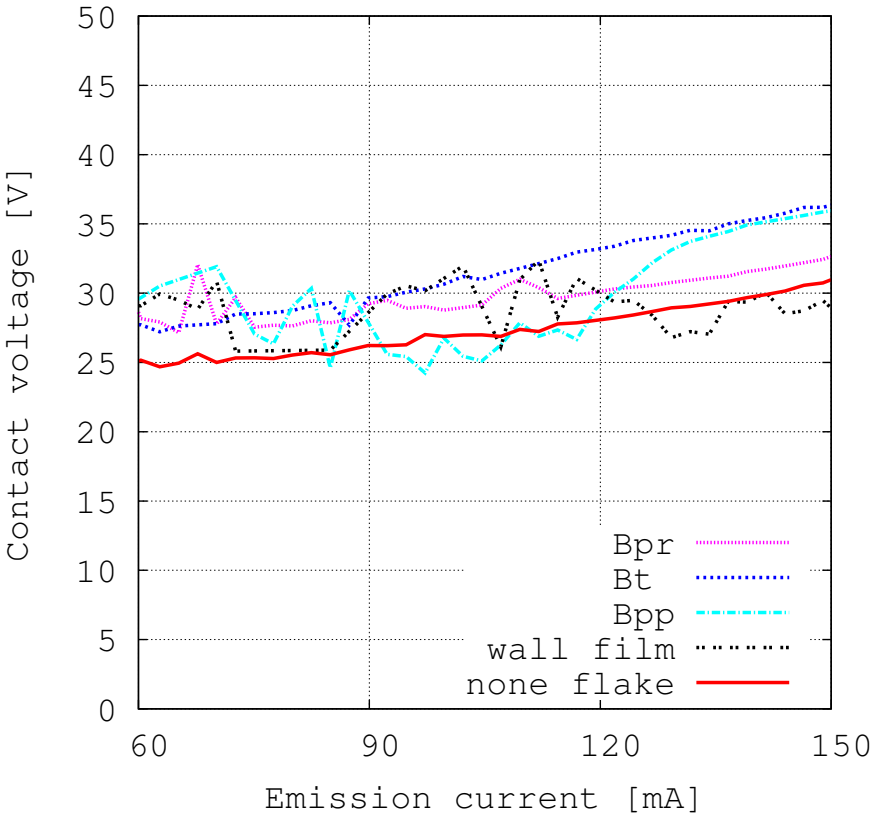

Figure4.3: Results for each setup.

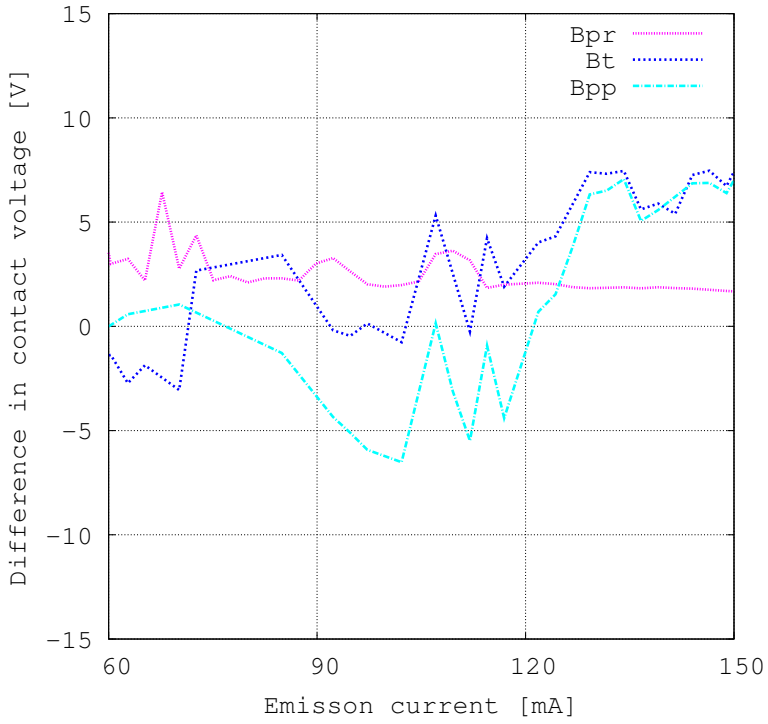

Figure4.4: Changes in the contact voltage and emission current with and without the imitation flakes (0.5 *sccm*).

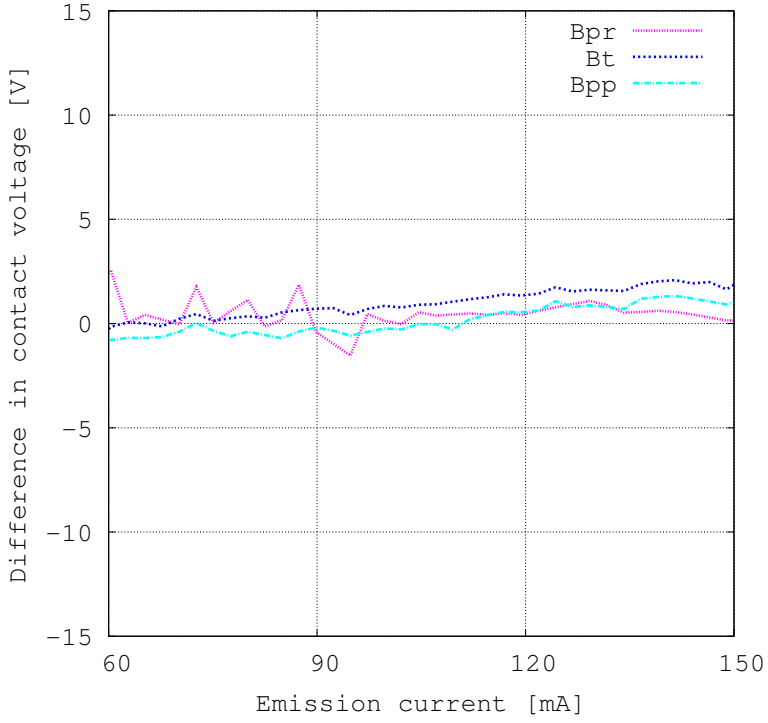

Figure4.5: Changes in the contact voltage and emission current with and without the imitation flakes (0.7 *sccm*).

4.3 Contamination of the dielectric

The effect of contamination on the dielectric was investigated as follows. A new neutralizer, the dielectric of which was artificially contaminated, was subjected to the diode test. Fig.4.6 and Fig.4.7 shows the upstream magnetic circuit of the neutralizer. In Fig.4.6, the surface of the dielectric is contaminated by metal. The results were compared with those after removal of the contamination, as shown in Fig.4.8. The potential was found to change by more than 20 V. In other words, the contamination of the dielectric has a large effect on the neutralizer performance and is consequently thought to be a major influence on the performance degradation. However, quantitative verification in space operation is difficult because of artificial contamination.

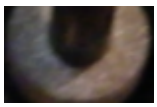

Figure4.6: Contamination on the dielectric surface.

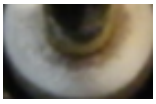

Figure4.7: After grinding the dielectric surface.

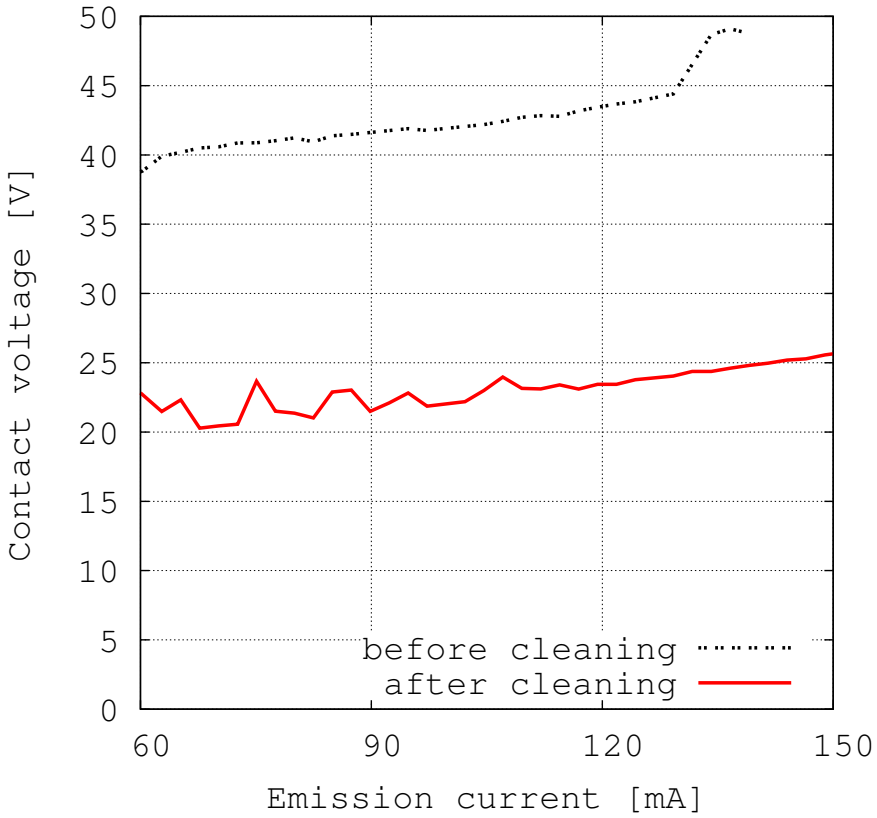

Figure4.8: Performance before and after grinding the contamination from the dielectric surface.

4.4 Summary

Fig.4.9 results a degradation mechanism.The principal cause of the performance degradation of the neutralizer is contamination of the dielectric surface due to sputtering from the flakes on the magnetic circuit. This degradation can be avoided by suppressing the sputtering by means of a lower contact voltage and by inhibiting flakes formation. These countermeasures will be explained in Chapters 6 and 7.

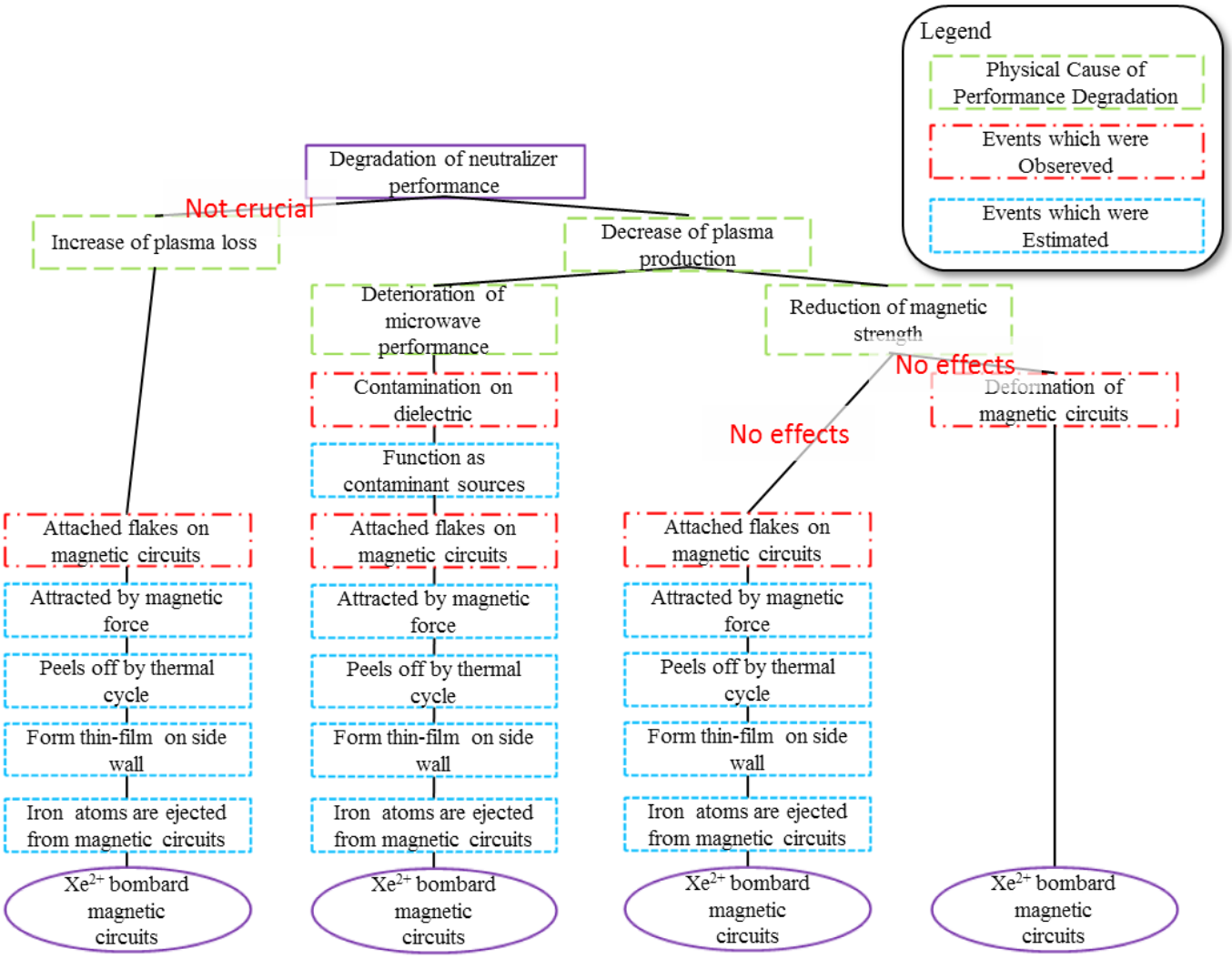

Figure4.9: Verified degradation mechanism. Fault tree analysis form.

5 Experimental investigation of the neutralizer conditions

The principal cause of the performance degradation of the neutralizer is the contamination of the dielectric surface due to the sputtering from flakes on the magnetic circuit. This degradation can be avoided by suppressing the sputtering by using a lower contact voltage and by inhibiting flakes formation. In this chapter, several measures by which to suppress the contact voltage are explained. We measured the net ion current distribution in the neutralizer, which enables us to know which neutralizer assembly should be improved.

5.1 Refurbished design assemblies

The ECR neutralizer, as shown in Fig.5.1, is composed of major assemblies: magnets, an upstream magnetic circuit, an antenna, a dielectric antenna holder, a sidewall, a downstream magnetic circuit, and an orifice plate. In order to reduce the contact voltage, we should first determine which assembly should be improved. The net ion current distribution measurement method was used for this purpose.

5.1.1 Net ion current distribution measurement method

When the ECR neutralizer emits electrons, the same charge of xenon ions bombard the inside of the neutralizer as a counterpart. This charge flows to the earth ground or standard voltage of the satellite, as shown in Fig.5.2. We measured the net ion current by insulating each assembly of the neutralizer, as shown in Fig.5.1, i.e., it is called as a separated electrodes in common, and investigated the net ion current distribution when running the neutralizer. Based on these measurements, we can determine what assemblies of the neutralizer are crucial for collecting ions, i.e., emitting electrons. Therefore, we can determine areas for improvement in the neutralizer. Such measurements are advantageous in that they are non-invasive and real-time measurements. Fig.5.3 shows the differences in the contact voltage compared to the nominal neutralizer and the assemblies-insulated neutralizer. Despite insulating all of the assemblies in the neutralizer, there is no significant difference in the contact voltage. Fig.5.4 shows the experimental setup of the net ion current distribution measurement

system. In operational mode, the neutralizer emits electrons into a plasma beam. In order to measure the net ion current of the antenna we used a microwave connector called a “ bias-tee ”, which was a high-pass filter for microwaves, and the core of the coaxial cable can be electrostatically separated from the upstream circuits. Using the bias-tee connector, we can consider the antenna to be a cylindrical probe and measure the ion saturation current and the floating potential [44].

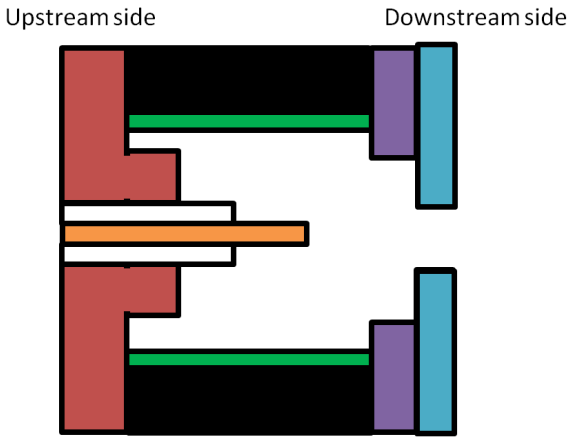

Figure5.1: Schematic diagram of the ECR neutralizer, which is composed of the magnets (black), an upstream magnetic circuit (red), an antenna (orange), a dielectric antenna holder (white), a sidewall (green), a downstream magnetic circuit (purple), and an orifice plate (blue).

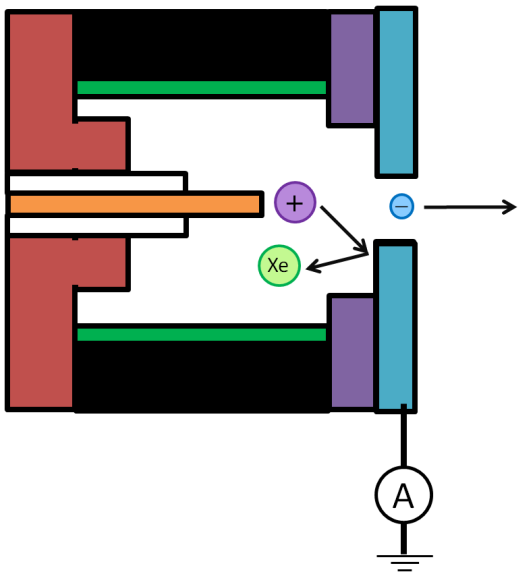

Figure5.2: Schematic diagram of the net ion current measured at the orifice plate. When the neutralizer emits electrons, the same charge of ions strike the surface, in this case the orifice plate, and is neutralized.

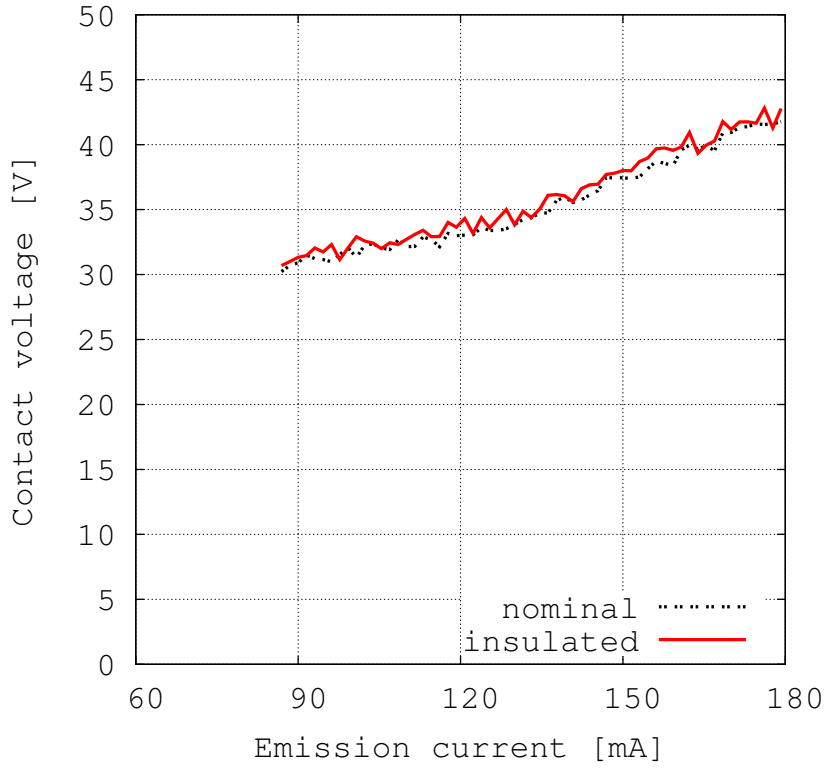

Figure5.3: Difference in performance between nominal and insulated neutralizers.

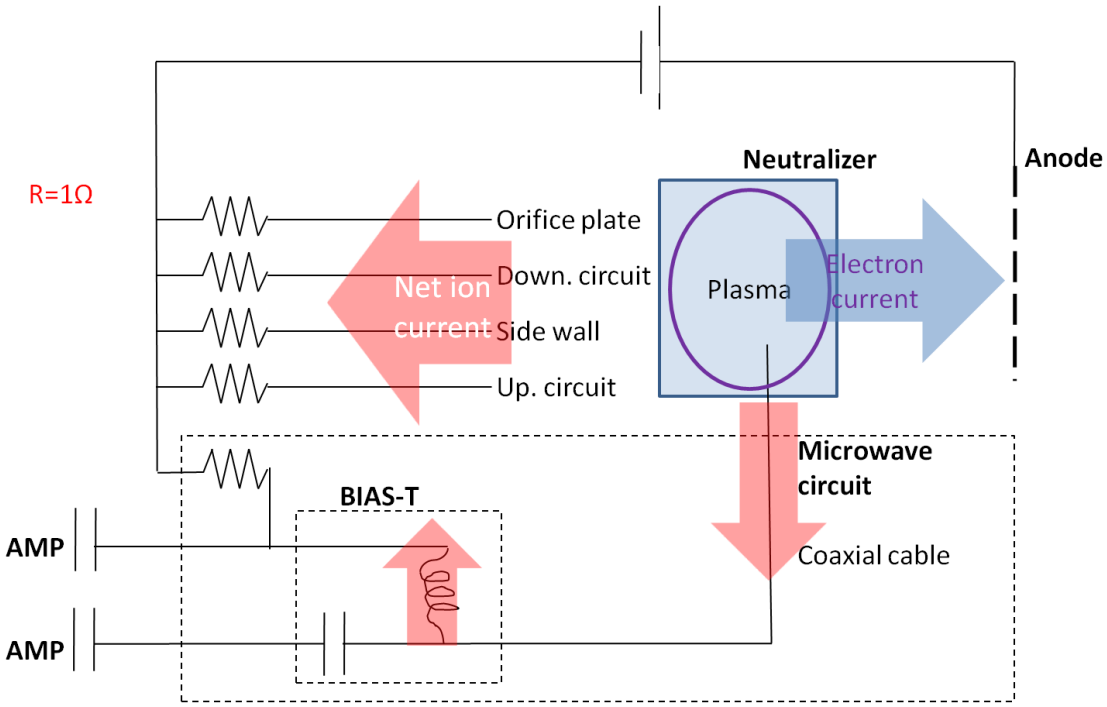

Figure5.4: Schematic diagram of the net ion current measurement circuit. Summary of the electron current and the net ion current is zero. The power source supplies the contact voltage.

5.1.2 Experimental results: net ion current distribution of the nominal neutralizer

Fig.5.5 shows the results for the net ion current distribution of the neutralizer. The ion saturation current is also shown in Fig.5.5 which is mentioned in the discussion of Section 5.1.2. Fig.5.6 shows the results for the net ion current distribution of the neutralizer as a percentage, i.e., $(each\,net\,ion\,current)/(emission\,current)$. Fig.5.7 shows the results for the net ion current distribution density of the neutralizer. The colors in the figure correspond to those in Fig.5.1. Fig.5.5 and Fig.5.6 show that

1. the sidewall collects the greatest portion of the net ion currents and
2. the antenna collects numerous electrons.

In addition to 1), Fig.5.7 shows that the density of net ion current is approximately the same in the sidewall, the upstream magnetic circuit, and the downstream magnetic circuit. The current densities in these components are approximately 0.1-0.2 mA/mm^2. For instance, at 160 mA, the current density in the upstream magnetic circuit is 0.08 mA/mm^2, the current density in the sidewall is 0.15 mA/mm^2, the current density in the downstream magnetic circuit is 0.12 mA/mm^2, and the current density in the orifice plate is 0.08 mA/mm^2. In addition to 2), the neutralizer emits electrons, and so the antenna adversely affects the neutralizer performance.

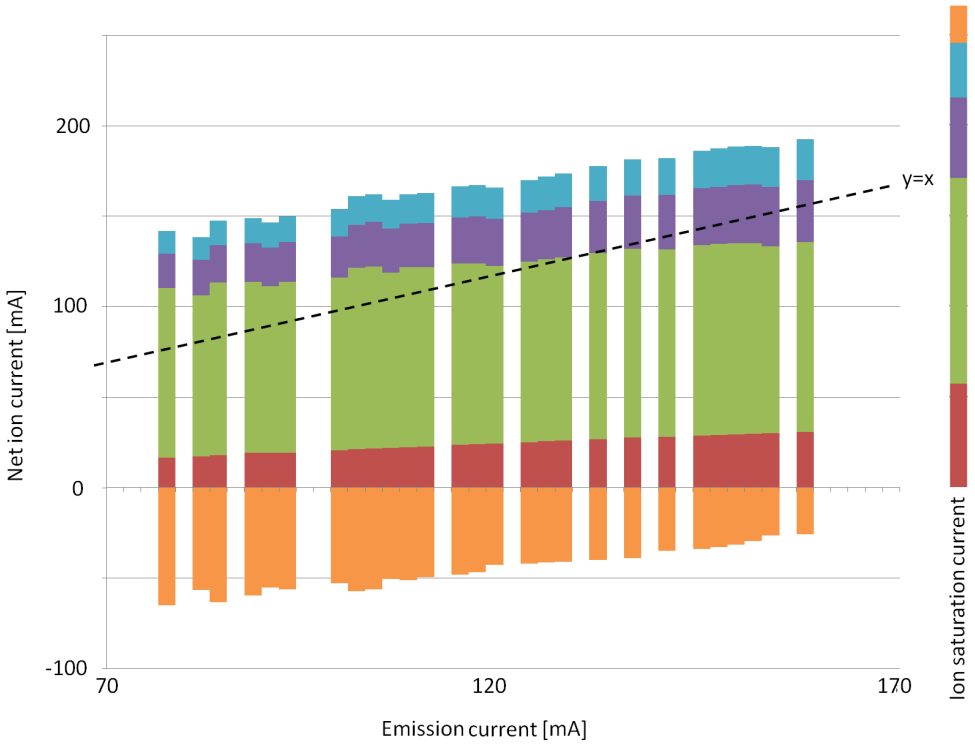

Figure5.5: Net ion current distribution of the nominal neutralizer. The colors correspond to those described in Fig.5.1.

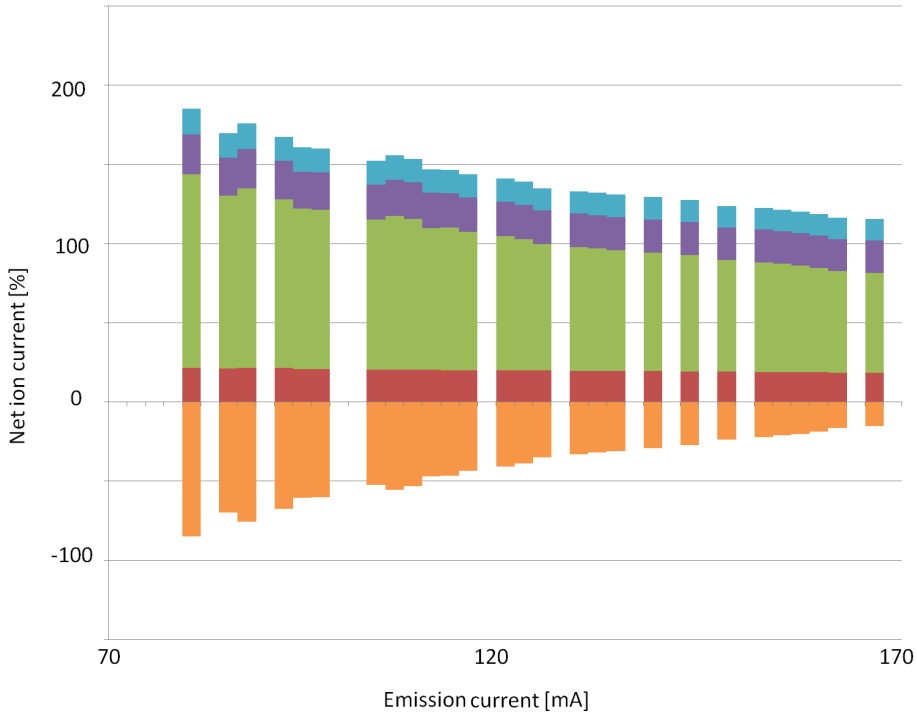

Figure5.6: Net ion current distribution of the nominal neutralizer as a percentage. The colors correspond to those described in Fig.5.1.

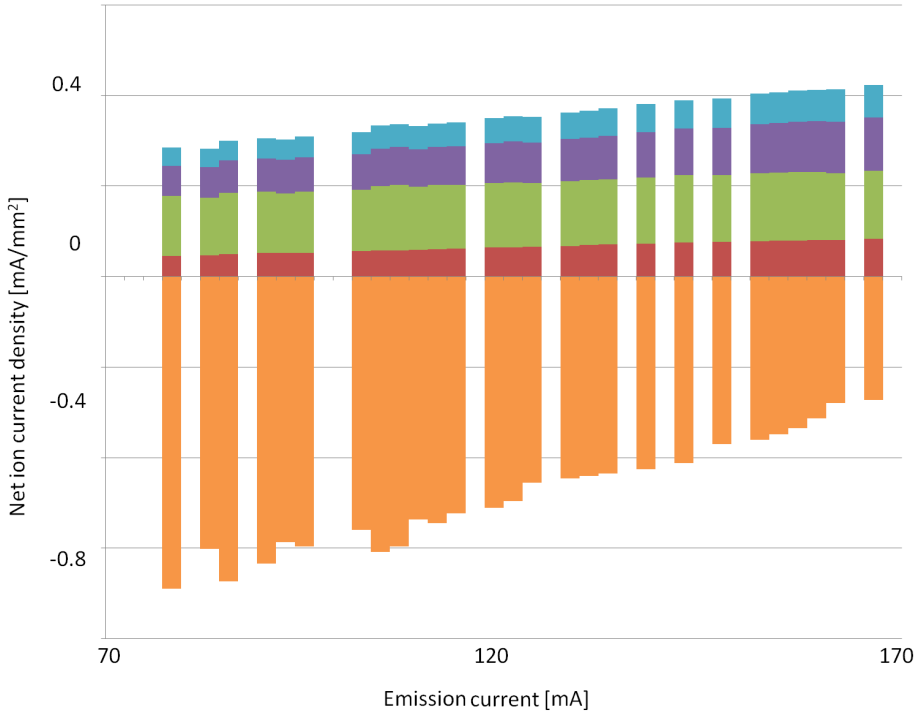

Figure5.7: Net ion current density distribution of the nominal neutralizer. The colors correspond to those described in Fig.5.1.

Discussion

According to Fig.5.5, net ion current increases with increasing emission current. There are two causes for this, the increase of ion current to the surface, or the decrease of electron current to the surface. Now, the ion temperature is approximately 350 K, since the ions ejection from the neutralizer doesn't change in increasing of emission current, i.e., contact voltage. The input power and the gas flow rate are constant in the experiment, and this results in the constant plasma parameter. Thus, the net current increasing with increase emission current due to the decrease of electron current. This results in the constant ion current and the degradation by sputtering only determined by sputtering voltage. The electron temperature inside the discharge chamber is approximately 2 to 3 eV, and the space voltage is approximately 20 V which is shown in Table 1.7. The difference between the space voltage and the wall voltage is much more greater than the electron temperature, and it is expected that the breakdown of the net ion current is almost ion current. Fig.5.8 shows the results of the probe (electron) current, which uses the orifice as a Langumir probe, when the emission current is constant at 135 mA. Due to the magnetic field and the disturbance of the neutralizer performance, when the orifice voltage is large, the disturbance is also large, and it is difficult to calculate the plasma parameters. As a result, the ion saturation current density is approximately $0.1 mA/mm^2$. Fig.5.9 shows the results for the probe (electron) current, where the antenna is used as a Langumir probe, when the emission current is constant at 135 mA. The probe current at 0 V is not saturated. This is because the electron temperature near the antenna is higher than it is in the other areas. For this reason, according to Fig.5.9, the ion current density is also large at approximately $0.3 mA/mm^2$ for a 22.4 mA saturation current. The ion saturation current except the antenna and the orifice are assumed as the following. According to Fig.5.7, at 160 mA, the current density in the upstream magnetic circuit is 0.08 mA/mm^2, the current density in the sidewall is 0.15 mA/mm^2, the current density in the downstream magnetic circuit is 0.12 mA/mm^2, and the current density in the orifice plate is 0.08 mA/mm^2. The ion saturation current of the orifice is 0.1 mA/mm^2. Thus the 80% of ion current is measured as the net ion current at 160 mA. Assuming the 80% of ion current is measured as the net ion current at 160 mA in the other assemblies except the antenna, the results of the ion saturation current are in Table 5.1.

Table5.1: Ion saturation current of each assembly.

Assembly	Ion saturation current, mA/mm^2	Detail
Upstream magnetic circuit	0.112	calculated
Side wall	0.187	calculated
Downstream magnetic circuit	0.15	calculated
Orifice plate	0.1	measured
Antenna	0.3	measured

Assuming the Bohm sheath model, the ion current flux is insusceptible to the magnetic force, the ion current flux is given as follows:

$$j_i = qe^{-\frac{1}{2}} n_0 \sqrt{\frac{kT_e}{m_i}} \tag{5.1.1}$$

where j_i is the ion current flux A/m^2, q is the quantum of electricity, n_0 is the number density of plasma, k is the Boltzmann coefficient, T_e is the electron temperature, and m_i is the mass of the ion. Using the electron tempertature of Table 1.7 and the ion saturation currents of Fig.5.8, and Fig.5.9, the plasma densities are calculated as Table 5.2. Both number densities exceed the plasma cutoff density of 4.25 GHz which is $2.1 \times 10^{17} m^{-3}$. The number density measured by the orifice is

equivalent to the result of Table 1.7, but the other is relatively high. This is because the measured plasma is near to the antenna which emits microwave. In addition to this, the diameter of the discharge chamber is smaller than the wave length of 4.25 *GHz*. Accordingly, there is a plasma whose density is above the cutoff density inside discharge chamber.

Table5.2: Plasma densities of inside discharge chamber.

Measured at	Plasma density $\times 10^{17} m^{-3}$
Orifice	6.7
Antenna	27

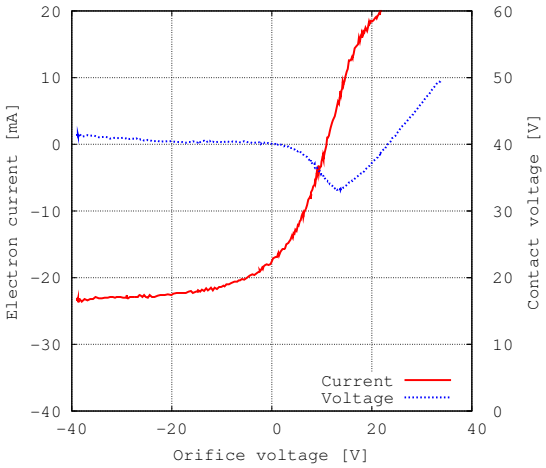

Figure5.8: Orifice electron current and contact voltage with respect to the change in the orifice voltage.

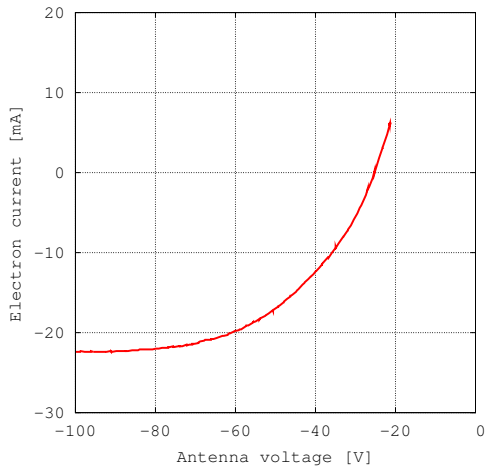

Figure5.9: Variation in the antenna electron current with respect to the change in the antenna voltage.

5.2 Improvement of the neutralizer performance

In this section, we explain how we improved the performance of the neutralizer based on the results of net ion current distribution measurements.

5.2.1 Antenna

Through the use of a floating antenna, the electron loss shown in Fig.5.5 can be suppressed. Fig.5.10 shows the results of the net ion current distribution when the antenna is floating. The ion saturation current is also shown in Fig.5.10 which is mentioned in Section 5.1.2. Fig.5.11 shows the results of the net ion current distribution of the neutralizer as a percentage, which is obtained as $(each\,net\,ion\,current)/(emission\,current)$. Fig.5.12 shows the results for the net ion current distribution density of the neutralizer. The results were compared for the cases of floating and non-floating antenna, as shown in Fig.5.13. Fig.5.14 graphs the antenna floating voltage.

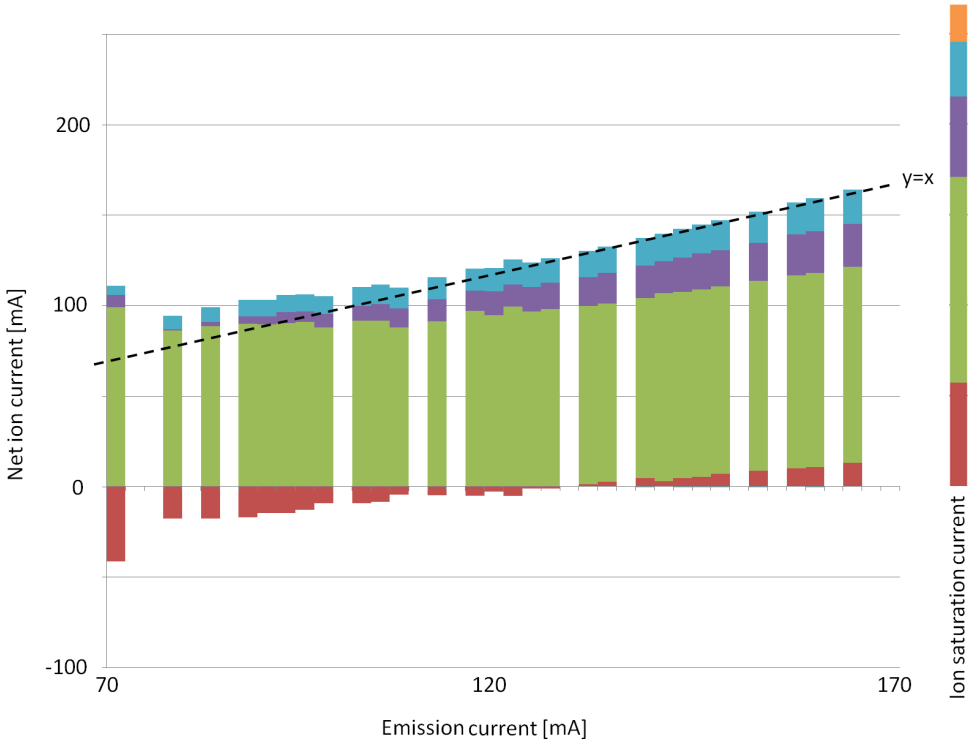

Figure5.10: Net ion current distribution of the floating antenna neutralizer. The colors correspond to those described in Fig.5.1.

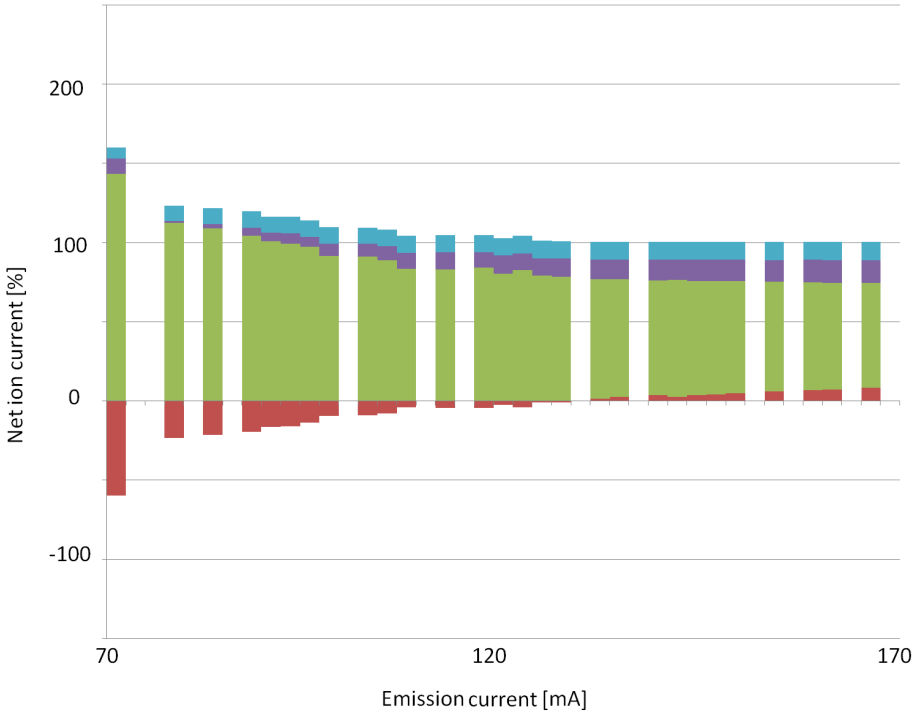

Figure5.11: Net ion current distribution of the floating antenna neutralizer. The colors correspond to those described in Fig.5.1.

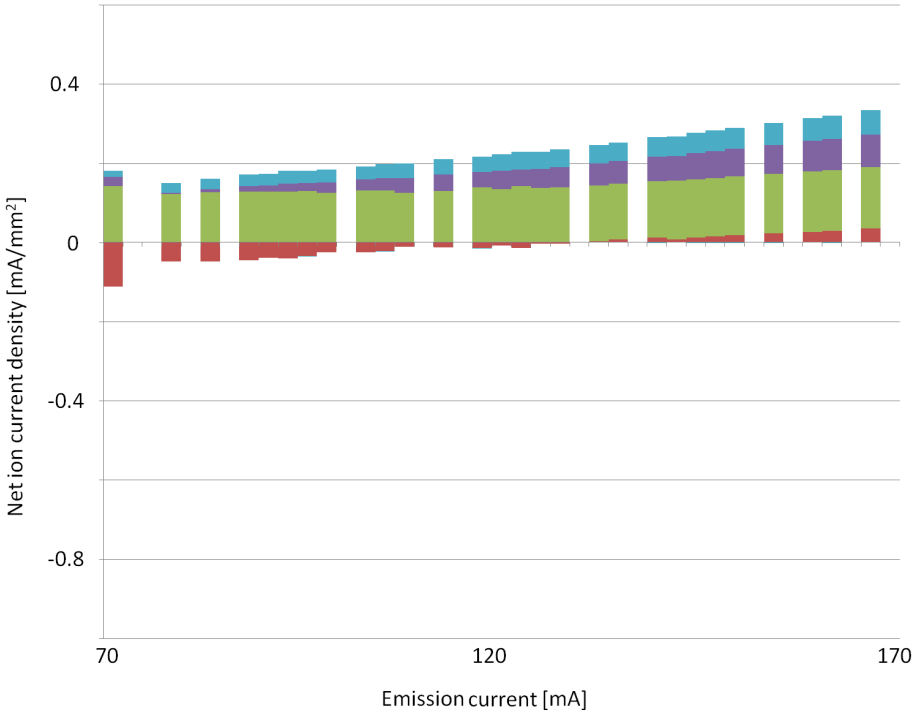

Figure5.12: Net ion current density distribution of the floating antenna neutralizer. The colors correspond to those described in Fig.5.1.

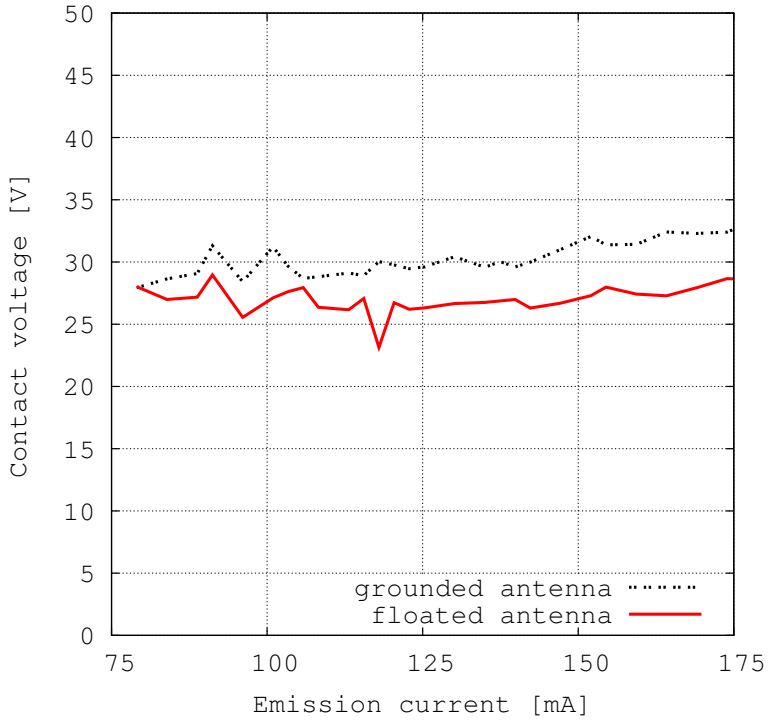

Figure5.13: Change in performance with and without the floating antenna.

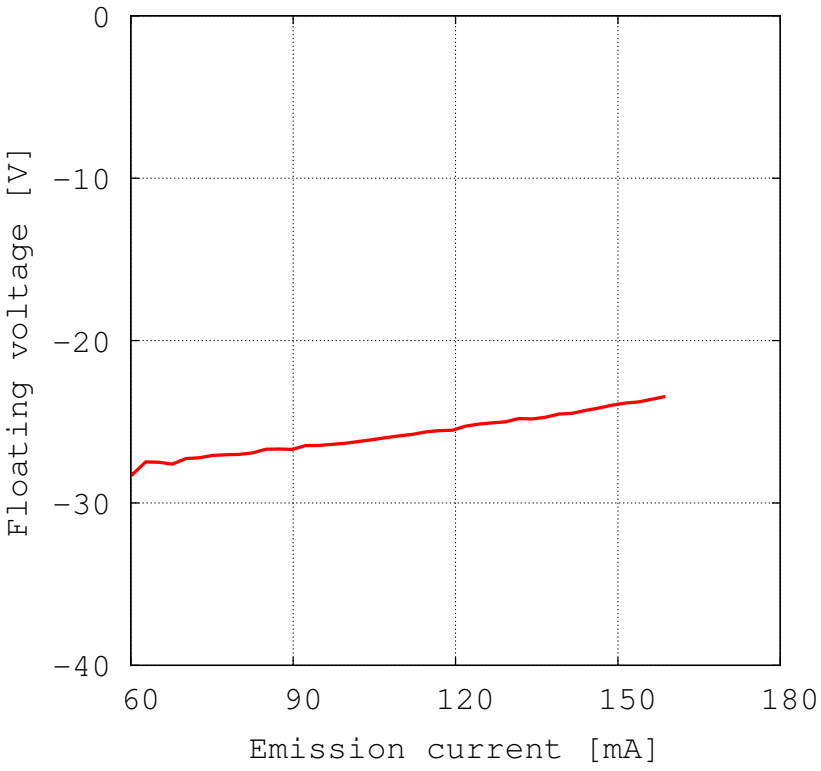

Figure5.14: Floating antenna voltage.

Discussion

The contact voltage was reduced by inhibiting electron collection in the antenna. In Fig.5.11, the percentage of net ion current of the upstream magnetic circuit and the downstream magnetic circuit increases more than those of the other components when the emission current increases. For instance, the downstream magnetic circuit percentage is 7% at 90 *mA*, and 14% at 150 *mA*, which is a two-fold increase. This is because the antenna is neglected, the electrons mainly struck the magnetic circuit because of the motion parallel to the magnetic line.

According to Fig.5.14, in the case of the floating antenna, the contact voltage will become several volts lower, but the antenna floating voltage is reduced by approximately 25 V. This means that sputtering of the antenna will be increased.

With respect to the endurance enhancement, there is a 5 V decrease in the contact voltage and a 25 minus 5 V increase in the sputtering voltage for the antenna. Since the antenna is constructed of molybdenum, it has higher resistance to sputtering than the other assemblies, which are made of iron. The lifetime of the floated antenna neutralizer will be discussed in Section 6.2.1.

5.2.2 Orifice plate

As mentioned in Subsection 5.1.2, the components of the neutralizer other than the antenna collect more ions than electrons, so floating the components may worsen the performance. However, when we floated an orifice, the performance improved, as shown in Fig.5.8. In Fig.5.8, the performance of the neutralizer is best when the orifice voltage is 15 V. We constructed a novel three-sectioned orifice plate, as shown in Fig.5.15. Fig.5.16 graphs the net ion current distribution of the new neutralizer. The grey area is approximately the same as that shown in Fig.5.5. Fig.5.16 shows that the downstream side (green) does not have any effect on the current. Fig.5.17 shows the performance difference between the nominal neutralizer and the orifice floated neutralizers. Fig.5.17 shows that the floating inner orifice is effective for improving the performance of the neutralizer. This indicates that the outer side of the orifice is dominant in collecting ions.

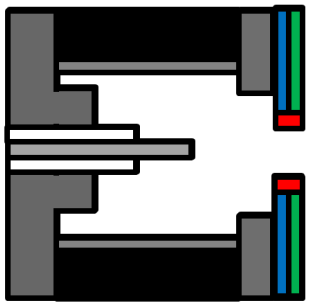

Figure5.15: Schematic diagram of the three-sectioned orifice plate neutralizer. The radial thickness of the red area is 1 *mm*.

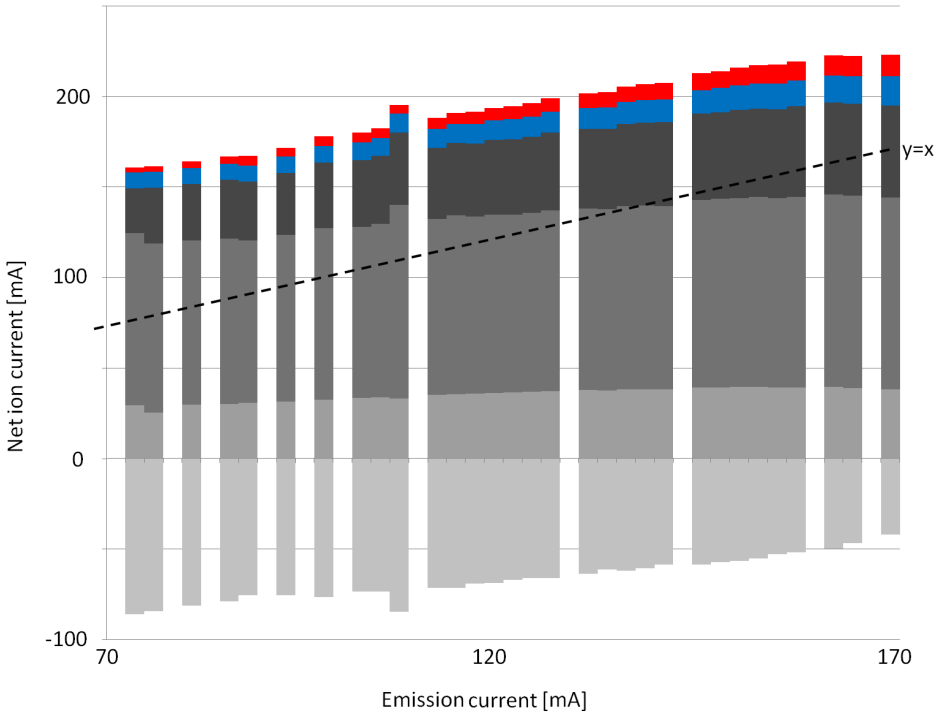

Figure5.16: Net ion current distribution of the three-sectioned orifice plate neutralizer. The colors correspond to those described in Fig.5.15

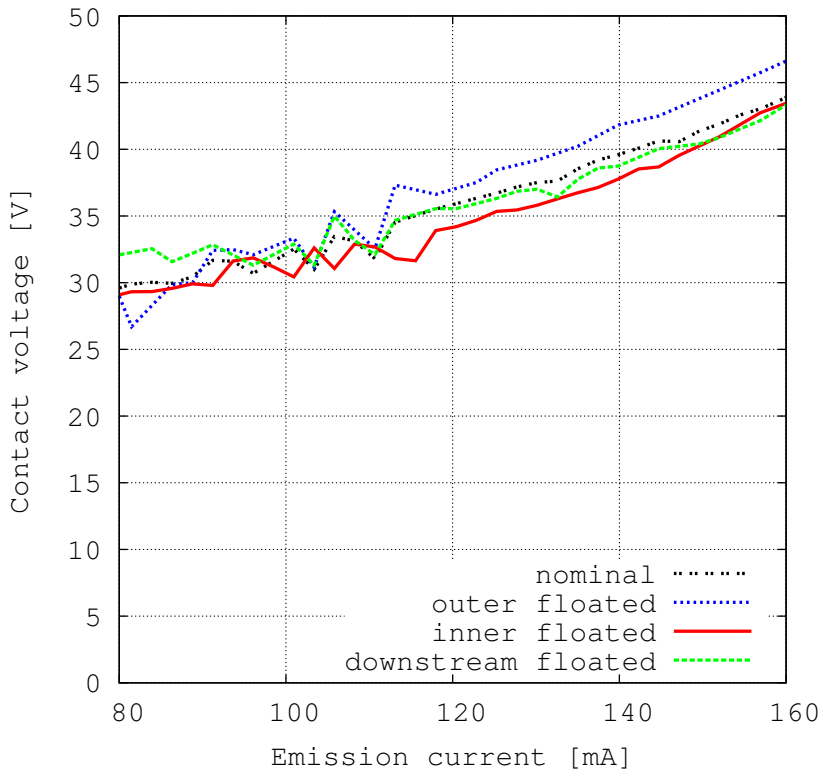

Figure5.17: Performance of nominal neutralizer and the three-sectioned orifice plate floating neutralizers.

For further study, we newly constructed the four-sectioned orifice plate neutralizer shown in Fig.5.18. The axial length of each orifice plate which is shown in red, green, and blue in Fig.5.18 is 1.5 *mm*. Fig.5.19 shows the performances for different floating conditions. The floating downstream orifice plate is effective for improving the performance. In addition, floating all of the orifice plate is also effective.

We checked these phenomena occurs not only in diode mode operation. We operated the neutralizer with an ion source using the facilities mentioned in Section 3.3. Fig.5.20 graphs the results for the performance of the grounded orifice (nominal condition) and the floating downstream orifice neutralizer with an ion source.

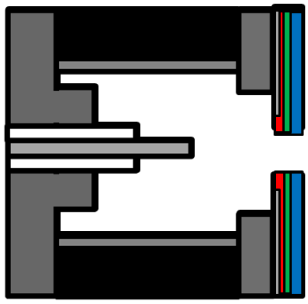

Figure5.18: Schematic diagram of the four-sectioned orifice plate neutralizer.

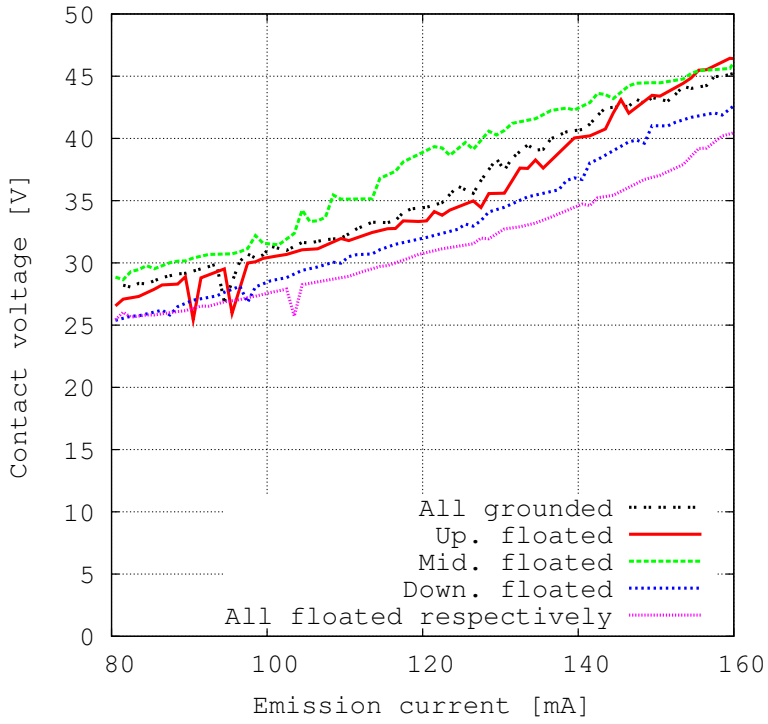

Figure5.19: Performance of the nominal neutralizer and the four-sectioned orifice plate floating neutralizers.

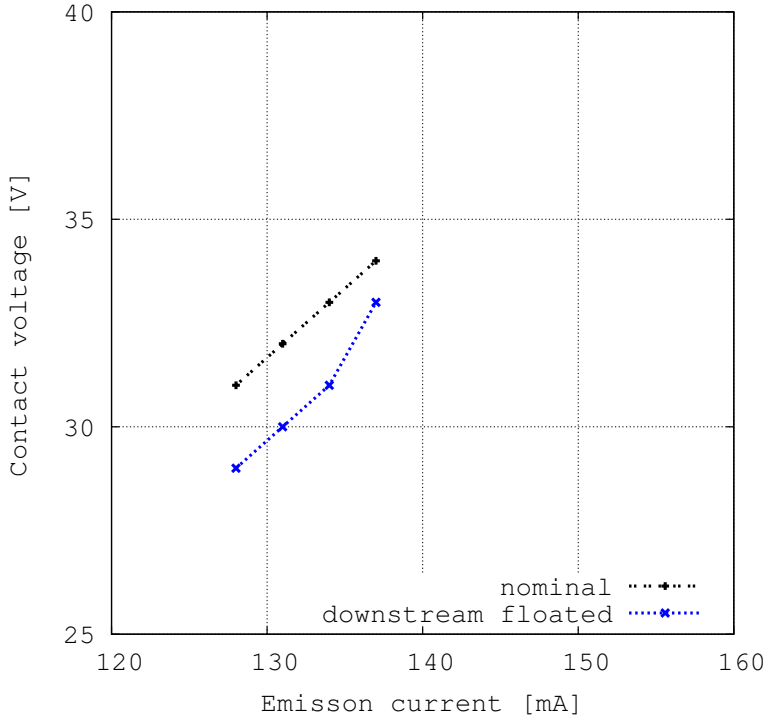

Figure5.20: Performance of the nominal neutralizer and the four-sectioned orifice plate downstream floated neutralizer with an ion source.

Discussion

Next, we discuss why the contact voltage is suppressed by the floating orifice. Table 5.3 shows the floating voltage of 135 *mA*. It is assumee that the contact voltage get less by floating orifice because of the change in space voltage, which is shown in Fig.5.21. When the orifice was floated, the space voltage decreased from the red line to the blue line in following reasons: The plasma in narrow orifice area, which is a cylindrical positive column, the magnetic field of the area is less than 10 mT so that the plasma parameters can be predicted by the free-fall theory of Tonks and Langumir. From the energy balance equation of electrons in a positive column, the reduced axial electric field E_z/P can be expressed as follows

$$E_z = (G\frac{3\nu k(T_e - T_g)}{2q\mu_e} + \frac{3kT_e\Phi}{2n_e})^{0.5} \tag{5.2.1}$$

Where T is the temperature, m is the mass, n is the density, G is the collision factor due to inelastic and elastic collisions, Φ is the total electron loss to the orifice wall per second, k is Boltzmann ' s constant, q is the elementary charge, and the subscripts e and g refer to electron and gas respectively [45] [46]. The experimental results of E_z/P are shown in Fig.5.22 which were reported by Kaneda et.al [4]. The experiments were conducted with the tubes with inner diameters of 0.5, 0.8, and 3 *mm* DC discharge tube, and 2 *mm* long cylindrical electrostatic probes were used for the measurements. Discharge current is 20-30 *mA* in this experiment. Using the parameter of neutralizer, $10^{-2}Torr$ and 2 *mm* for pR in the Fig.5.22, we got $E_z/p = 500V/(cmTorr)$. This results in the increase of 2.5 V in the space voltage between the inlet and the outlet of the orifice. When the orifice is floated, ion flux to the surface reduces. This results in the lower plasma loss so that the needs of high electron temperature to maintain plasma eliminates. The lower electron temperature results in the lower electric field, so that the space voltage of outlet of orifice decreases.

Table5.3: Floating voltage for each condition.

Condition	Up. voltage, V	Mid. voltage, V	Down. voltage, V
Up. floated	9.5	0	0
Mid. floated	0	14.5	0
Down. floated	0	0	16.1
Floating respectively	9.8	14.3	16.7

The space voltage should be changed which are marked A to C on Fig.5.21. Table 5.4 and Fig.5.23 shows the space voltage of A to C measured by emissive probe. Anode ' is the anode voltage when emissive probe is used. G is grounded, F is floated in Fig.5.23. There were no difference between the cases in which the orifice was floating or not floating.

Table5.4: Space voltage of the downstream.

Upstream	Mid.stream	Downstream	A(3mm)	B(6mm)	C(8mm)	Anode(11mm)	Anode'
GND	GND	GND	23.2	23.8	23.8	37.5	39.8
GND	GND	FLT	23.0	23.6	23.6	35.3	39.1
GND	FLT	GND	23.2	23.5	23.5	40.9	40.6
FLT	GND	GND	23.1	23.8	23.8	37.2	39.9
FLT	FLT	FLT	23.2	23.8	23.8	34.2	40.1

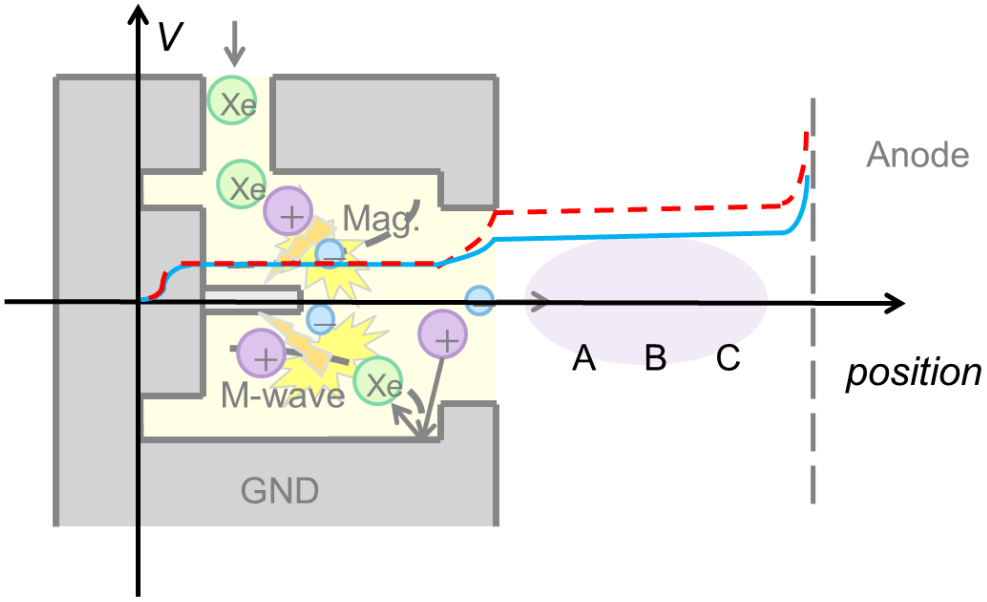

Figure5.21: Space voltage image of the floating orifice or not.

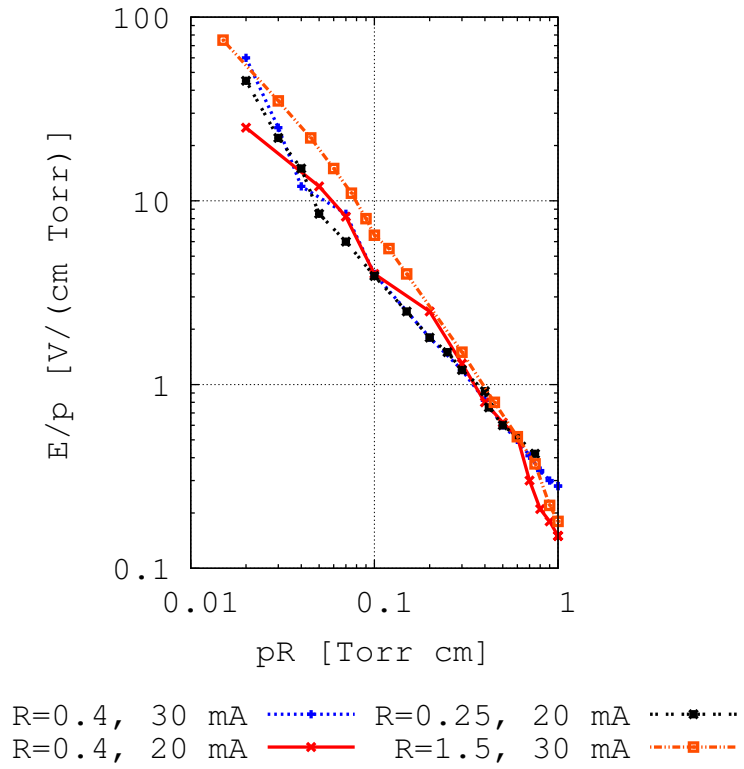

Figure5.22: The axial electric field as function of *pR*. [4]

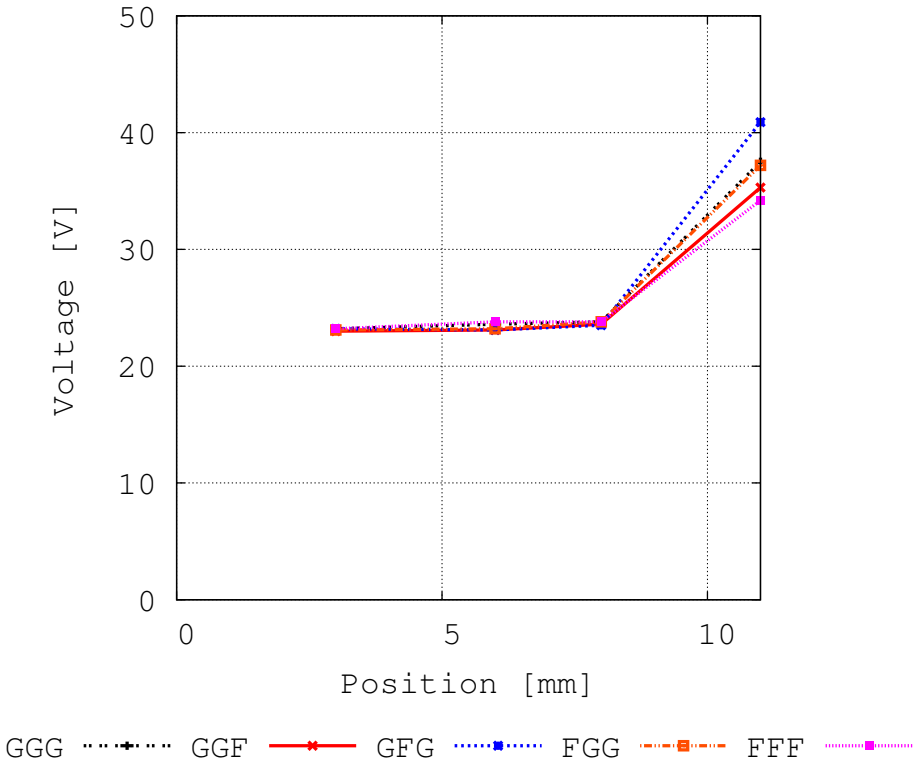

Figure5.23: The space voltage of the downstream.

5.2.3 Dielectric orifice neutralizer

Results of Fig.5.19, floating orifice plate all respectively is effective to the lower contact voltage. Floating the orifice plate all respectively is equivalent to replacing the orifice as the dielectric, as shown in Fig.5.24. The performance results for this redesign are shown in Fig.5.25. Replacing the molybdenum inner orifice plate with a dielectric is effective for reducing the contact voltage.

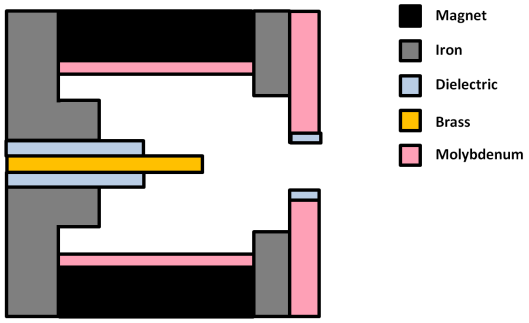

Figure5.24: Schematic diagram of the dielectric inner orifice plate neutralizer.

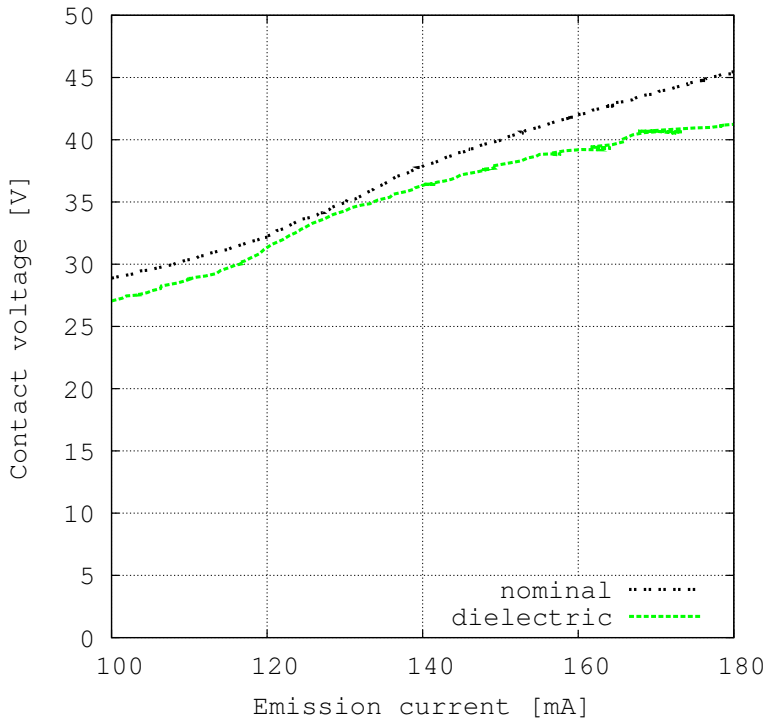

Figure5.25: Performance of the nominal neutralizer and the dielectric inner orifice plate neutralizer.

Discussion

The reason why the contact voltage becomes lower is the same as the floating orifice neutralizer. Dielectric surface is always floating. The low plasma loss results in the lower electric field, so that the space voltage of outlet of orifice decreases.

5.2.4 Stronger magnet

Assuming the Bohm sheath model, the ion current flux and the electron current flux to the wall are given as follows:

$$j_i = qe^{-\frac{1}{2}} n_0 \sqrt{\frac{kT_e}{m_i}} \tag{5.2.2}$$

$$j_e = \frac{1}{4} q n_0 v_e e^{\frac{-q\phi}{2kT_e}} \tag{5.2.3}$$

where j_i is the ion current flux A/m^2, j_e is the electron current flux A/m^2, q is the quantum of electricity, n_0 is the number density of plasma, k is the Boltzmann coefficient, T_e is the electron temperature, m_i is the mass of the ion, v_e is the electron speed, and ϕ is the space voltage. In order to increase the ion current flux and decrease the electron current flux, increasing the space voltage or the electron temperature is important. Therefore, we strengthen the magnetic field by 1.2 times in order to better confine the plasma. The net ion current distribution is shown in Fig.5.26. The ion saturation current is also shown in Fig.5.26 which is mentioned in Section 5.1.2. Fig.5.27 shows the results for the net ion current distribution of the neutralizer as a percentage, as follows $(each\,net\,ioncurrent)/(emission\,current)$. Fig.5.28 shows the results for the net ion current distribution density of the neutralizer. The performance varies as shown in Fig.5.29 and Fig.5.30. The higher magnetic flux density has a beneficial effect on suppressing the contact voltage.

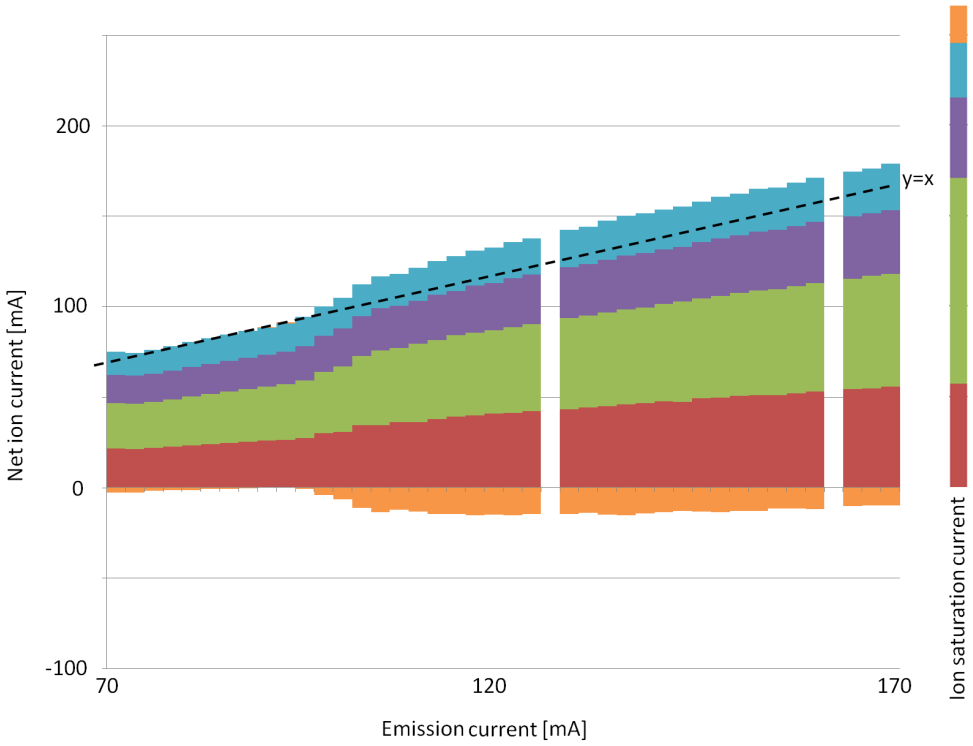

Figure5.26: Net ion current distribution of the neutralizer with a 1.2-times stronger magnet. The colors correspond to those described in Fig.5.1.

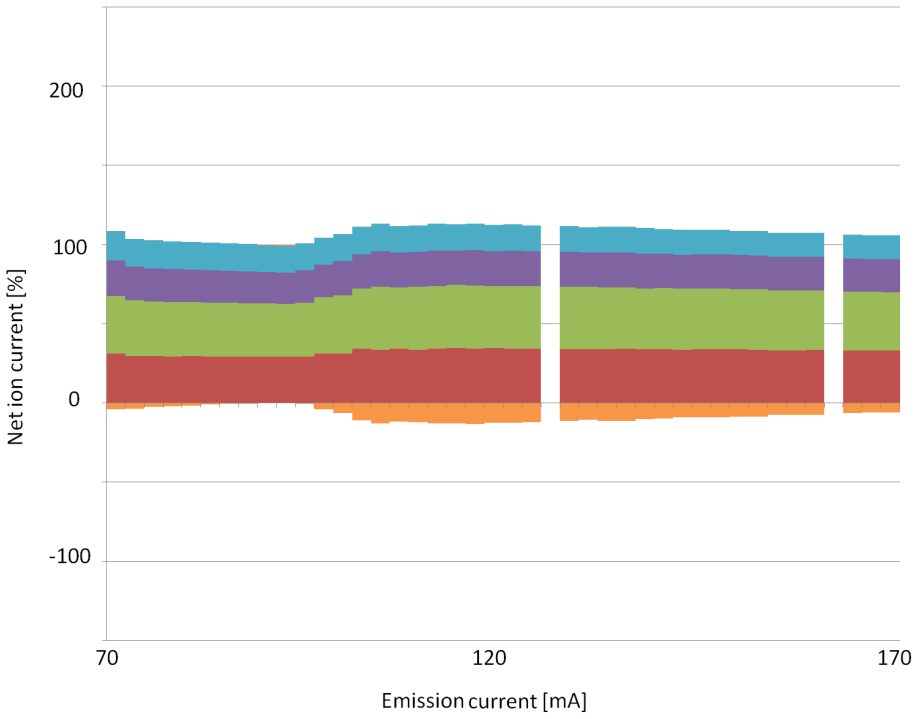

Figure5.27: Net ion current distribution of the neutralizer with a 1.2-times stronger magnet as a percentage. The colors correspond to those described in Fig.5.1.

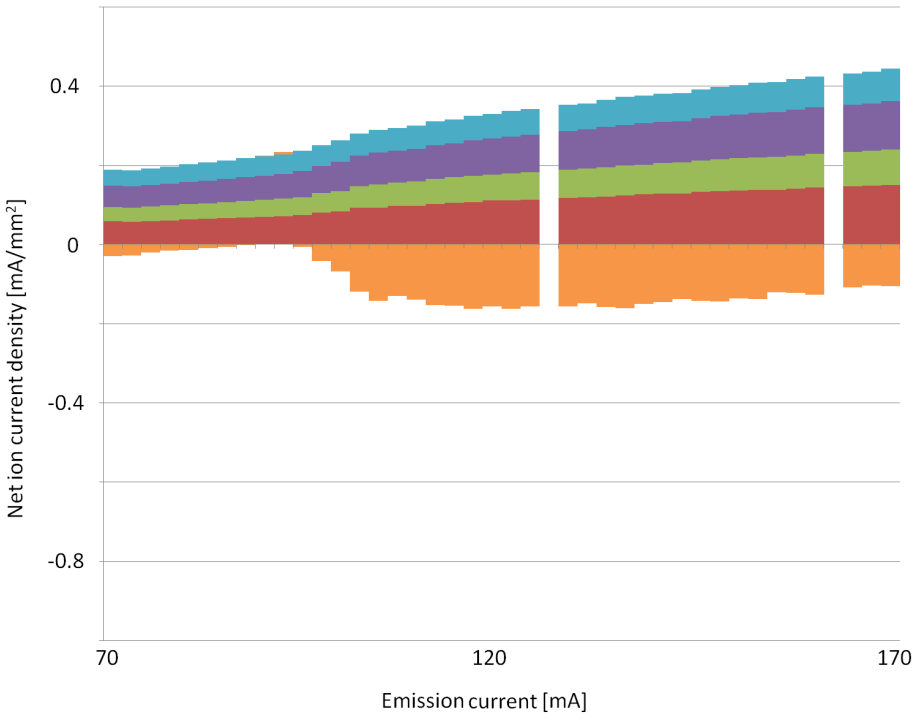

Figure5.28: Net ion current distribution of the neutralizer with a 1.2-times stronger magnet. The colors correspond to those described in Fig.5.1.

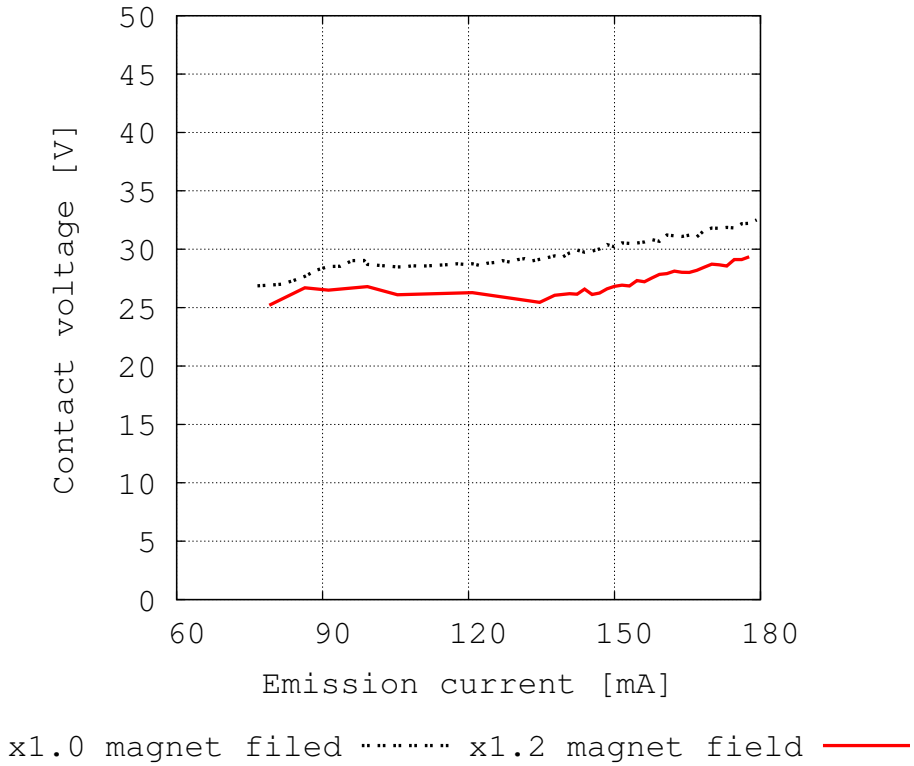

Figure5.29: Performance of the nominal neutralizer and the neutralizer with a higher magnetic flux density (0.5 *sccm*).

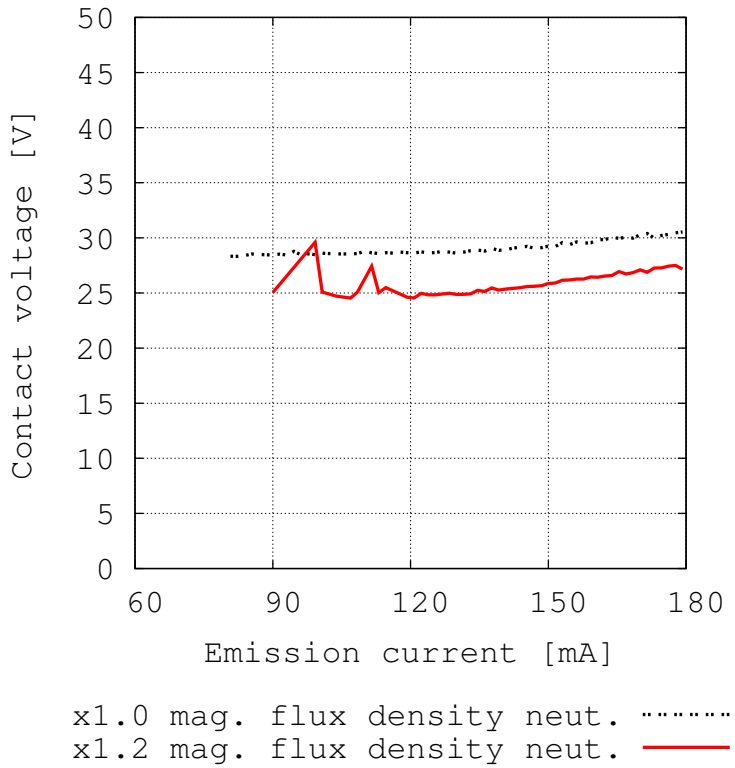

Figure5.30: Performance of the nominal neutralizer and the neutralizer with a higher magnetic flux density (0.7 *sccm*).

Discussion

Comparing Fig.5.26 and Fig.5.5, the electron current of the antenna and the net ion current of the sidewall decreased. Fig.5.31 shows the experimental results which are the same as the results in the Fig.5.29 and the calculated results which are shown in blue line. The blue line was plotted by the following: The blue line is contact voltage v.s. ion current. The ion current is calculated from Fig.5.5. For instance, at 120 mA emission current, the ion current is 120 minus the negative current, i.e., the antenna current. Thus, the ion current is 160 mA. In this case, the blue line is plotted with contact voltage of 120 mA emission current and the ion current of 120 mA emission current, i.e., 160 mA. In Fig.5.31, the blue line is equivalent to the red line. This results in the fact that the plasma generation performance is conserved in the both neutralizers. The neutralizer performance improved with suppressing the amount of electron current to the surface inside the neutralizer. This is explained by the following: Discussion form Section 5.1.2, the net ion current mainly changes in electron current to the surface. This results in the mobility of the electron suppressed. The reason for this is as follows: with the magnet field, diffusion coefficient and the mobility transverse to the magnetic line is

$$D_{\perp} = \frac{D}{1+\omega_H^2\tau^2} \tag{5.2.4}$$

$$\mu_{\perp} = \frac{\mu}{1+\omega_H^2\tau^2} \tag{5.2.5}$$

where $D_{\perp}$ is the diffusion coefficient transverse to the magnetic line, D is the diffusion coefficient without magnetic field, ω_H^2 as a cyclotron frequency, τ is a mean time between collisions, $\mu_{\perp}$ is the mobility transverse to the magnetic line, and mu is a mobility without magnetic field.

ω_H^2 is approximately $1\times10^9 Hz$, if τ is larger than $1\times10^{-8}s$, $D_{\perp}$ and $\mu_{\perp}$ increase as the inverse square of magnetic fulx density. Now we estimate the minimum of τ.

$$\tau = \frac{1}{vN\sigma} \tag{5.2.6}$$

where, v is thermionic velocity of electron m/s, N is the number density of neutral particle m^{-3}, and σ is cross section of elastic collision m^2. Assuming the electron temperature as 10 eV, pressure as 1 Pa, and σ as $4\times10^{-19}m^2$ [47], the τ is $4.9\times10^{-9}s$. It is less than $1\times10^{-8}s$, but when ω_{H^2} is approximately $1\times10^9 Hz$, $\omega_H^2\tau^2$ is 25. This results in $D_{\perp}$ and $\mu_{\perp}$ increase as the inverse square of magnetic flux density with less than $\frac{1}{25}$ error. By increasing magnetic field ad 120%, the mobility decreases to approximately 70 %.

In addition to this, the plasma confinement also improved. This is explained by the following. The plasma leakage is proportional to the line cusp area. The line cusp area is the product of magnetic circuit tip perimeter and the cusp width. Where cusp width is the twice of the geometric mean of ion Larmor radius and electron Larmor radius [48].

As a result,

1. The plasma confinement was improved, so that the distance between the plasma and the wall surface increased.
2. The electron current, which was collected by the antenna, was reduced.
3. The electron current collected by other assemblies were also decreased.

The neutralization cost of the normal neutralizer and 1.2 times higher magnetic flux density neutralizer are calculated as the following: The neutralization cost of 180 mA in Fig.5.29, the former neutralizer is $(8+33\cdot0.18)/0.18 = 77\ W/A$ using 1.5.2. Considering the anode fall which is mentioned in Section 3.4, the cost is 69 W/A. The latter neutralizer neutralization cost of 180 mA in Fig.5.29, is $(8+30\cdot0.18)/0.18 = 74\ W/A$. Considering the anode fall, the cost is 66 W/A.

This is equivalent to the cost which is discussed in Section 1.5, results in the the fact that the 1.2 times higher magnetic flux density neutralizer is operated in almost maximum theoretical performance. Fig.5.32 shows the neutralization cost and gas utilization efficiency of the latter neutralizer. The blue and red line are the same as the Fig.1.10.

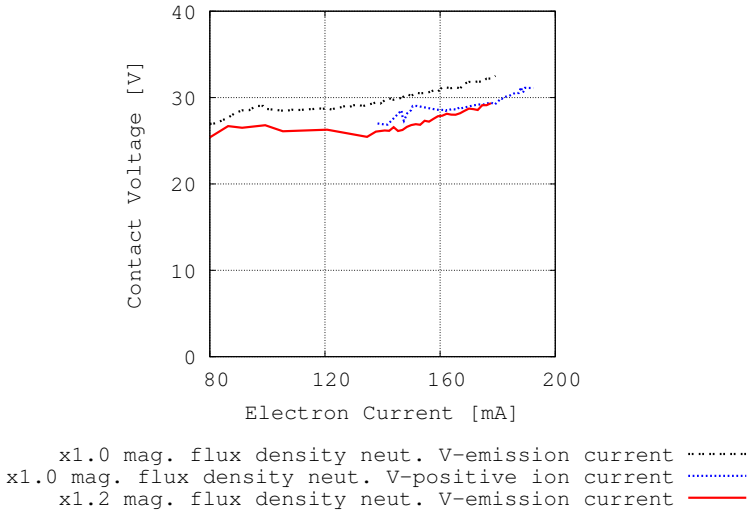

Figure5.31: Relationship between the performance of the nominal neutralizer and the neutralizer with a higher magnetic flux density (0.5 *sccm*).

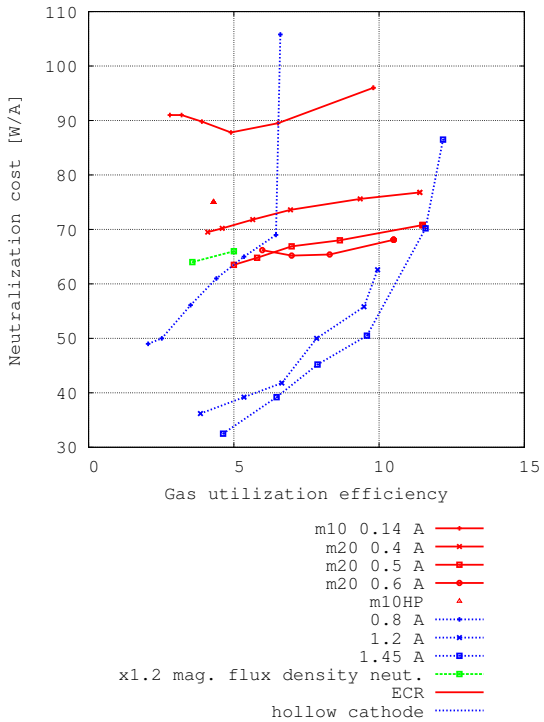

Figure5.32: Neulization cost v.s. gas utilzation efficiency of higer magnetic flux density neutralizer and the other cathodes. [3]

5.3 Summary

The net ion current distribution measurement method revealed the neutralizer performance is determined by the amount of electron current to the surface of inside the neutralizer, because the ion current to the surface of inside the neutralizer is constant in the variation of contact voltage. This results in the degradation rate by sputtering only determined by contact voltage, i.e., sputtering voltage, not determined by electron emission current of the neutralizer. The net ion current distribution measurement method also revealed that refurbishing antenna and orifice condition result to the lower contact voltage. Table 5.5 lists the results of measures taken to realize a lower contact voltage.

Table5.5: Results of countermeasures to realize lower contact voltage.

Measure	Effects on the lower contact voltage	Reason
Floated antenna	Realized	Increases the electrons rejection which are absorbed to the antenna
Floating orifice	Realized	Low space voltage increase at orifice
Dielectric orifice	Realized	Low space voltage increase at orifice
Strengthen magnet	Realized	Suppressed the electron mobility

6 Lifetime enhancement

The principal cause of the performance degradation of the neutralizer is the contamination of the dielectric surface due to sputtering from flakes on the magnetic circuit. This degradation can be avoided by suppressing the sputtering by using a lower contact voltage and by inhibiting flakes formation. In this chapter, the lifetime enhancement procedure will be described. We conducted 10,000-hour class endurance tests in order to demonstrate the effectiveness of lowering the contact voltage and inhibiting flake formation.

6.1 Estimation of the neutralizer lifetime

The ion currents of each area are already revealed. The degradation rate can be calculated if we set the sputtering yield and the sputtering voltage. By using the degradation rate for the indicator, the lifetime is estimated. In this section, we will explain the association between calculation and experiment results will be explained.

6.1.1 Degradation rate measurement

We newly constructed a neutralizer and operated it for 600 hours. This experiment was conducted by diode mode, 135 *mA* of emission current, 0.5 *sccm* of operational gas flow rate, 35 *V* of contact voltage. Fig.6.1 graphs the degradation of the upstream magnetic circuit. In this operation, we measured the upstream magnetic circuit weight four times, before operation, after 171 hours, 460 hours, and 582 hours of operation. In order to measure the weight, we ceased the operation and disassembled the neutralizer. After measurement, we reassembled the neutralizer.

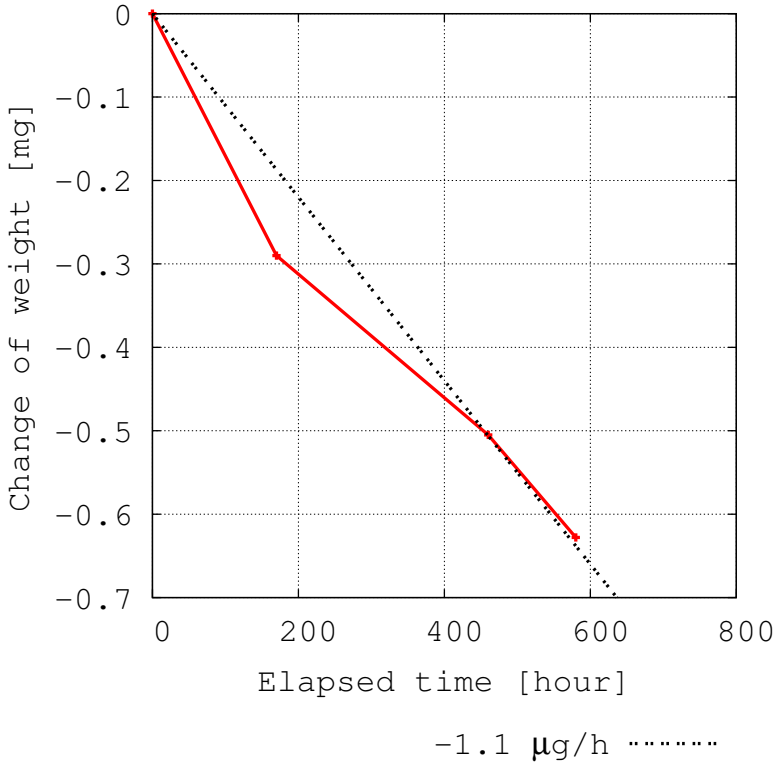

Figure6.1: Variation in upstream magnetic circuit weight measurement.

6.1.2 Discussion of flake forming speed

Now, we can calculate the degradation rate using the ion current density. The upstream magnetic circuit ion current distribution density is approximately 0.112 mA/mm^2. The ratio of singly ionized ion and doubly ionized ion number density in the neutralizer is 470:1 shown in Table 1.7, with the assumption which the ratio of them is the same as the outside the neutralizer in entire area. Using sputtering yield of Yamaura et.al [38] which is shown by Fig.6.2, assuming the sputtering voltage of singly ionized ions to be the contact voltage and the sputtering voltage of the doubly ionized ions to be twice the contact voltage, the upstream magnetic circuit degradation rate is shown in Fig.6.3. We call this as a calculated degradation rate. When the sputtering voltage is less than 35 V, degradation due to doubly ionized ions is dominant. Now, we assume the sputtering voltage inside the neutralizer as the contact voltage in coupling mode operation. From the Fig.3.6 in 3.4, the contact voltage of the diode mode at 135 mA is 5 V less than coupling mode. We assume the sputtering voltage of this experiment as 30 V. This assumption is likely by following reason. The space potential of outside the neutralizer to the anode is measured in Section 5.2.2 and it is shown in Fig.5.23. There are anode fall in Fig.5.23 and the difference of the contact voltage of the diode mode and coupling mode due to this anode fall. The thickness of the anode fall area is significantly thin. The ionization due to the collisions between electrons and neutral particles are not active due to the thickness. This anode fall do not contribute to the degradation of the neutralizer. By this assumption, the calculated degradation rate which is shown in Fig.6.3 is 3.2-times greater than the real degradation rate, which is shown in Fig.6.1. It results that 67 % of the sputtered particles were reattached. These particles are from not only the upstream magnetic circuit but also the other areas, such as the side wall. In these calculations, we used the initial surface area of the magnetic circuit. The change in the surface area by sputtering is negligible because it is less than 3 %, as explained in 2.2.

However, the surface area also changes with the formed flakes. The average size of the flake was about 1 *mm* square. There were hundreds of flakes, and the surface area of the flakes are equivalent to the surface area of the magnetic circuit and it is approximately 25 % of total surface area of the neutralizer. This results in the degradation rate, which is shown in Fig.6.1 being 50 % faster.

The reason of the calculated degradation rate was 3.2-times greater than the real degradation rate is explained as follows. Set the model as Fig.6.4. In Fig.6.4, we assumed there are only two parts inside the neutralizer, the iron part and the molybdenum part. We also assumed the sputtering only occurs to the iron. This means sputtering voltage is less than 25 V. f_f is the weight of the iron particles ejected from the iron part per unit time, and f_m is the weight of the iron particles ejected from the molybdenum part per unit time. The latter ejection only occurs when the iron was accumulated on the molybdenum part. r is the probability of reattachment to the iron part. We assumed the neutralizer is isolated from the outside so that no particles are ejected from the neutralizer, because the area of the orifice is significantly small than the area of whole neutralizer. The weight variation per unit time of the iron part dFe are the summary of the degradation and the accumulation so that it can be written by

$$dFe = (f_f + f_m)r - f_f \tag{6.1.1}$$

also the molybdenum part dMo can be written by

$$dMo = (f_f + f_m)(1-r) - f_m \tag{6.1.2}$$

From the parameter of 135 mA in Fig.5.5, $f_f = \frac{55}{80} f_m$. Thus

$$dFe = (1.6875r - 1) f_f \tag{6.1.3}$$

Now, r is associated with the ratio of iron area and molybdenum area assuming the phenomena of reattachment is the same between them. r is approximately 0.4, so that $dFe = -0.325 f_f$. This result is well accorded with the fact of calculated degradation rate was 3.2-times greater than the real degradation rate. In addition to this, average accumulation rate of the molybdenum parts is $(f_f + f_m)(1-r) = 1.47 f_m$. The principal cause of the performance degradation of the neutralizer is the contamination of the dielectric surface due to sputtering from flakes on the magnetic circuit. This flakes are mainly peeled off from the molybdenum surface, so that dMo is an important indicator of the lifetime.

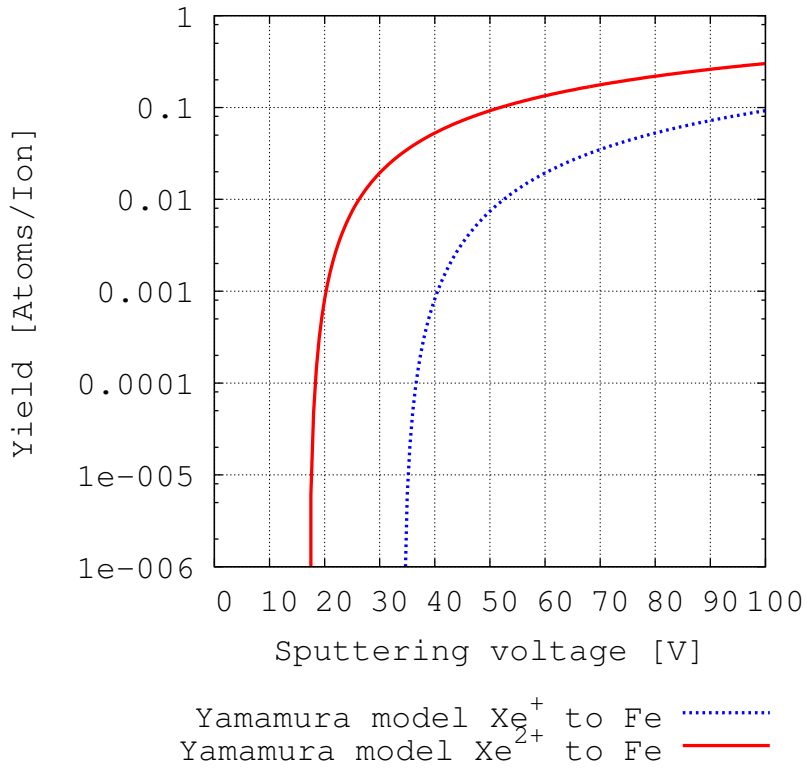

Figure6.2: Sputtering yield ratio of iron.

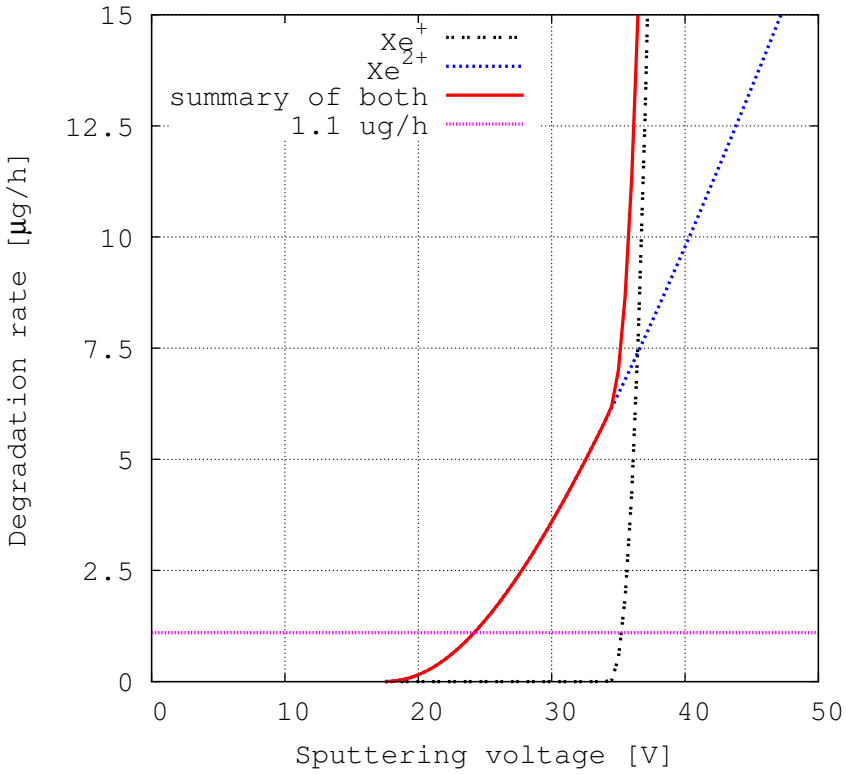

Figure6.3: Degradation rate of the upstream magnetic circuit.

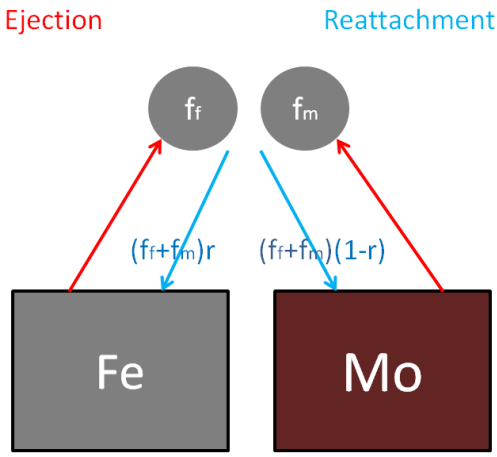

Figure6.4: Model of sputtering and reattachment.

6.1.3 Indicator of the neutralizer lifetime

Using the discussion of 6.1.2, the degradation rate of the 20,000-hour endurance test which is shown by Fig.2.4 can be calculated. The integral of the dMo ((6.1.2)) in the operation time is calculated as Fig.6.5. Now we define the integral of the dMo as the accumulated metal. The accumulated metal in 20,000-hour is 46 mg. It is approximately 4.9 mm^3, using the density of the flakes of approximately 9 g/cm^3, and it is compatible to the experimental results of Section 2.2. The weight of accumulated metal when the accumulation increases exponentially, i.e., accumulated metal of 18,000 hour is approximately 9 mg. Now we define 9 mg accumulated metal for the neutralizer lifetime. The reason we set the lifetime as 9 mg not as 46mg as follows. Once the performance degradation started, the neutralizer stops its function sooner or later. This indicator is reasonable when there are sufficient times of the thermal cycles and the maximum and the minimum temperature is equivalent to the prototype model endurance test using the discussion of 2.3.

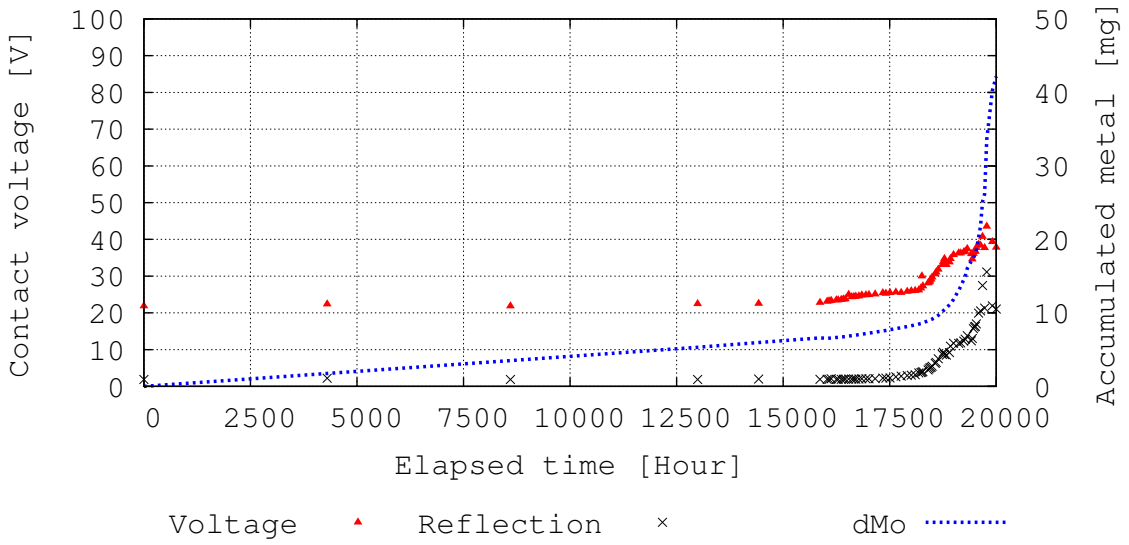

Figure6.5: Variation in parameters in 20,000-hour endurance test.

Discussion of repetition of accumulating and vanishing

By the way, 9 *mg* of accumulated metal is equivalent to $1.0mm^3$. The surface area of the molybdenum parts are approximately 1,000 mm^3, so that the average thickness of the film is $1.0\mu m$. This results in that the fact that the accumulation is occurred locally. This is because peeling mainly occurs when the thickness of the film is larger than 10 μm. The detail is explained by followings.

The formed films are vanished when the ion bombardment is strong. The expectation value of number of repetition of forming and vanishing is followings. Assuming sputtering only occurs to the iron but both iron parts and molybdenum parts, the expectation value of number of repetition E which attaches to the molybdenum part is

$$E = \sum_{1}^{\infty}(n-1)(1-r)^n \tag{6.1.4}$$

where n is the number of repetition. For instance, when n is two, the first formed film attaches to the molybdenum part. Its probability is $(1-r)$. Than it vanishes and attaches to the molybdenum again. Its probability is $(1-r)$. This means it reattached 1 time. When $r = 0.4$, $E = 2.8$. In this estimation, 2.8-time repetitions results into the accumulation of the low sputtering area on the molybdenum part. This accumulated iron forms the flakes which were attracted to the tips of the magnetic circuit and contaminate the surface of dielectric. This results in the performance degradation which was explained in Section 2.3.

6.2 Lower-contact-voltage neutralizer

The lower contact voltage is effective for mitigating the performance degradation. The measures for lowering the contact voltage are listed in Table 6.1. We strengthened the magnetic field in order to determine whether lowering the contact voltage will extend the lifetime of the neutralizer. We conducted preliminary experiments in order to make this determination.

Table6.1: Promising measures for reducing the contact voltage.

Measures	Reason
Floated antenna	Increase the electrons rejection which are absorbed to the antenna
Floating orifice	Low space voltage increase at orifice
Dielectric orifice	Low space voltage increase at orifice
Strengthen magnet	Suppressed the electron mobility

6.2.1 Extension of the lifetime of a lower-contact-voltage neutralizer: preliminary study

Lifetime discussion of floated antenna neutralizer

1.Degradation rate of floated antenna neutralizer

In the case of the floating antenna, the contact voltage will become several volts lower, but the antenna floating voltage is reduced by approximately 25 V which was explained in 5.2.1. This means that sputtering of the antenna will be increased. With respect to the endurance enhancement, there is a 5 V decrease in the contact voltage and a 25 minus 5 V increase in the sputtering voltage for the antenna. Since the antenna is constructed of molybdenum, it is higher resistance to sputtering than the other assemblies, which are made of iron. The degradation rate $\mu g/h$ are calculates under the following assumptions.

The ion current density of the antenna is 0.3 mA/mm^2 and the ion current densities of the other components are 0.1-0.187 mA/mm^2, based on the discussion in 5.1.2. The number density ratio of singly, and doubly ionized ions in the neutralizer is 470:1 as shown in Table 1.7. The sputtering voltage of the antenna for singly ionized ions is $Contactvoltage - 20$, and that for doubly ionized ions is $2 \cdot (Contactvoltage - 20)$ when the antenna is floating. Here, the electric field of the microwave, 3,000 V/m [49] is not considered, because the force due to the field affects the sputtering energy by only several percent. Using the sputtering yield ratio reported by Yamamura et al. [38], the molybdenum [5], the iron, nickel, and tungsten sputtering yield results in Fig.6.6, Fig.6.2, Fig.6.7, and Fig.6.8. Fig.6.9 results the difference of the sputtering rate between grounded and floated antenna. This is the calculated degradation rate. From the discussion in 6.1.2, average accumulation rate is 147 % of average degradation rate of molybdenum part. The average ion saturation current of molybdenum part is 0.16 mA/mm^2 based on the discussion in 5.1.2 and considering the surface area. This results in the net degradation rate as the $-0.3+1.47\times0.16=-0.065$, so that the net degradation rate is approximately quarter (-0.065 /0.3) of the Fig.6.9 and it is shown in Fig.6.10. The lines which indicate 10,000 and 20,000-hour lifetime are the degradation rate which the antenna size will be the 75 % in those times, assuming the antenna lifetime is determined by the antenna size. Fig.6.11 shows the expected lifetime, i.e., the time to be 75 % of the antenna size, with variation of sputtering voltage. To endure 20,000-hour operation, keeping the sputtering voltage, i.e., contact volate of coupling mode less than 32 V is required. Assuming the lifetime of the antenna is determined by 80, 85, 90, and 95 % of its size, the lifetime is 90.4 %, 81.6 %, 73.1 %, and 64.4 % to the lifetime of the 75 %. The reasons of the lifetime are not $\frac{75}{80}$, $\frac{75}{85}$, $\frac{75}{90}$, and $\frac{75}{95}$ to the lifetime of the 75 % are that

the sputtering rate is proportional to the surface area of the antenna, and it gets smaller when the volume gets smaller. For summary, when the antenna is grounded, lifetime is limited by accumulated metal, i.e., flakes forming, and when the antenna is floated, it is also limited by antenna lifetime. There are 5-15% errors in lifetime due to Yamamura model.

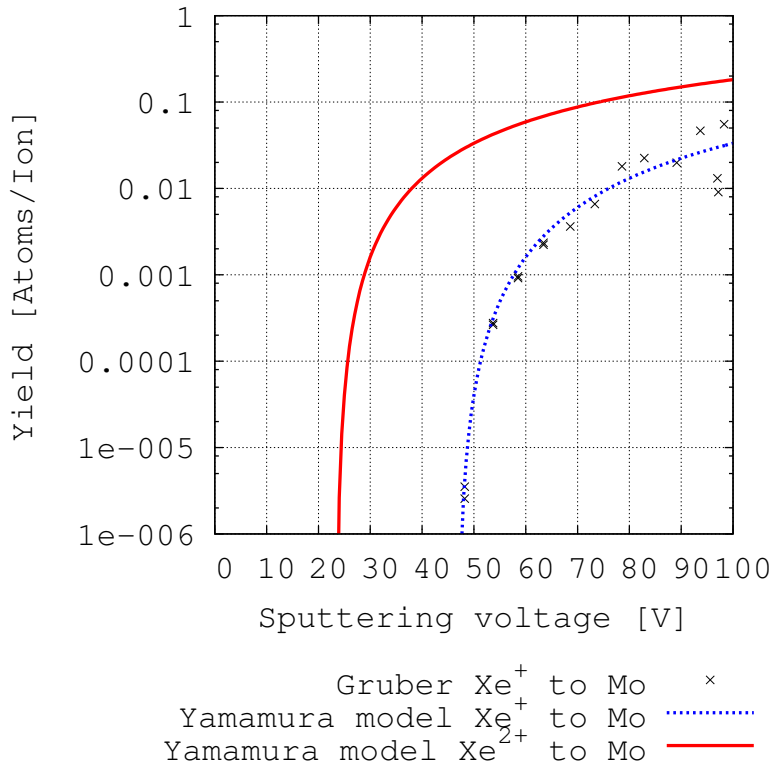

Figure6.6: Sputtering yield ratio of molybdenum. [5]

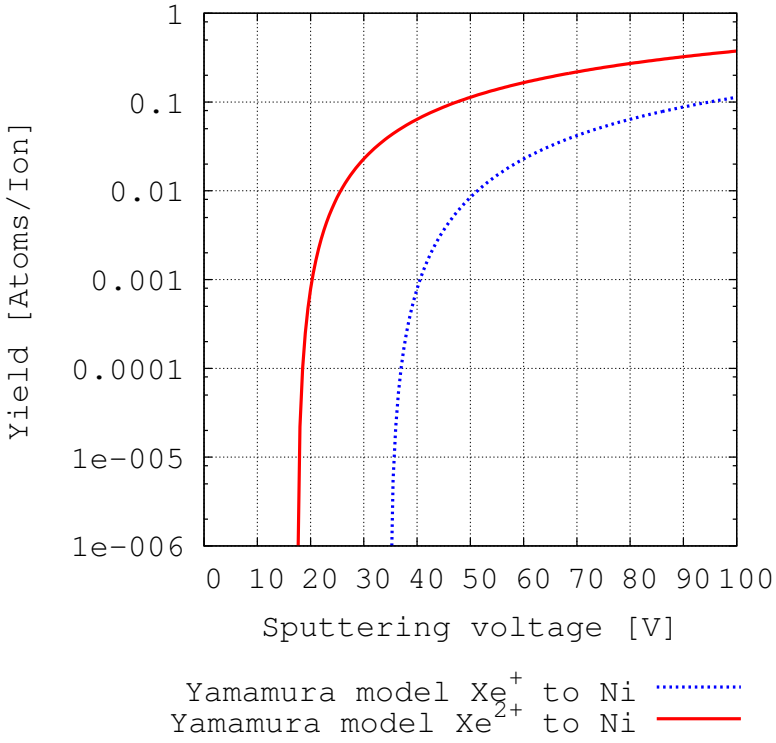

Figure6.7: Sputtering yield ratio of nickel.

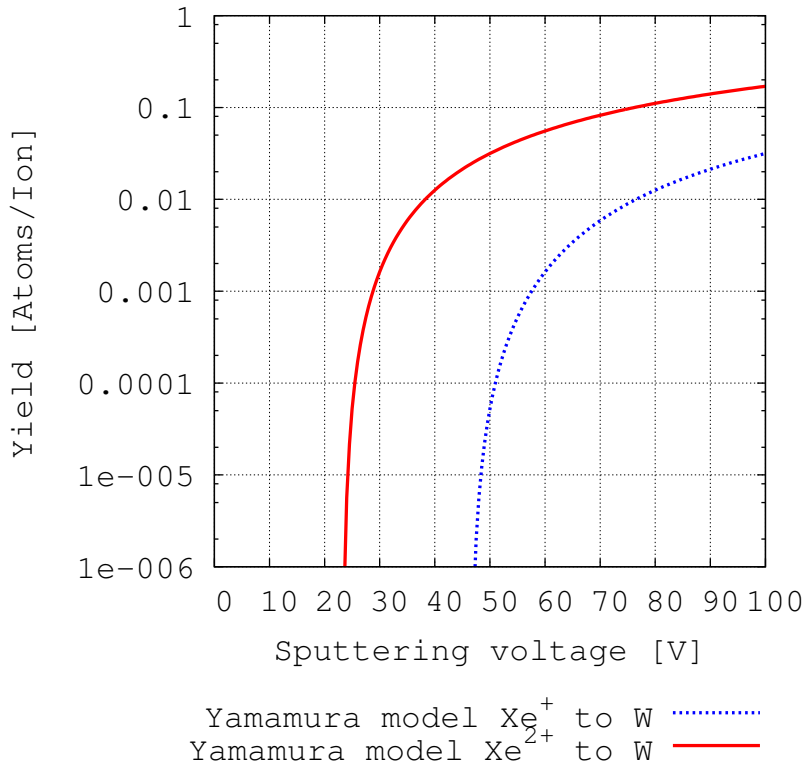

Figure6.8: Sputtering yield ratio of tungsten.

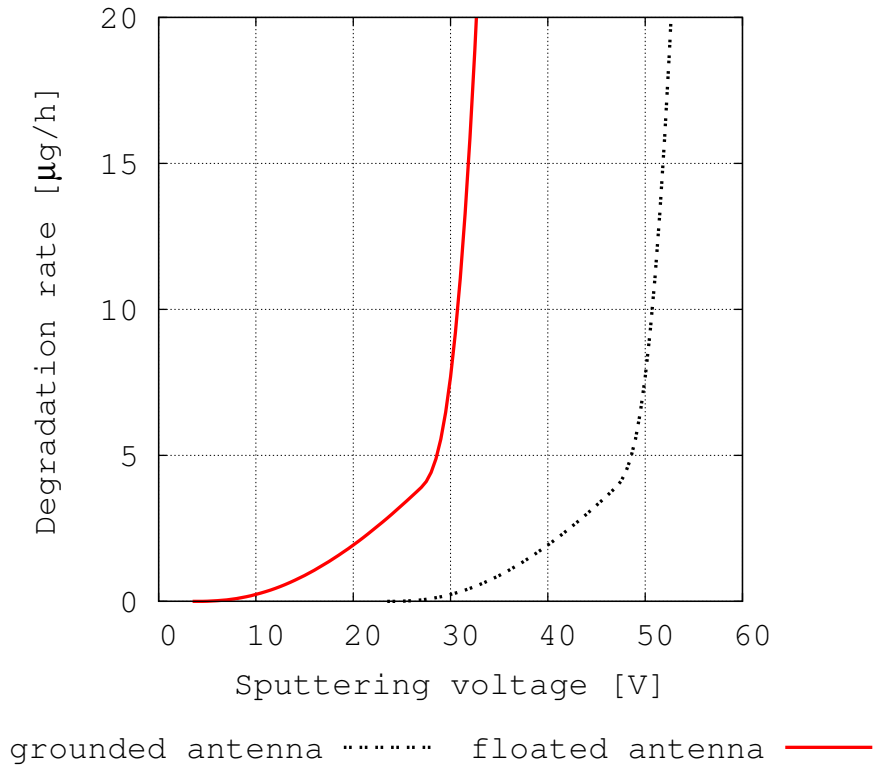

Figure6.9: Difference in calculated antenna weight degradation rate with antenna conditions.

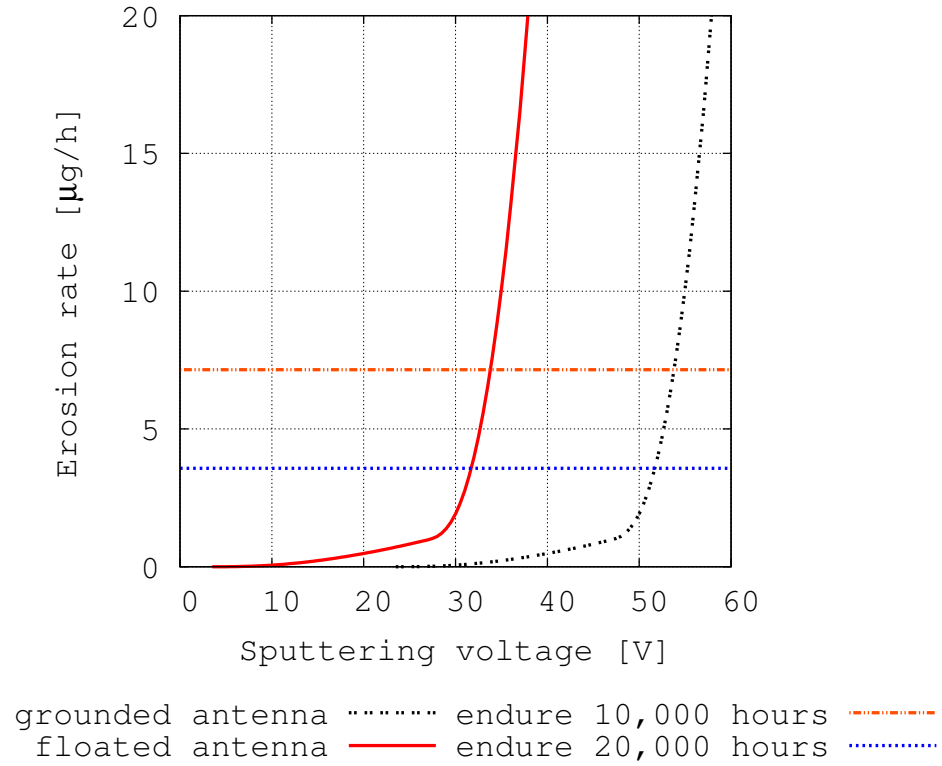

Figure6.10: Difference in net antenna weight degradation rate with antenna conditions.

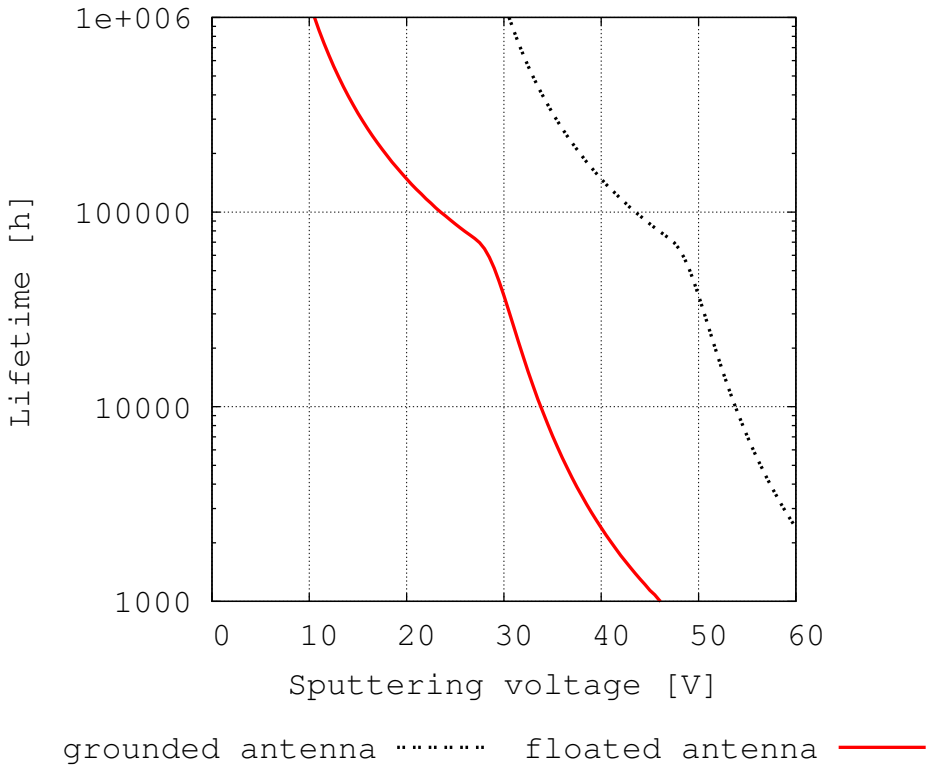

Figure6.11: Expected antenna lifetime with antenna conditions.

2.Plasma cleaning of the dielectric surface

As we explained in 2.3, and 6.1.2, there are ion bombardments to the entire surface inside the neutralizer. If the ion bombardments rate is greater than accumulation rate, the surface is kept clean. In this section, we discuss about the plasma cleaning of the dielectric surface when the antenna is floated.

In the 6.1.1 experiment, the dielectric surface was kept clean. The ion bombardment rate of the surface is equivalent to the ion bombardment rate of the nearby upstream magnetic circuit. This ion bombardment rate is the calculated degradation rate which was explained in 6.1.2, and it is approximately 3.3 $\mu g/h$. Thus, the surface kept clean while the accumulation rate is less than 3.3 $\mu g/h$. However, when the antenna is floated, the degradation rate of the antenna increases which is shown in Fig.6.9, and it results in the greater contamination rate. To sustain the degradation rate less than 3.3 $\mu g/h$, the 24 V contact voltage is required at a maximum. From this reason, the floated antenna also does harm to the lifetime.

From discussion of 6.2.1 and this, it is concluded that the floated antenna neutralizer endurance is worse than the grounded antenna neutralizer.

Lifetime discussion of floated orifice and dielectric orifice neutralizer

From discussions of Section 2.3, and 6.1.2, the sputtering voltage inside neutralizer is dominant to the neutralizer lifetime. By floating orifice, the sputtering voltage is reduced, so that there is no injurious effect on the lifetime.

Lifetime discussion of stronger magnetic field neutralizer

1.Experimental result in the degradation rate and magnetic field

Fig.6.12 shows the weight change of upstream magnetic circuit depending on the magnetic force. This experiment was conducted as explained in 6.1.2. As Fig.6.12 shows, the stronger magnetic force decreases the rate of degradation, which means that strengthening the magnetic force does not adversely affect the lifetime of the neutralizer.

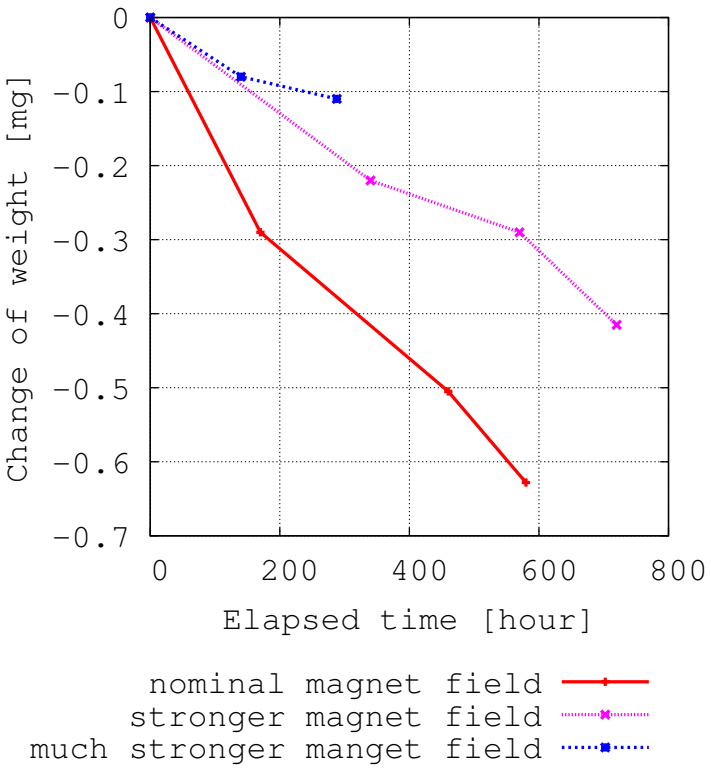

Figure6.12: Change in upstream magnetic circuit weight.

2.Experimental result in the effects of flakes and the magnetic field

The experiment described in Section 4.2 was conducted in a strong magnetic field. According to Fig.6.13 and Fig.6.14, higher magnetic flux density has a beneficial effect on the performance degradation caused by the flakes.

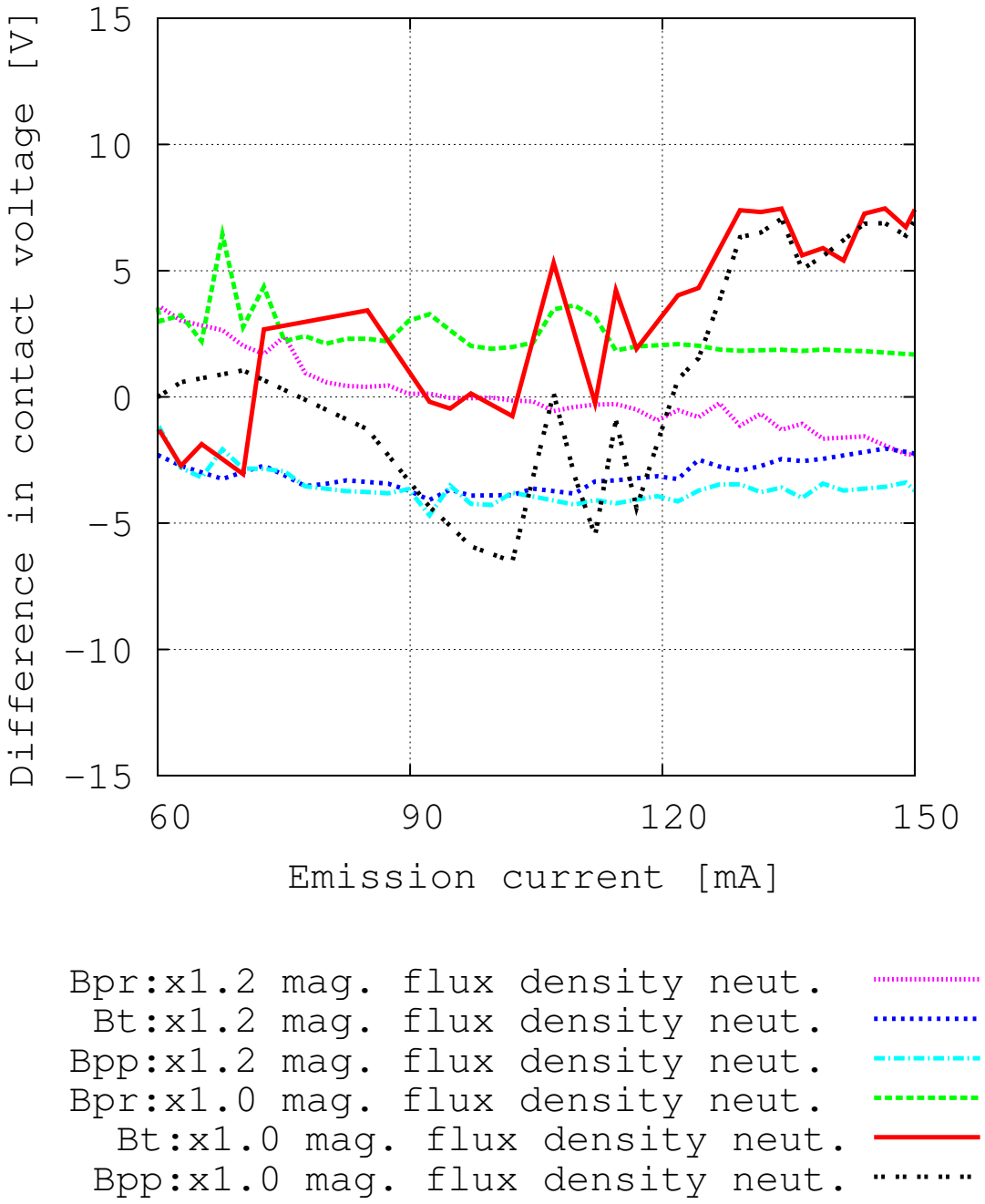

Figure6.13: Flake effects and magnetic field (0.5 sccm).

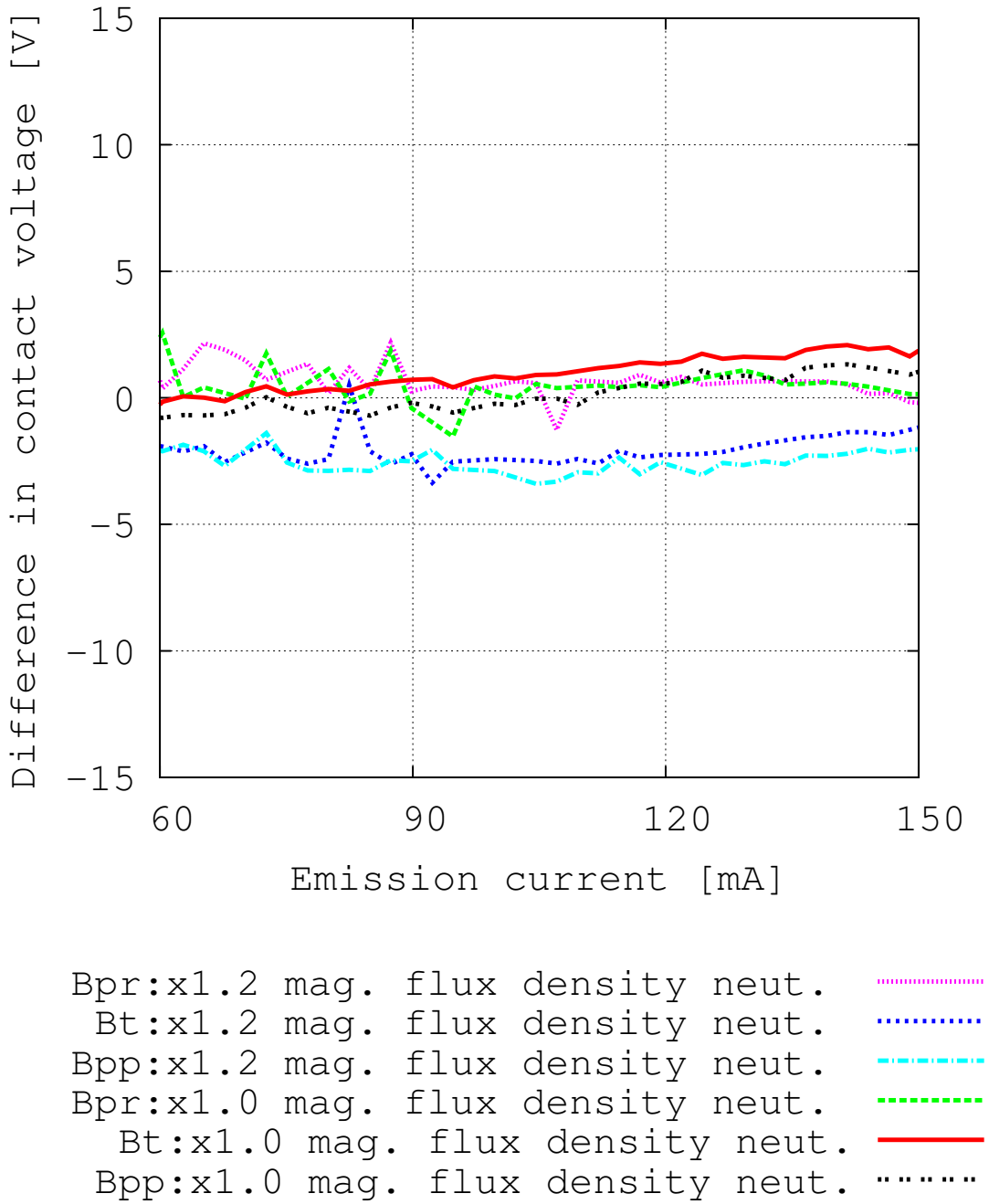

Figure6.14: Flake effects and magnetic field (0.7 sccm).

6.2.2 Demonstration of lower-contact-voltage neutralizer lifetime enhancement: endurance test

Experimental results

As indicated by the results shown in Sections 5.2.4, 6.2.1, and 6.2.1, strengthening the magnetic field appears to be effective for extending the lifetime of the neutralizer. Based on these facts, we conducted an endurance test using a $\times 1.15$ stronger magnet neutralizer. Fig.6.15 shows the result of the endurance test. The endurance test was conducted under the following conditions: The operational gas flow rate is 0.7 *sccm*, and the input microwave power is constant at 8 W. At the start of the week, the neutralizer has stopped for thirty minutes, and its temperature was approximately 5 degrees Celsius. There was no performance degradation after 12,000 hours of operation, and the contact voltage was constant at 30 V.

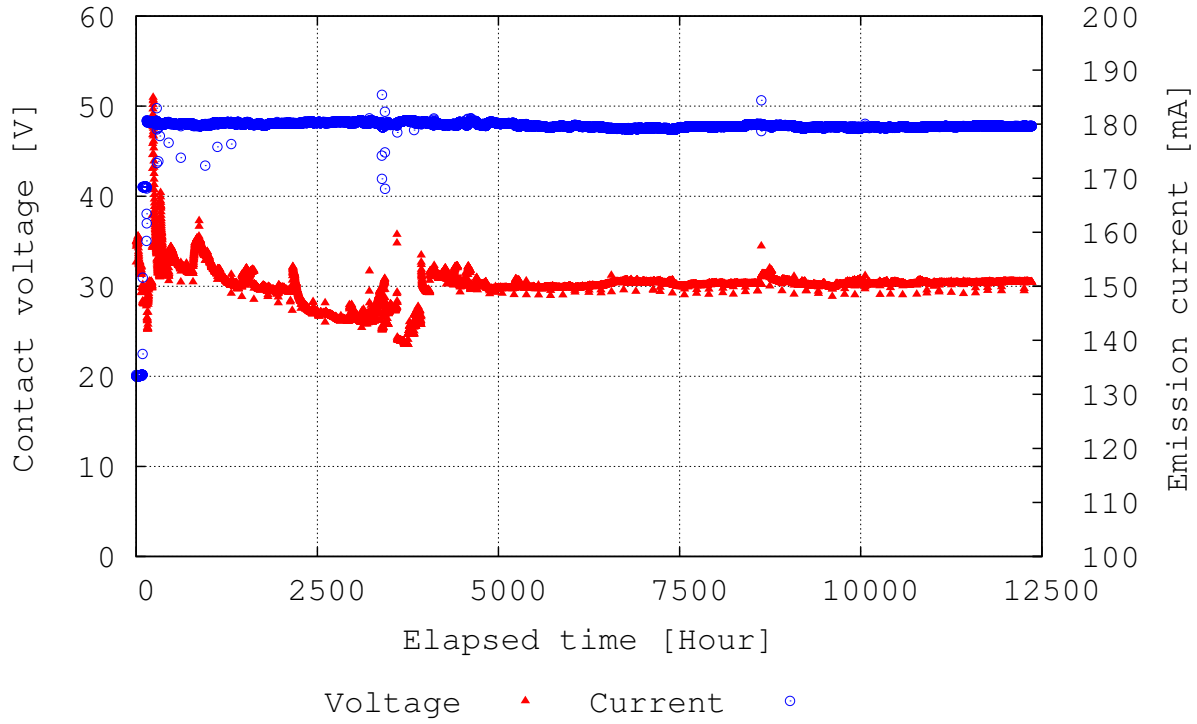

Figure6.15: Performance transition of the $\times 1.15$ stronger magnet neutralizer.

Discussion

The contact voltage of the endurance test was 30 V when the emission current was 180 mA. This seems significantly greater than the 20,000-hour endurance test Fig.2.4, so that the lifetime seems to be shorter than 20,000-hour. This is not correct. From the Fig.3.6 in Section 3.4, the contact voltage of the diode mode at 135 mA 0.7 $sccm$ is 5 V less than the coupling mode. The contact voltage of the diode mode at 150 mA 0.7 sccm is 5 V less than the coupling mode, and at the 165 mA it is 7.5 V less than the other. We assume the contact voltage of 180 mA 0.7 $sccm$ which is the condition of this experiment is less than 22.5 V. This assumption is likely by the reason which was discussed in 6.1.2. Fig.6.16 shows the sputtering rate with the variation of the sputtering voltage. Fig.6.17 shows the expected lifetime with the variation of the sputtering voltage. When the sputtering voltage is 22.5 V, it reaches the 9 mg of the accumulated metal in 22,000-hour. This neutralizer also has an advantage in minimizing the redesigning of the neutralizer from the flight model which has achieved 10,000-hours of space operation. The errors of the expected lifetime are due to the following.

1. The errors due to the sputtering model. Yamamura model has 5-15% difference to the experimental results [5].
2. The errors due to the estimation of the anode fall due to the difference between coupling mode and the diode mode. Anode fall gap is several V.
3. The errors due to the ion saturation current errors.
4. The errors due to the peeling mechanism.

The first errors are reduced by using more resonable sputtering model. The second errors are reduced by obtaining the precise anode fall gap in the same neutralizer. The ion saturation current were measured only at the antenna and at the orifice plate. The currents of others are assumued the same as the orifice plate. In addition to this, the ion saturation current includes the secondary electron current caused by ion, excited particle collision against the surface. This results in expecting 0.8 % lifetime shorter [33]. The forth errors are reduced by controlling the operating temperature and operating with the sufficient number of thermal cycles. However, the peeling mechanism which was mentioned in Section 2.3 is not entirely true with the phenomena in the neutralizer, and further verification is needed.

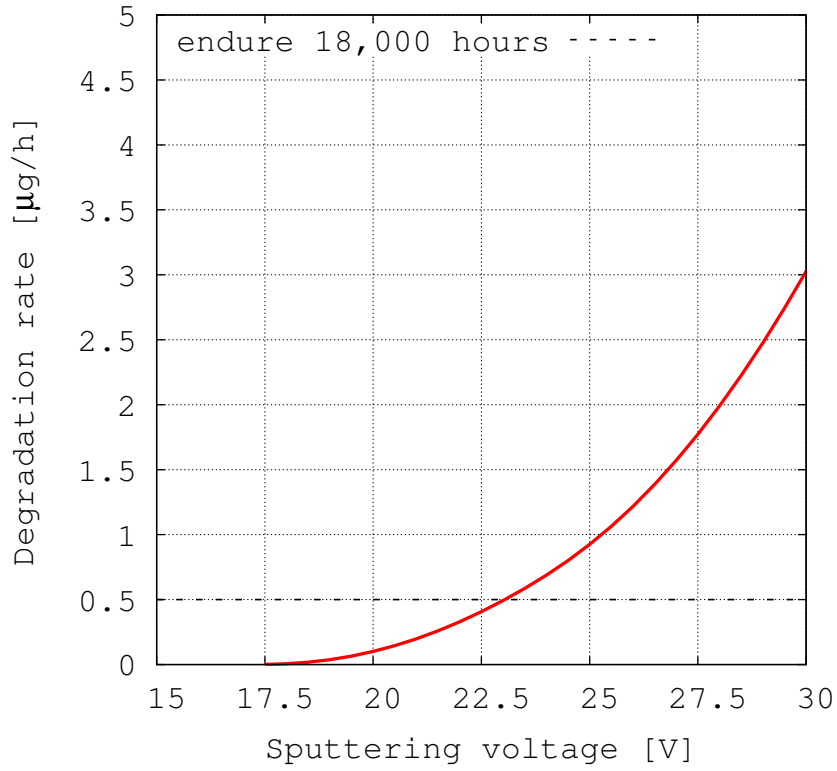

Figure6.16: Sputtering rate of the ×1.15 stronger magnet neutralizer.

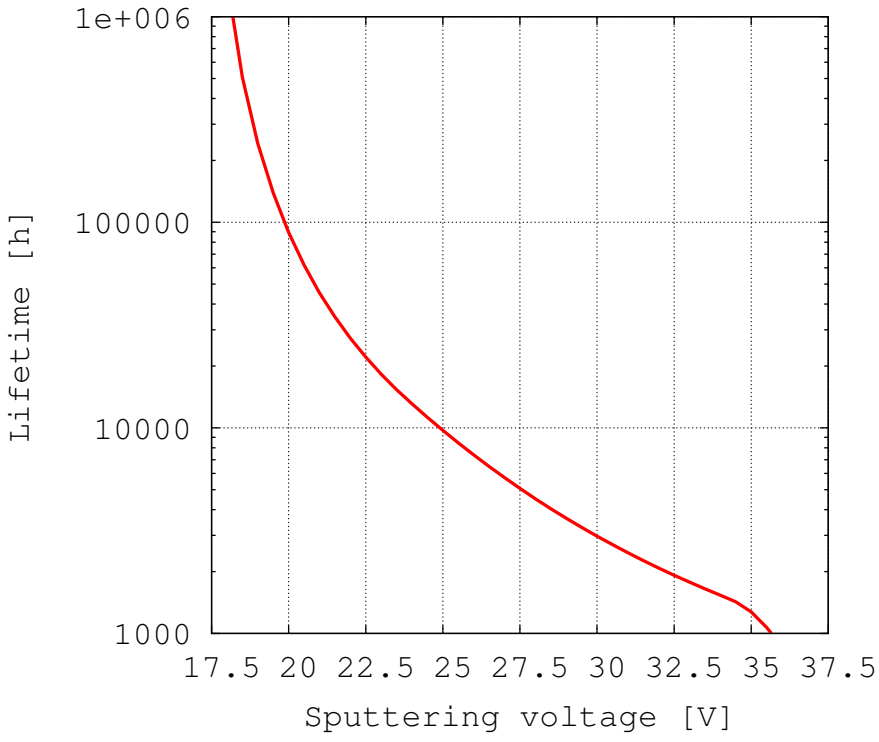

Figure6.17: Expected lifetime of the ×1.15 stronger magnet neutralizer.

6.3 Molybdenum-covered neutralizer

In order to mitigate the performance degradation, bombardment by doubly ionized xenon ions results in ferromagnetic flakes at the magnetic circuit tips. This degradation can be avoided by increasing the resistance of the surfaces of the magnetic circuit to sputtering by using doubly charged ions. Coating the surfaces of the magnetic circuit with molybdenum should be effective because molybdenum has a high threshold energy of 50 eV for xenon sputtering, compared to 30 eV for iron [38] In addition, if sputtering does occur, thin films of molybdenum will be produced on the sidewalls of the discharge chamber. Since the sidewalls are made of the same material, there is no difference in thermal expansivity, so that thermal cycling is unlikely to cause the films to peel off. Finally, even if the thin molybdenum films do exfoliate into flakes, they will not be attracted to the magnetic circuits because they are nonmagnetic.

6.3.1 Demonstration of non-flake neutralizer lifetime enhancement: Preliminary study

A molybdenum cover of 300 μm in thickness was manufactured for a preliminary study. Fig.6.18 shows the nominal neutralizer, and Fig.6.19 shows the newly designed neutralizer.Fig.6.20 shows the performance of neutralizers with and without molybdenum covers. The resulting voltage-current characteristics are worse with covers because the mirror ratio $(edge/ECRarea)$ was decreased to confine plasma. The magnetic field is strengthened so that the magnetic field is the same at the edge of the cover, which is indicated by the green circle in Fig.6.19, and at the edge without the cover, which is indicated by the green circle in Fig.6.18, and the resulting voltage-current characteristics are plotted in Fig.6.21. The performance is identical to the original neutralizer which lacks a molybdenum cover. As mentioned in 6.2.1, the stronger magnetic force suppresses the degradation rate. This means that strengthening the magnetic force does not adversely effect endurance. The covered neutralizer was tested for 400 hours. The covered neutralizer maintained an emission current of 135 mA at a contact voltage of 35 V. After the test, the molybdenum cover was found to have lost 0.5% of its weight. Such a molybdenum cover is predicted to extend the lifetime of the neutralizer by several tens of thousands of hours.

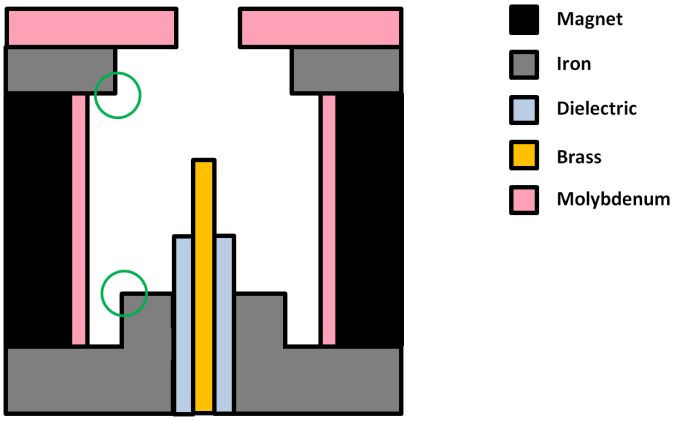

Figure6.18: Schematic diagram of the nominal experimental neutralizer.

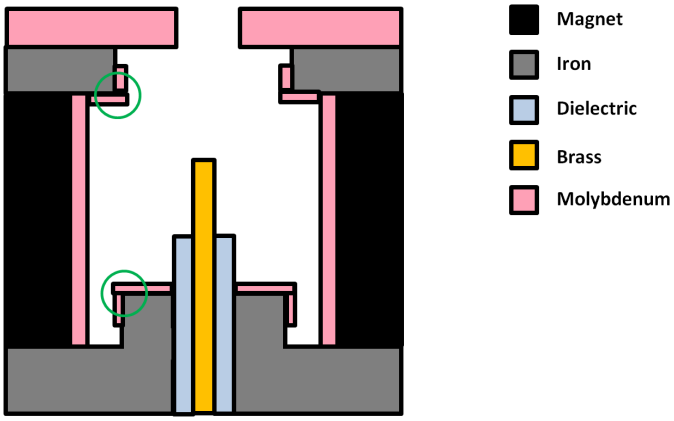

Figure6.19: Schematic diagram of the molybdenum covered neutralizer of the preliminary study.

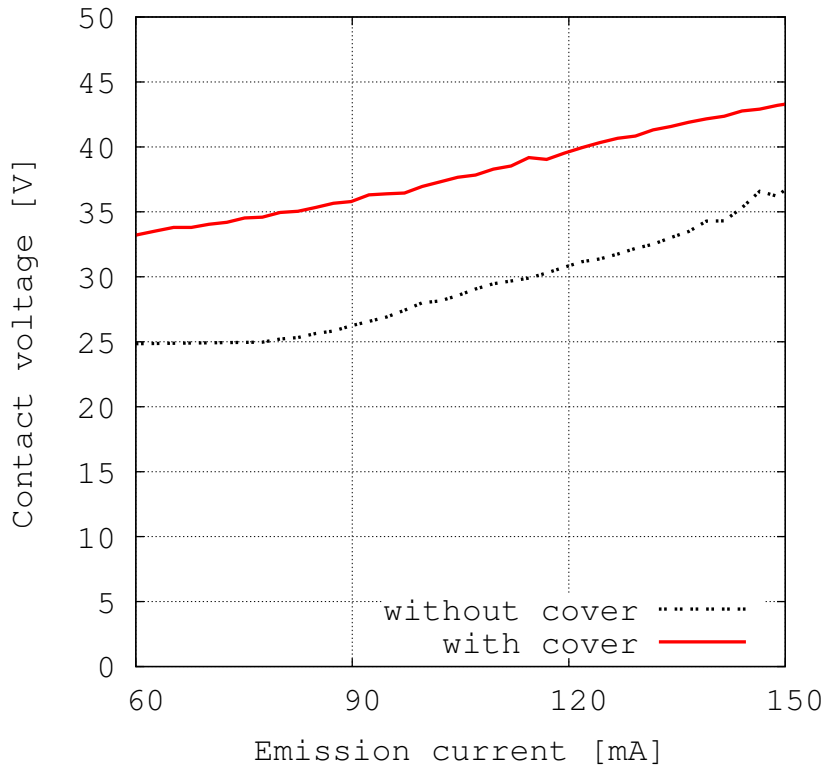

Figure6.20: Performance of neutralizers with and without a molybdenum cover. Normal magnetic force.

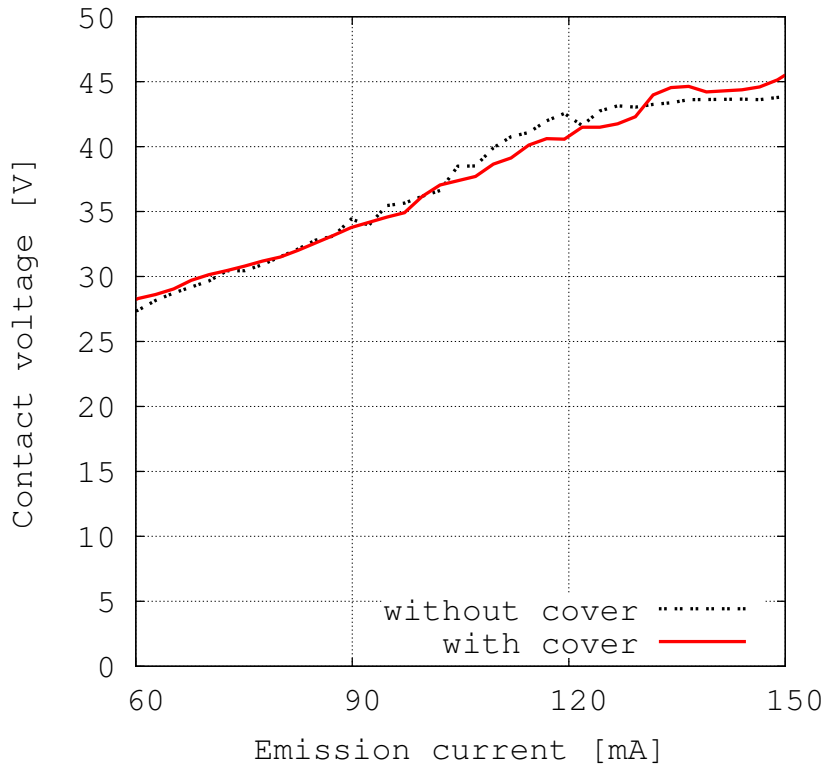

Figure6.21: Performance of neutralizers with and without a molybdenum cover. Strong magnetic force.

6.3.2 Demonstration of non-flake neutralizer lifetime enhancement: endurance test

Experimental results

A preliminary study revealed that the molybdenum-covered neutralizer is promising method by which to enhance the lifetime of the neutralizer. In order to more precisely verify the effectiveness of this method, we performed an endurance test. In this experiment, we newly manufactured a molybdenum-covered neutralizer, in which the entire magnetic circuit is covered. In addition, the antenna was changed from brass to molybdenum. By this redesign, the surface that touches the plasma is composed of molybdenum. Fig.6.22 shows the redesigned neutralizer. The cover thickness is also 300 μm in this experiment. We also strengthen the magnetic field in order to make the magnetic field the same at the edge of the cover and at the edge without the cover. The reason for this is described in the preliminary study. Fig.6.23 shows the performance transition of the redesigned molybdenum-covered neutralizer. The neutralizer performance is not getting worse after 2,500 hours of operation. The experimental condition is 8 W microwave power and 0.7 *sccm* operational gas (0.5 *sccm* up until 84 hours).

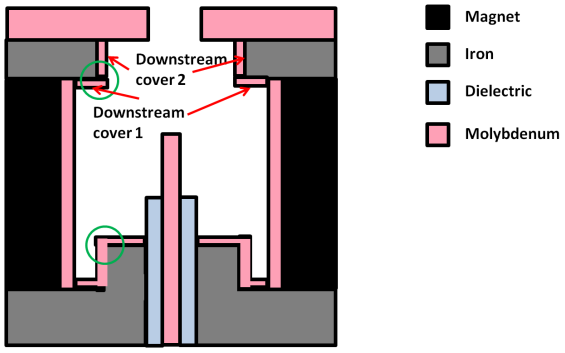

Figure6.22: Schematic diagram of the fully molybdenum-covered neutralizer.

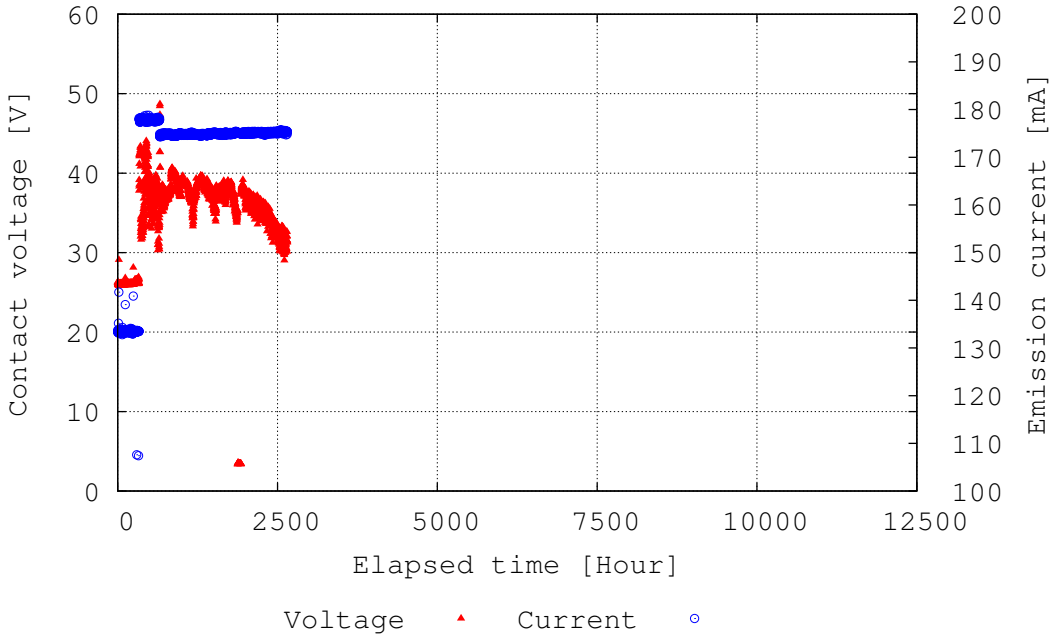

Figure6.23: Performance transition of the molybdenum-covered neutralizer.

Internal inspection of the neutralizer after the 2,500-hour endurance test revealed the following. The flakes were attached on the orifice plate.The flake thickness is approximately 14 μm. Table 6.2 lists the weight change and the degradation or accumulation rate of each assemblies which were calculated from the weight change, the surface area, and the ion current.

Table6.2: Weight change and degradation or accumulation rate of each assembly. When the parameter is positive, it indicates accumulation.

	Weight difference, mg	Rate, atoms/mC
Upstream cover 1	7.9	2.9e+11
Upstream cover 2	8.6	3.2e+11
Side wall and downstream cover1	-21	-1.84e+11
Downstream cover2	10.4	7.0e+11
Orifice plate	-28.4	-7.8e+11
Antenna	-1	1.1e+11
Peeled flake	6	
Summary	-17.5	

Discussion

The flake thickness which was peeled from the orifice plate is only 14 μm. This is explained by the lack of cleaning and the lack of heating of the base material [50]. First, the attachment energy of the film become lower when the base material is dirty. In this experiment, the neutralizer was only wiped by alcohol cotton before the endurance test. Second, the sufficient surface diffusion is also needed for uniform attachment. For the sufficient surface diffusion, it is required that the base material is heated above the 50% of melting temperature of the film material, i.e., approximately 2,900 K in molybdenum. In this experiment, the neutralizer was operated in approximately 280-450 K. Fig.6.24 shows the sputtering yield against inner plasma of the neutralizer. The accumulation or degradation rate of the Table 6.2 should be several times larger or smaller than the parameter of the 23-33 V considering the anode fall and the discussion of 6.1.2. The difference of the degradation or accumulation rate from the Fig.6.24 is explained by the foreign material inside the neutralizer. As mentioned, the neutralizer was only wiped by alcohol cotton before the endurance test. This error is reduced by cutting off the initial weight change because the plasma cleans the surface. Thus, the degradation or accumulation rate should be discussed after obtaining the second weight change. In the case of molybdenum-covered neutralizer, lifetime is limited by the degradation of the antenna most often. This is because the flakes, which peeled off from the surface, are not attracted to the magnetic circuit near the antenna by magnetic force. This results in the contamination of the dielectric surface not occuring more than the usual non-molybdenum-covered neutralizer. The following lifetime expectation is assuming that the molybdenum flake doesn't attach to the magnetic circuit near the antenna. As we discussed in 6.2.1, assuming the lifetime of the antenna is determined by 75 % of its size. Assuming the lifetime of the antenna is determined by 80, 85, 90, and 95 % of its size, the lifetime is 90.4 %, 81.6 %, 73.1 %, and 64.4 % to the lifetime of the 75 %. The reasons of the lifetime are not $\frac{75}{80}$, $\frac{75}{85}$, $\frac{75}{90}$, and $\frac{75}{95}$ to the lifetime of the 75 % are that the sputtering rate is proportional to the surface area of the antenna, and it gets smaller when the volume gets smaller. As the discussion of 6.1.2, set the model as Fig.6.25. In Fig.6.25, we assumed there are only two parts inside the neutralizer: the antenna and rest. m_a is the weight of the molybdenum particles ejected from the antenna per unit time, and m_m is the weight of the molybdenum particles ejected from the rest per unit time. s is the probability of reattachment to the antenna. We assumed the neutralizer is isolated from the outside so that no

particles are ejected from the neutralizer, because the area of the orifice is significantly smaller than the area of the whole neutralizer. This assumption is reasonable from the results of Table 6.2. The particles which emitted from the neutralizer is 17.5 *mg*. The particles which stayed inside the neutralizer, i.e., forming flakes or reattached is 32.9 *mg*. This results in 65 % of the particles stayed inside the neutralizer. This error is much less than the errors caused by the sputtering voltage. The weight variation per unit time of the antenna dAn are the summary of the degradation and the accumulation so that it can be written by

$$dAn = (m_a + m_r)s - m_a \tag{6.3.1}$$

also of the rest dO can be written by

$$dO = (m_a + m_r)(1-s) - m_r \tag{6.3.2}$$

From the parameter of ion current densities in 5.1.2, using surface area of all assemblies, $m_r = \frac{252}{21} m_a$. Thus

$$dAn = (13r - 1)m_a \tag{6.3.3}$$

Now, s is associated with the ratio of area of antenna and the rest assuming the phenomena of reattachment is the same between them. s is approximately 0.04, so that $dAn = -0.48m_a$. The net antenna degradation rate is 48 % of calculated rate. Fig.6.26 shows the expected lifetime, i.e., the time to be 75 % of the antenna size, with variation of sputtering voltage. The neutralizer lifetime is expected 32 V contact voltage of diode mode, which is 22 V sputtering voltage is more than 1,000,000-hours. To accellerate the endurance test, conducting with the larger emission current is effective. By the larger emission current, the contact voltage gets larger, but the ion saturation current unchanges.

The errors of the expected lifetime are due to the following.

1. The errors due to the sputtering model. Yamamura model has 5-15% difference to the experimental results [5].
2. The errors due to the estimation of the anode fall due to the difference between coupling mode and the diode mode. Anode fall gap is several V.
3. The errors due to the ion saturation current errors.

The first errors are reduced by using more resonable sputtering model. The second errors are reduced by obtaining the precise anode fall gap in the same neutralizer. The ion saturation current were measured only at the antenna and at the orifice plate. The currents of others are assumued the same as the orifice plate. In addition to this, the ion saturation current includes the secondary electron current caused by ion, excited particle collision against the surface. This results in expecting 0.8 % shorter lifetime [33].

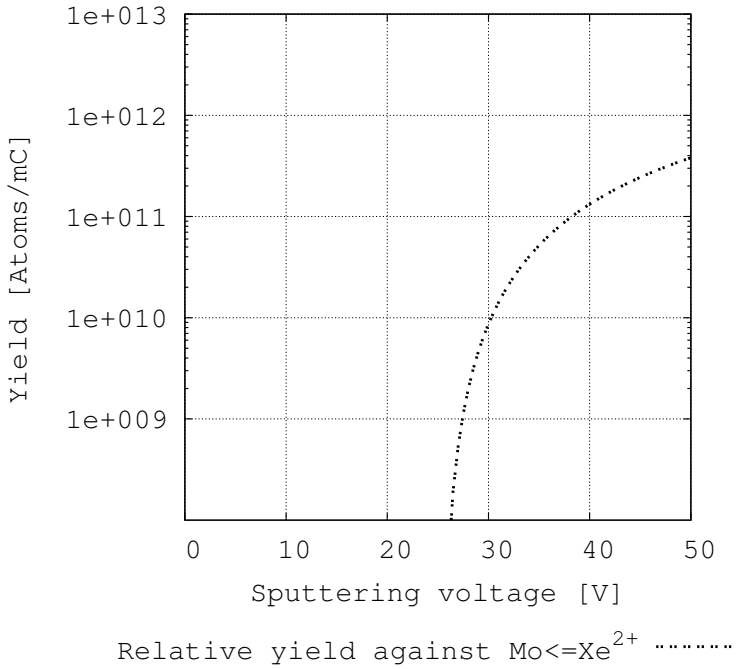

Figure6.24: Sputtering yield from inner plasma of neutralizer.

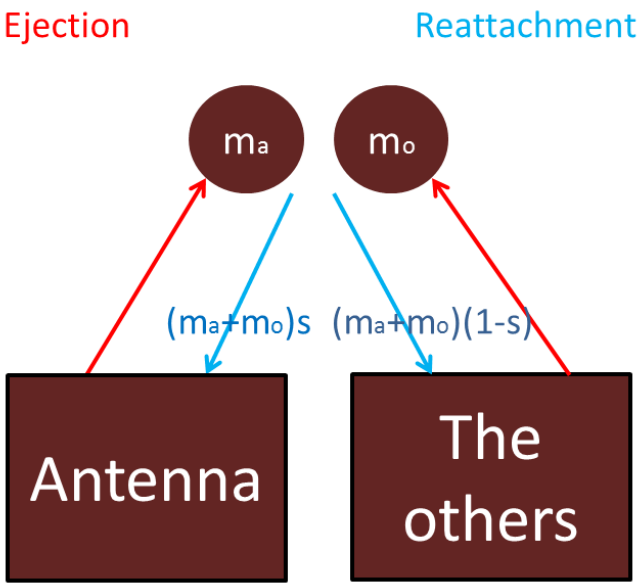

Figure6.25: Model of sputtering and reattachment with the antenna.

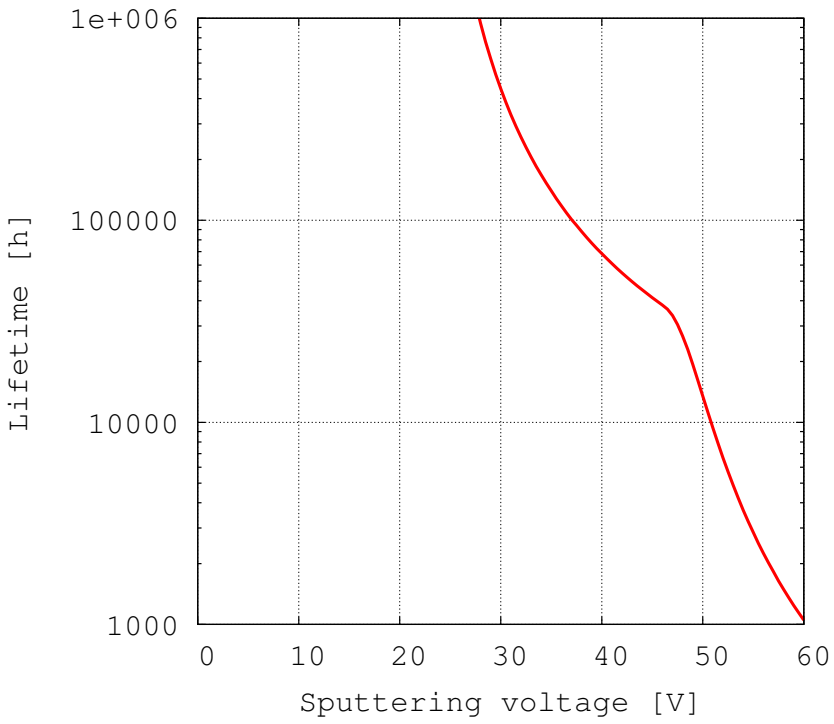

Figure6.26: Expected lifetime of the non-flake neutralizer.

6.4 Summary

1. Inside the neutralizer, there are repetition of accumulation and vanishing due to sputtering. It results in the 30% of sputtered particles accumulate on the molybdenum surface.
2. The neutralizer lifetime is expected by using the accumulation weight as an indicator.
3. Floated orifice, dielectric orifice, strengthen of magnet, and molybdenum-covered neutralizer are promising methods by which to enhance the lifetime.
4. Higher magnetic flux density neutralizer is demonstrating the constant performance in 12,000-hour endurance test, and its lifetime is expected to be 22,000 hours.
5. Higher magnetic flux density neutralizer have an advantage in minimizing the redesigning of the neutralizer from the flight model which had acheived 10,000 hours of space operation.
6. Molybdenum-covered neutralizer is demonstrating the favorable performance in 2,500-hour endurance test, and its lifetime is expected to be 1,000,000 hours more than the molybdenum-covered neutralizer.

7 Conclusion

The performance degradation mechanism of the ECR neutralizer was clarified. According to this mechanism, the principal cause of the performance degradation of the neutralizer is contamination of the dielectric surface due to sputtering from flakes on the magnetic circuit. This degradation can be avoided by suppressing the sputtering by means of a lower contact voltage and by inhibiting flake formation.

Net ion current distribution measurement was conducted to refurbish the design assemblies for endurance enhancement. The measurement revealed several measures. Among these measures, we chose to make higher magnetic flux density and to fully cover the neutralizer with molybdenum and demonstrated the result of improved performance through an endurance test. The neutralizer performances are not getting worse in the 12,000-hour and 2,500-hour endurance tests.

We discussed degradation inside neutralizer applying the Yamamura et.al sputtering model [38] to the results of the net ion current distribution. According to the discussion, the 30 % of sputtered iron accumulates on the molybdenum surface. This results in the formed flakes by repeating the vanishing and accumulating for 2.8-times in average, and finally peels off from the low sputtering area inside the neutralizer.

Using the total accumulation weight for the indicator of the lifetime, the higher magnetic flux density neutralizer which are running through the endurance test, is expected 22,000-hours lifetime, in spite of 135 % emission current of its prototype model. The fully covered neutralizer is expected 1,000,000-hours lifetime. The fully covered neutralizer has an advantage in the lifetime than the higher magnetic flux density neutralizer, but the latter also has an advantage in minimizing the redesigning of the neutralizer from the flight model which had achieved 10,000 hours of space operation.

The degradation mechanism and the theory for the lifetime enhancement are revealed. For the further study, particular net ion current distribution measurement is required especially at magnetic circuit tips. In these areas, the accumulation and the degradation rate are different from average rate. Figuring out these phenomena, the lifetime expectation accuracy will be improved.

Reference

[1] M. Hayashi, “Determination of electron-xenon total excitation cross-sections, from threshold to 100 ev, from experimental values of townsend’s alpha,” *Journal of Physics D: Applied Physics*, Vol. 16, pp. 581–589, 1983.

[2] E. Krishnakumar and S. K. Srivastava, “Ionisation cross sections of rare-gas atoms by electron impact,” *Journal of Physics B: Atomic, Molecular and Optical Physics*, Vol. 21, pp. 1055–1082, 1988.

[3] M. J. Patterson, “Neutralizer optimization,” *22nd International Electric Propulsion Conference*, Vol. IEPC91-151, 1991.

[4] T. K. T. Kaneda and J.-S. Chang, “Plasma parameters in noble-gas narrow-tube and capillary-tube discharge, positive column plasmas,” *Journal of Physics D: Applied Physics*, Vol. 23, pp. 500–503, 1990.

[5] J. Gruber, “Low-energy sputter erosion of various materials in a t5 ion thruster,” *27th International Electric Propulsion Conference*, Vol. IEPC-01-307, 2007.

[6] McGraw-Hill, *Physics of Electric Propulsion*, 1968.

[7] 栗木恭一 and 荒川義博, **電気推進ロケット入門**. 東京大学出版, 2003.

[8] S. S. H. Kuninaka, “Development of microwave discharge ion thruster for asteroid sample return mission,” *32nd AIAA/ASME/SAE/ASEE Joint Propulsion Conference and Exhibit*, Vol. AIAA-1996-2979, 1996.

[9] S. Hosoda and H. Kuninaka, “The homeward journey of asteroid explorer ”hayabusa” powered by the ion engines,” *Journal of Plasma and Fusion Research*, Vol. 86(No.5), pp. 282–292, 2010.

[10] H. Kuninaka and S. Satori, “Development and demonstration of cathode-less electron cyclotron resonance ion thruster,” *Journal of Propulsion and Power*, Vol. 14, pp. 1022–1026, 1998.

[11] 細田聡史 and 國中均, “イオンエンジンによる小惑星探査機「はやぶさ」の帰還運用,” *Journal of Plasma and Fusion Research*, Vol. 86, pp. 282–292, 2010.

[12] H. K. et. al, “Asteroid rendezvous of hayabusa explorer using microwave discharge ion engine,” *29th International Electric Propulsion Conference*, Vol. IEPC-2005-010, 2005.

[13] D. M. Goebel and I. Katz, *Fundamentals of Electric Propulsion:Ion and Hall Thrusters*. JPL space scienceand technology series, 2008.

[14] 渡邉裕樹, “誘導結合プラズマ電子源のイオンスラスタへの適用研究,” Ph.D. dissertation, 首都大学東京大学院, 2012.

[15] M. Frandia and L. Arrington, “Staus of the next ion thruster long duration test,” *41st AIAA/ASME/SAE/ASEE Joint Propulsion Conferene & Exhibit*, Vol. AIAA2005-4065, 2005.

[16] H. L. L Arrington, H. Bassner and R. Kukies, “Rita ion propulsion artemis - results close to the completion of thelife test,” *37th AIAA/ASME/SAE/ASEE Joint Propulsion Conference & Exhibit*, Vol. AIAA-2001-3490, 2001.

[17] A. N. R. Killinger, R. Kukies and L. Amorosi, “Artemis: Ion propulsion - satellite interactions,” *41st AIAA/ASME/SAE/ASEE Joint Propulsion Conference & Exhibit*, Vol. AIAA-2005-3670, 2005.

[18] G. C. et. al, “Review of qualification activities on the neutralizer for the rit 10 ion thruster,” *23rd International Electric*

Propulsion Conference, Vol. IEPC-93-109, 1993.

[19] H. e. Bassner, "Recent results on qualification of rita components for the artemis satellite," *28th AIAA/ASME/SAE/ASEE Joint Propulsion Conference & Exhibit*, Vol. AIAA-1992-3207, 1992.

[20] 碓井美由紀, "マイクロ波放電式イオン源のプラズマ生成に関する解析的および実験的研究," **東京大学修士論文**, No. 4, 2008.

[21] R. Tsukizaki, "Plasma diagnostics of the microwave ion thruster utilizing optical fiber probes," Ph.D. dissertation, The University of Tokyo, 2013.

[22] 荒川義博, 國中均, 中山宜典, and 西山和孝, **イオンエンジンによる動力航行**. コロナ社, 2006.

[23] T. R. Sarver-Verhey, "28,000 hour xenon hollow cathode life test results," *Proceedings of 25th International Electric Propulsion Conference*, pp. 1030–1037, 1997.

[24] K. Nishiyama and H. Kuninaka, "Discussion on performance history and operations of hayabusa ion engines," *Proceedings of 28th International Symposium on Space Technology and Science*, Vol. 2011-def-04, 2011.

[25] 小泉宏之, "500ma 級マイクロ波放電式中和器の dubaissat-2 ホール推進システムへの適用," **平成** *24* **年度宇宙輸送シンポジウム**, Vol. STEP-2012-085, 2013.

[26] S. H. K. Nishiyama and H. Kuninaka, "Operational characteristics of a microwave discharge neutralizer for the ecr ion thruster μ20," *International Electric Propulsion Conference*, Vol. IEPC-2009-21, 2009.

[27] J. Brophy, "Nasa's deep space 1 ion engine," *Review Scientific Instruments*, Vol. 73(2), pp. 1071–1078, 2002.

[28] 伊勢俊之, "電気光学素子ファイバプローブを用いたマイクロ波放電式イオンスラスタの内部現象解明," Master's thesis, 東京大学, 2013.

[29] J. Brophy and P. Wilbur, "Calculation of plasma properties in ion source," *AIAA Journal*, Vol. 24, pp. 1516–1523, 1986.

[30] H. K. et. al, "Microwave plasma contactor," *Proceedings of 24th International Electric Propulsion Conference*, Vol. IEPC-93-040, 1993.

[31] C. Garner and J. Brophy, "Fabrication and testing of carbon-carbon grids for ion optics," *28th Joint Propulsion Conference and Eshibit*, Vol. AIAA 92-3149, 1992.

[32] 中野正勝, 梶村好弘, and 船木一幸, "電気推進の数値的な寿命評価-イオン加速グリッド耐久認定用数値解析 (jiedi) ツールの開発-," **第** *54* **回宇宙科学技術連合講演会**, 2010.

[33] 小野寺範義, 竹ヶ原春貴, 西山和孝, 船木一幸, and 國中均, "マイクロ波放電型中和器の電子放出機構," **日本航空宇宙学会論文集**, Vol. 49, pp. 27–31, 2001.

[34] 宮坂武志, 安里勝雄, F. B. Bharudin, 小林勉, and 杉山仁志, "イオンエンジングリッド損耗解析における電子モデルの検討," **平成** *22* **年度宇宙輸送シンポジウム**, Vol. STEP2010-030, 2011.

[35] 西山和孝 and 國中均, "はやぶさイオンエンジンの性能履歴と運用に関する考察," **平成** *22* **年度宇宙輸送シンポジウム**, Vol. STEP-2010-054, 2011.

[36] H. K. et.al, "Results of 18,000-hour endurance test on microwave discharge ion thruster engineering model," *36th AIAA/ASME/SAE/ASEE Joint Propulsion Conference and Exhibit*, Vol. AIAA-2000-3276, 2000.

[37] 大道渉, 小泉宏之, 細田聡史, 西山和孝, and 國中均, "マイクロ波放電式中和器の性能低下モデルとその実験的検証," **平成** *22* **年度宇宙輸送シンポジウム**, Vol. STEP-2010-58, 2011.

[38] Y. Yamamura and H. Tawara, "Energy dependence of ion-induced sputtering yields from monatomic solids at normal incidence," *Atomic Data and Nuclear Data*, Vol. 62, pp. 149–253, 1996.

[39] 金原粲, **薄膜の基本技術**. 東京大学出版, 2008.

[40] R.V.Stuart, 毛利衛, and 数坂昭夫, **入門　真空・薄膜・スパッタリング**. 技報堂出版, 1985.

[41] I. F. et.al, "Verification tests of carboncarbon composite grids for microwave discharge ion thruster," *Journal of Propul-*

sion and Power, Vol. 18(1), pp. 169–175, 2002.

[42] Y. S. H. Kuninaka, I. Funaki and K. Toki, "Endurance test facility and test status of microwave discharge ion thruster," *21st International Symposium on Technology and Science*, Vol. ISTS 98-a-2-21P, 1998.

[43] ——, "Endurance test of microwave discharge ion thruster system for asteroid sample return mission muses-c," *25th International Electric Propulsion Conference*, Vol. IEPC-97-137, 1997.

[44] I. F. S. Satori and H. Kuninaka, "Plasma coupling of microwave neutralizer," *34th AIAA/ASME/SAE/ASEE Joint Propulsion Conference & Exhibit*, Vol. AIAA-1998-3478, 1998.

[45] T. Dote and T. Kaneda, "Remarks on the collision loss factor of electrons," *Japanese Journal of Applied Physics*, Vol. 15(7), pp. 1399–1400, 1976.

[46] P. B. et.al, "Effective collison frequency of electrons in noble gases," *Journal of Physics B: Atomic, Molecular Physics*, Vol. 14(8), pp. 1485–1495, 1981.

[47] K. P. Subramanian and V. Kumar, "Total electron scattering cross sections for argon, krypton and xenon at low electron energies." *Journal of Physics B: Atomic, Molecular Physics*, Vol. 20, pp. 5505–5515, 1987.

[48] N. H. K. N. Leung and K. R. MacKenzie, "Plasma confinement by localized cusps," *The Physics of Fluids*, Vol. 19, pp. 1045–1053, 1976.

[49] I. T. et.al, "Electric field measurement of ecr ion thruster u 10 with optical fiber sensor," *48th AIAA/ASME/SAE/ASEE Joint Propulsion Conferene & Exhibit*, Vol. AIAA 2012-4185, 2012.

[50] 情報機構, **ディスプレイ・光学部材における薄膜製造技術**, 2007.

Acknowledgment

Since the beginning of the Ph. D course, I have been supported by a lot of people. In order to express my best gratitude, please let me remark the acknowledgment in Japanese.

はじめに、本研究を 2009 年より 5 年間に渡りご指導くださった國中先生に感謝申し上げます。小惑星探査機「はやぶさ」のイオンエンジンの長寿命化という大変やり甲斐と、そして責任の伴うテーマを与えていただきました。学生の立場ながら実ミッションの研究に関わることができるということは、私が ISAS での研究で求めていたもので大変な幸運でした。テーマは大変に重いものでしたが、こうして論文という形に出来たのは國中先生のご指導の賜物です。学術的なところはもちろんですが、先生の宇宙開発や技術開発に対しての哲学は、どのようにすれば世界で通じるもの作りができるのかということへの本質を少しでも理解する上で、感銘を受けることばかりでした。5 年間先生のもとで学ばせていただけたのは、私の人生のよろこびです。

西山先生には、先生でいらっしゃいながら気さくに様々なことでお助けいただき、その技術力や研究力など多くのことを学ばせていただきました。輪講でのご指摘にはいつも勉強させていただきました。小泉さんには、機械工学科出身で右も左も分からない自分に対し、プラズマの基礎や道具の使い方まで何もかも教えて下さり、その丁寧なご指導で、曲がりなりにもすぐに一人で実験ができるようになりました。細田さん、清水さん、上野さんには実験装置の使い方や注意点、事故を起こさない工夫など研究生活全般で多数のご指導を賜りました。先生方のみならず、スタッフとして教育以外の実務についていらっしゃる皆様に師事できたことは、私の研究生活を大変実りのあるものにしてくれました。

船田さんには、学会や実験装置の購入の手続きから、急な発注などイレギュラーな事態をいつもカバーしていただきました。安藤さんには実験室の環境を日頃から整えていただきました。実験や研究にに集中することができ、あらためてお礼申し上げます。

研究室で楽しく研究できたのは、いつでも協力してくれたり話し相手になってくれた先輩方・同期・後輩のおかげです。月崎さんには研究の進め方や論文の書き方など、大きなものから小さなものまで数多く教えていただきました。同期の久本くんや後輩の神田くんには常に気軽に相談に乗ってくれて、いつも助けられました。木下くん、杉田くんには最後の最後まで英文校正を手伝っていただけました。また、仕事の合間に英文校正をしてくれた学部時代の同期である古川くん、ありがとうございました。同じく英文校正を手伝ってくれて、また家族としても支えてくれた兄と、ここまで学ぶことができるような環境を作ってくれた母、育ててくれた家族に感謝致します。

皆様、ありがとうございました。

2014 年 3 月

大道　渉